Oxidation of Mercury in Products of Coal Combustion

Final Scientific/Technical Report

Reporting period start: September 15, 2004
Reporting period end: September 14, 2009

Peter M. Walsh, Giang Tong, and Neelesh S. Bhopatkar
University of Alabama at Birmingham, Birmingham, AL

Thomas K. Gale and George A. Blankenship
Southern Research Institute, Birmingham, AL

Conrad W. Ingram, Selasi Blavo, Tesfamariam Mehreteab,
Victor Banjoko, and Yohannes Ghirmazion
Clark Atlanta University, Atlanta, GA

Heng Ban
Utah State University, Logan, UT

April Freeman Sibley
Southern Company Services, Birmingham, AL

Report issued: March 2011

DOE Award Number: DE-FG26-04NT42195

University of Alabama at Birmingham
1530 3rd Avenue South
Birmingham, AL 35294-4461

Disclaimer

This report was prepared as an account of work sponsored by an agency of the United States Government. Neither the United States Government nor any agency thereof, nor any of their employees, makes any warranty, express or implied, or assumes any legal liability or responsibility for the accuracy, completeness, or usefulness of any information, apparatus, product, or process disclosed, or represents that its use would not infringe privately owned rights. Reference herein to any specific commercial product, process, or service by trade name, trademark, manufacturer, or otherwise does not necessarily constitute or imply its endorsement, recommendation, or favoring by the United States Government or any agency thereof. The views and opinions of authors expressed herein do not necessarily state or reflect those of the United States Government or any agency thereof.

Abstract

Laboratory measurements of mercury oxidation during selective catalytic reduction (SCR) of nitric oxide, simulation of pilot-scale measurements of mercury oxidation and adsorption by unburned carbon and fly ash, and synthesis of new materials for simultaneous oxidation and adsorption of mercury, were performed in support of the development of technology for control of mercury emissions from coal-fired boilers and furnaces.

Conversion of gas-phase mercury from the elemental state to water-soluble oxidized form ($HgCl_2$) enables removal of mercury during wet flue gas desulfurization. The increase in mercury oxidation in a monolithic V_2O_5-WO_3/TiO_2 SCR catalyst with increasing HCl at low levels of HCl (< 10 ppmv) and decrease in mercury oxidation with increasing NH_3/NO ratio during SCR were consistent with results of previous work by others. The most significant finding of the present work was the inhibition of mercury oxidation in the presence of CO during SCR of NO at low levels of HCl. In the presence of 2 ppmv HCl, expected in combustion products from some Powder River Basin coals, an increase in CO from 0 to 50 ppmv reduced the extent of mercury oxidation from 24 ± 3 to 1 ± 4%. Further increase in CO to 100 ppmv completely suppressed mercury oxidation. In the presence of 11-12 ppmv HCl, increasing CO from 0 to ~120 ppmv reduced mercury oxidation from ~70% to 50%. Conversion of SO_2 to sulfate also decreased with increasing NH_3/NO ratio, but the effects of HCl and CO in flue gas on SO_2 oxidation were unclear.

Oxidation and adsorption of mercury by unburned carbon and fly ash enables mercury removal in a particulate control device. A chemical kinetic mechanism consisting of nine homogeneous and heterogeneous reactions for mercury oxidation and removal was developed to interpret pilot-scale measurements of mercury oxidation and adsorption by unburned carbon and fly ash in experiments at pilot scale, burning bituminous coals (Gale, 2006) and blends of bituminous coals with Powder River Basin coal (Gale, 2005). The removal of mercury by fly ash and unburned carbon in the flue gas from combustion of the bituminous coals and blends was reproduced with satisfactory accuracy by the model. The enhancement of mercury capture in the presence of calcium (Gale, 2005) explained a synergistic effect of blending on mercury removal across the baghouse. The extent of mercury oxidation, on the other hand, was not so well described by the simulation, because of oversensitivity of the oxidation process in the model to the concentration of unburned carbon.

Combined catalysts and sorbents for oxidation and removal of mercury from flue gas at low temperature were based on surfactant-templated silicas containing a transition metal and an organic functional group. The presence of both metal ions and organic groups within the pore structure of the materials is expected to impart to them the ability to simultaneously oxidize elemental mercury and adsorb the resulting oxidized mercury. Twelve mesoporous organosilicate catalysts/sorbents were synthesized, with and without metals (manganese, titanium, vanadium) and organic functional groups (aminopropyl, chloropropyl, mercaptopropyl). Measurement of mercury oxidation and adsorption by the candidate materials remains for future work.

Table of Contents

Disclaimer ii

Abstract iii

List of Tables vii

List of Figures viii

Acknowledgments xii

Executive Summary xiii

1. Introduction 1

2. Mercury and Sulfur Dioxide Oxidation during Selective Catalytic Reduction of Nitric Oxide 2

   2.1. Processes Occurring in Selective Catalytic Reduction Catalysts 2

   2.2. Laboratory Experiments 3

      2.2.1. Southern Research Institute Catalyst Test Facility 3
      2.2.2. Quartz Cell, Flow System, and Gas Analysis 4
      2.2.3. Catalyst and Test Conditions 6
      2.2.4. Determination of Elemental and Total Mercury 8
      2.2.5. Determination of Sulfate 10
      2.2.6. Experimental Procedure 11

   2.3. Experimental Results and Discussion 13

      2.3.1. Program of Laboratory Measurements of SCR Performance 13
      2.3.2. Reactor Containing Sand 13
      2.3.3. Dependence of Mercury Oxidation on HCl 18
      2.3.4. Interaction between Mercury Oxidation and NO Reduction 20
      2.3.5. Inhibition of Mercury Oxidation by Carbon Monoxide 21
      2.3.6. Sulfate Formation 23

   2.4. Model for Reactions in the SCR Catalyst 28

      2.4.1. Nitric Oxide Reduction and Mercury Oxidation 28
      2.4.2. Inhibition of Mercury Oxidation by Carbon Monoxide 32
      2.4.3. Sulfur Dioxide Oxidation to Sulfate 34

3. Mercury Oxidation and Adsorption by Unburned Carbon and Fly Ash 37

   3.1. Pilot-Scale Experiments 37

   3.2. Experiments with Bituminous Coals 38

   3.3. Experiments with Blends of Bituminous and Powder River Basin Coals 41

   3.4. Mechanism and Kinetics of Mercury Oxidation and Adsorption 43

   3.5. Comparison of the Model with the Pilot-Scale Measurements 45

Table of Contents (continued)

4. Toward the Development of Combined Catalysts and Sorbents for Low Temperature Oxidation and Removal of Mercury from Flue Gas 49
   4.1. Introduction 49
   4.2. Synthesis of the Catalysts/Sorbents 50
      4.2.1. Synthesis of SBA-15 50
      4.2.2. Synthesis of MCM-41 50
      4.2.3. Synthesis of MCM-41 Containing Transition Metal, Manganese 51
      4.2.4. Synthesis of MCM-41 Containing Transition Metal, Titanium 51
      4.2.5. Synthesis of MCM-41 Containing Transition Metals, Titanium and Vanadium 51
      4.2.6. Synthesis of MCM-41 Containing Amino Organic Functionality as Pendant 51
      4.2.7. Synthesis of MCM-41 Containing CPTMS Organic Functionality as Pendant 51
      4.2.8. Synthesis of MCM-41 Containing Mercapto Organic Functionality as Pendant 52
      4.2.9. Synthesis of MCM-41 Containing Transition Metal, Manganese, and Amino Organic Functionality as Pendant 52
      4.2.10. Synthesis of MCM-41 Containing Transition Metal, Manganese, and CPTMS Organic Functionality as Pendant 52
      4.2.11. Synthesis of MCM-41 Containing Transition Metal, Manganese, and MPTMS Organic Functionality as Pendant 52
      4.2.12. Synthesis of Nano-Zeolite Y 53
   4.3. Characterization of the Catalysts/Sorbents 53
      4.3.1. X-ray Diffraction 53
      4.3.2. BET Surface Area and Pore Size Analyses 57
   4.4. System Set Up for the Evaluation of Materials for Mercury Oxidation and Adsorption 60
      4.4.1. Mercury Adsorption 60
      4.4.2. Mercury Analysis by Cold Vapor Atomic Adsorption Spectrophotometry 60
5. Summary and Conclusion 63
   5.1. Mercury and Sulfur Dioxide Oxidation during Selective Catalytic Reduction of Nitric Oxide 63
   5.2. Mercury Oxidation and Removal by Unburned Carbon and Fly Ash 67
   5.3. Toward the Development of Combined Catalysts and Sorbents for Low Temperature Oxidation and Removal of Mercury from Flue Gas 68

Table of Contents (continued)

References 70

List of Acronyms, Abbreviations, and Symbols 76

Appendix: One-Dimensional Radial Diffusion and Heterogeneous Reaction Model for NO Reduction by NH_3, Mercury Oxidation by HCl, and SO_2 Oxidation to SO_3 in SCR A1

List of Tables

2.2.1. SCR Catalyst Properties and Experimental Conditions. 7

2.3.1. Measurements of NO Reduction, Mercury Oxidation, and Sulfate Formation in the SCR Catalyst, as Functions of HCl, NO, NH_3 to NO Ratio, and CO in the Simulated Flue Gas. 14

2.3.2. Averages and Standard Deviations of the Measurements of SO_2 Conversion to Sulfate, Shown in Figure 2.3.5. 27

2.4.1. Reaction Rate Coefficients and Adsorption Equilibrium Constants in the Radial Diffusion and Heterogeneous Reaction Model. 29

3.2.1. Unburned Carbon in Fly Ash and Flue Gas Compositions during the SRI Experiments with Bituminous Coals (Gale, 2006). 38

3.2.2. Fraction of Total Mercury in the Oxidized State and Fraction of Total Mercury Adsorbed on Fly Ash and Unburned Carbon at Different Quench Rates and Temperatures during the SRI Experiments with Bituminous Coals (Gale, 2006). 40

3.3.1. Unburned Carbon in Fly Ash, Calcium Oxide in Ash, and Flue Gas Compositions during the SRI Experiments Firing Blends of PRB Coal with Bituminous Coals (Gale, 2005). 41

3.3.2. Fraction of Total Mercury in the Oxidized State and Fraction of Total Mercury Adsorbed on Fly Ash and Unburned Carbon at the Inlet to the Baghouse during the SRI Experiments with Blends of PRB Coal with Bituminous Coals (Gale, 2005). 43

3.4.1. Arrhenius Parameters for Rate Coefficients of Mercury and Chlorine Reactions in Products of Combustion of the Bituminous Coals and Coal Blends. 45

List of Figures

2.2.1. The Catalyst Test Facility at Southern Research Institute. 4

2.2.2. Quartz glass reactor cell with catalyst. 5

2.2.3. Test specimen of selective catalytic reduction (SCR) catalyst. 6

2.2.4. System for reduction of mercury from the oxidized to the elemental state at 750 ^{o}C followed by introduction of hydrogen gas to consume oxygen and inhibit reoxidation of mercury on cooling (Van Pelt and Meischen, 1999; Meischen et al., 2004). 9

2.2.5. Mercury concentration measurements at the catalyst outlet during equilibration of mercury vapor with the catalyst, adjustment of flow rates, an upset condition, and arrival at steady state, in the absence of HCl, NO, NH_3, and CO. 12

2.2.6. Example of mercury concentration measurements in the presence of HCl, NO, and NH_3. 12

2.3.1. Dependence of mercury oxidation in the square channel monolithic catalyst on the volume fraction of HCl, in the presence and absence of NO and NH_3, and absence of CO. 19

2.3.2. Dependence of mercury oxidation in the square channel monolithic catalyst on NH_3/NO ratio at the catalyst inlet, in the presence of 1 ppmv HCl and 10 to 11 ppmv HCl, with 300 to 345 ppmv NO at the catalyst inlet, in the absence of CO. 20

2.3.3. Dependence of mercury oxidation in the square channel monolithic catalyst on the volume fractions of CO and HCl, in the presence of 313 and 329 ppmv NO and NH_3/NO ratio from 0.91 to 0.94 at the catalyst inlet. 22

2.3.4. Dependence of mercury oxidation in the square channel monolithic catalyst on the volume fractions of CO and HCl, in the presence of 313 and 329 ppmv NO and NH_3/NO ratio from 0.91 to 0.94 at the catalyst inlet. The data are from Figure 2.3.3, shown on an expanded CO scale, corresponding to the practical range of CO in flue gas. 23

List of Figures (continued)

2.3.5. Dependence of SO_2 oxidation to sulfate in the square channel monolithic catalyst, and in the reactor containing sea sand, on HCl, in the presence of 300 to 350 ppmv NO and NH_3/NO ratio from 0.91 to ~1 at the inlet to the reactor, and CO in the ranges 0 to 50, 101 to 511, and 1013 to 2053 ppmv. 24

2.3.6. Dependence of SO_2 oxidation to sulfate in the square channel monolithic catalyst, and in the reactor containing sea sand, on NH_3/NO ratio at the inlet to the reactor, in the presence of 300 to 345 ppmv NO at the inlet, 0 to 102 ppmv CO, and HCl in the ranges 1 to 2.2, 10 to 12, and 49 ppmv. 25

2.3.7. Dependence of SO_2 oxidation to sulfate in the square channel monolithic catalyst, and in the reactor containing sea sand, on CO, in the presence of 300 to 350 ppmv NO and NH_3/NO ratio from 0.91 to ~1 at the inlet to the reactor, and HCl in the ranges 1 to 3, 10 to 12, and 49 to 50 ppmv. 26

2.4.1. Comparison of calculated and measured dependence of mercury oxidation in the square channel monolithic catalyst on NH_3/NO ratio at the catalyst inlet. 30

2.4.2. Comparison of calculated and measured dependence of mercury oxidation in the square channel monolithic catalyst on the volume fraction of HCl. 31

2.4.3. Comparison of calculated and measured dependence of mercury oxidation in the square channel monolithic catalyst on the volume fractions of CO and HCl. 33

2.4.4. Comparison of calculated and measured dependence of SO_2 oxidation to sulfate in the square channel monolithic catalyst on NH_3/NO ratio at the inlet to the reactor and the volume fraction of HCl. 35

2.4.5. Comparison of calculated and measured dependence of SO_2 oxidation to sulfate in the square channel monolithic catalyst on the volume fraction of HCl. 36

3.2.1. The temperature-time histories of flue gas in the convection section of the SRI Combustion Research Facility under the high and normal quench rate conditions, while firing the bituminous coals (Gale, 2006). 39

List of Figures (continued)

3.3.1. The temperature-time histories of flue gas in the convection section of the SRI Combustion Research Facility, under the high and low baghouse temperature conditions, while firing the blends of PRB coal with bituminous coals (Gale, 2005). 42

3.5.1. Comparison of experimental and simulated relationships between unburned carbon, HCl volume fraction, mercury oxidation, and mercury removal (Bhopatkar, 2006). 47

3.5.2. Comparison of the simulation of mercury oxidation and removal with experimental measurements while firing the bituminous coals (Bhopatkar, 2006). 48

3.5.3. Comparison of the simulation of mercury oxidation and removal with experimental measurements while firing the blends of PRB coal with bituminous coals (Bhopatkar, 2006). 48

4.1.1. The hexagonal pore structure of MCM-41 and SBA-15 nanoporous silicas. 49

4.3.1. The catalysts/sorbents synthesized. 53

4.3.2. X-ray diffraction pattern of MCM-41. 54

4.3.3. X-ray diffraction pattern of MCM-41 containing titanium. 54

4.3.4. X-ray diffraction pattern of MCM-41 containing manganese. 55

4.3.5. X-ray diffraction pattern of MCM-41 containing APTES organic functionality as pendant. 55

4.3.6. X-ray diffraction pattern of MCM-41 containing manganese and amino functionality as pendant. 56

4.3.7. X-ray diffraction pattern of MCM-41 containing CPTMS organic functionality as pendant. 56

4.3.8. X-ray diffraction pattern of MCM-41 containing mercapto (−SH) organic functionality as pendant. 57

4.3.9. Nitrogen adsorption/desorption isotherms of SBA-15 sample. 58

List of Figures (continued)

4.3.10. Nitrogen adsorption/desorption isotherms of MCM-41 with mercapto (−SH) functionality. 58

4.3.11. Nitrogen adsorption/desorption isotherms of MCM-41 with CPTMS functionality. 59

4.3.12. Nitrogen adsorption/desorption isotherms of MCM-41 with amino functionality. 59

4.4.1. Photographs of the mercury oxidation/adsorption apparatus. 61

4.4.2. Photograph of the Perkin Elmer FIMS-100 Cold Vapor Atomic Adsorption Spectrometer, used for mercury analysis, and the mercury calibration curve. 62

Acknowledgments

The material presented in this report is based upon work supported by the U.S. Department of Energy, National Energy Technology Laboratory, under Award Number DE-FG26-04NT42195.

The authors acknowledge, with gratitude, the following valuable contributions to successful kickoff and execution of the project:

Cormetech, Inc., and the Gas Technology Institute for providing samples of selective catalytic reduction catalysts.

The Tennessee Valley Authority for permission to use its converter technology for reduction of oxidized mercury to elemental form for analysis.

Sandra J. Meischen, Edward A. Stephens, Jr., and Vincent James Van Pelt, of the Tennessee Valley Authority, for helpful discussions regarding the thermal mercury converter and the behavior of mercury during selective catalytic reduction.

J. Sammy O'Neal, now with PCT, Inc., for assembling and commissioning the thermal mercury converter, according to the specifications and guidance provided by the Tennessee Valley Authority.

Balaji Krishnakumar, in Joseph J. Helble's research group in the Thayer School of Engineering at Dartmouth College, for calculations examining the possibility that carbon monoxide could have an effect on homogeneous oxidation of mercury. Dr. Krishnakumar is now with Niksa Energy Associates.

W. Scott Hinton, of W. S. Hinton & Associates, for helpful discussion of the issues surrounding mercury oxidation in selective catalytic reduction catalysts, at the start of the project.

Joseph D. McCain, of Southern Research Institute, for helpful advice and discussion of methods and instrumentation for sampling and measurement of mercury.

Jared W. Cannon, now with Southern Company, for setting up the catalyst reactor and inaugurating the laboratory work for the project in the SRI Catalyst Test Facility.

Rosa Dominquez-Faus, now in the Department of Civil and Environmental Engineering at Rice University, for performing the first set of experimental measurements of catalyst performance for the project, under the difficult conditions that existed before implementation of the Tennessee Valley Authority's thermal converter for reduction of oxidized mercury.

Linda H. Vernon, for proofreading a draft of the report. However, the first author is solely responsible for any omissions or errors in the final version of the report.

Executive Summary

The work presented in this report supports the development and implementation of technology for removal of mercury from flue gas produced by combustion of coal in industrial furnaces and electric utility boilers. The research project had the following components: (1) laboratory measurements of the effects of HCl and CO in coal combustion products on mercury and sulfur dioxide oxidation in the presence of selective catalytic reduction (SCR) catalyst and the effect of NH_3/NO ratio in SCR, (2) simulation of pilot-scale measurements of mercury oxidation and adsorption by unburned carbon and fly ash from combustion of coal, and (3) synthesis of combined catalysts and sorbents for low temperature oxidation and capture of mercury from flue gas.

A large set of laboratory measurements was performed, documenting the dependence of mercury oxidation in a square-cell monolithic V_2O_5-WO_3/TiO_2 SCR catalyst on HCl, NO, NH_3/NO ratio, and CO. The experimental measurements of total mercury (oxidized + elemental) were greatly facilitated by use of the thermal converter developed at the Tennessee Valley Authority, for reduction of oxidized mercury to the elemental state for analysis.

As previously noted in work by others, mercury oxidation in SCR catalyst was highly sensitive to the concentration of HCl at low levels of HCl (< 10 ppmv) (Eswaran and Stenger, 2005), and is suppressed in the presence of NH_3 (Machalek et al., 2003; Niksa and Fujiwara, 2005b; Senior, 2006; Gale et al., 2006b), because NH_3 competes with one of more of the reactants (Hg, HCl) for active sites on the surface of the catalyst.

Carbon monoxide in flue gas was found to have a strong inhibitory effect on mercury oxidation at low levels of HCl. In the presence of 2 ppmv HCl, a level expected in combustion products from some Powder River Basin subbituminous coals, an increase in CO from 0 to 50 ppmv reduced the extent of mercury oxidation from 24 ± 3 to 1 ± 4%. A level of 100 ppmv of CO was sufficient to completely suppress mercury oxidation when only 2 ppmv of HCl were present. In the presence of 11-12 ppmv HCl, increasing CO from 0 to ~120 ppmv reduced the fraction of mercury oxidized from ~70% to 50%. Variation in the CO content of flue gas when burning low-chlorine coals, such as those from the Power River Basin, is thus another possible source of variability and uncertainty in the extent of mercury oxidation in SCR, in addition to the high sensitivity of mercury oxidation to HCl itself, at low HCl.

A one-dimensional model for reacting flow in an SCR catalyst channel, including radial diffusion of species and surface reactions, successfully reproduced the qualitative features of NO reduction by NH_3 and mercury oxidation by HCl in the presence of NH_3. The model overestimated mercury oxidation at high HCl levels (> 10 ppmv) and was unable to account for inhibition of mercury oxidation by CO.

Attempts were made to document the conversion of SO_2 to sulfate, in conjunction with the mercury measurements. Sulfate formation decreased with increasing NH_3/NO

ratio at the catalyst inlet. Trends in the dependence of sulfate formation on HCl and CO could not be identified, due to large scatter in the experimental measurements and uncertainty regarding the contribution of the SCR catalyst to SO_2 oxidation.

A chemical kinetic mechanism consisting of nine homogeneous and heterogeneous reactions for mercury oxidation and removal was developed to interpret measurements of mercury oxidation and adsorption by unburned carbon and fly ash in experiments at pilot scale in the Combustion Research Facility at Southern Research Institute, burning three high-volatile bituminous coals (Gale, 2006) and blends of bituminous coals with Powder River Basin (PRB) subbituminous coal (Gale, 2005). The blends provided systematic variation of the chlorine and unburned carbon contents of flue gas, and the CaO to unburned carbon ratio. Most of the measurements of elemental, oxidized, and adsorbed mercury were made at the baghouse. There was a clear correlation in the experimental data between unburned carbon and mercury removal, but only a weak correlation between unburned carbon and the extent of mercury oxidation. A synergistic effect of coal blending enhanced mercury removal across the baghouse. Change in the HCl volume fraction had relatively weak influence on mercury oxidation or removal, over the range investigated, from 10 to 190 ppmv HCl.

The model included chlorination of carbon sites by reaction with HCl(g) to form the adsorbed species, HCl(C) (the "C" in parentheses indicates adsorption on solid carbon surface); reaction of elemental vapor phase mercury, Hg(g), with the chlorinated sites to form adsorbed mercurous chloride, HgCl(C); and desorption of HgCl(C) back to the flue gas as HgCl(g). A mechanism proposed by Gale (2005), in which calcium reacts with HgCl(g) vapor after its desorption from carbon surface, but prior to its conversion to $HgCl_2$(g), was adopted to account for the enhancement of mercury removal by calcium. The removal of mercury by fly ash and unburned carbon in the flue gas from combustion of the bituminous coals, at both high and low temperatures, was reproduced with good accuracy by the simulation. The mercury removal measurements for the coal blends were approximately reproduced, with removal greatly overpredicted for only two runs. The extent of mercury oxidation, on the other hand, was not so well explained, because of oversensitivity of the oxidation process in the model to the concentration of unburned carbon.

Combined catalysts and sorbents for low temperature oxidation and removal of mercury from flue gas were based on surfactant-templated nanoporous silicas containing a transition metal and an organic functional group. The objective is to create crystalline or highly-ordered multifunctional nanoporous organosilicates, incorporating both metal ions and organic groups within the pore structure of the materials, to simultaneously oxidize elemental mercury, adsorb the resulting oxidized mercury, and adsorb oxidized mercury already present in the flue gas. Twelve templated mesoporous organosilicate catalysts/sorbents were synthesized, with and without metals (manganese, titanium, vanadium) and organic functional groups (aminopropyl, chloropropyl, mercaptopropyl). The catalysts/sorbents were characterized by x-ray diffraction and nitrogen porosimetry. A system was set up for measurement of mercury oxidation and adsorption by the candidate materials, to be investigated in future work.

1. Introduction

The motivation for the work described in the report is control of mercury emissions from combustion of coal in industrial furnaces and electric utility boilers (Senior, 2001; Senior et al., 2000b, 2006; Pavlish et al., 2003; Chang, 2008). Three of the possible approaches to mercury capture provided the focus for the research: (1) oxidation of elemental mercury to mercuric chloride by reaction with hydrogen chloride formed from chlorine in coal, followed by removal of mercuric chloride during wet flue gas desulfurization, (2) oxidation and absorption of mercury by unburned carbon and fly ash, followed by removal of the adsorbed mercury with the particles in a particulate control device, and (3) combined catalysts and sorbents for low temperature oxidation and removal of mercury from flue gas.

The investigation had the following components: (1) laboratory measurements of the effects of HCl, NH_3/NO ratio, and CO in coal combustion products on mercury and sulfur dioxide oxidation in the presence of SCR catalyst, (2) simulation of pilot-scale measurements of mercury oxidation, adsorption, and removal by unburned carbon and fly ash from combustion of coal, and (3) synthesis of candidate catalyst/sorbents for low temperature oxidation and removal of mercury from flue gas.

The partners in the project were the University of Alabama at Birmingham (UAB), Southern Research Institute (SRI), Clark Atlanta University (CAU), Gas Technology Institute (GTI), and Southern Company Services. UAB and SRI performed laboratory experiments in the Catalyst Test Facility at SRI. SRI shared data from its pilot-scale experiments in the SRI Combustion Research Facility. CAU and GTI developed new catalyst and sorbent formulations. UAB and SRI developed reaction mechanisms to describe SCR catalyst performance and oxidation and adsorption of mercury by unburned carbon and fly ash. Southern Company Services provided guidance and advice from the electric utility perspective.

The laboratory study of mercury and sulfur dioxide oxidation during selective catalytic reduction of nitric oxide is described in Section 2 of the report. The pilot-scale measurements and analysis of mercury oxidation and adsorption by unburned carbon and fly ash from pulverized coal combustion are discussed in Section 3. The synthesis and characterization of combined catalysts and sorbents for simultaneous oxidation and capture of mercury are presented in Section 4. The results and conclusions from the work are summarized in Section 5.

2. Mercury and Sulfur Dioxide Oxidation during Selective Catalytic Reduction of Nitric Oxide*

Giang Tong and Peter M. Walsh
University of Alabama at Birmingham

George A. Blankenship and Thomas K. Gale
Southern Research Institute

Mercury in coal appears in the products of combustion in boiler furnaces in its elemental state, Hg(0), and in its fully oxidized state, Hg(II), thought to be $HgCl_2$ in the presence of even small concentrations of chlorine from the coal. Mercuric chloride is soluble in water, while elemental mercury is not. An approach to removal of mercury from flue gas is to maximize its conversion from Hg(0) to $HgCl_2$, then capture the $HgCl_2$ during wet flue gas desulfurization (wet FGD). Though the oxidized state of mercury is thermodynamically favored under the conditions at the exit from the convection heat transfer section in an electric utility boiler and in wet FGD, oxidation of mercury downstream from the convection section is slow in the absence of a catalyst (Senior et al., 2000a, 2000b).

The state of development of catalysts for mercury oxidation, mechanisms of oxidation, and the prospects for advances in catalyst technologies were reviewed by A. A. Presto and E. J. Granite of the National Energy Technology Laboratory (Presto and Granite, 2006). Their comprehensive review included selective catalytic reduction (SCR) catalysts, carbon-based materials, and metals and metal oxides. The authors identified sources of uncertainty in the application of the approach to mercury capture described above, emphasizing the need for research "... determining the reaction mechanism and kinetics and searching for more cost-effective catalyst and support materials" (Presto and Granite, 2006).

2.1. Processes Occurring in Selective Catalytic Reduction Catalysts

The SCR catalyst's primary function is to remove NO_X from flue gas. Taking NO as the example, the reaction is between gas-phase NO and NH_3 adsorbed on the catalyst:

$$NO(g) + NH_3(ads) + 1/4\ O_2 \rightarrow N_2 + 3/2\ H_2O \qquad \text{(Reaction 2.1)}$$

Sulfate (SO_3, SO_4^{2-}, HSO_4^-, and H_2SO_4) formation in the catalyst is also of interest in connection with a number of operating and emissions problems in coal-fired utility boilers, such as excessive stack plume opacity, cold-end corrosion, precipitator performance, and air heater fouling. An SCR catalyst is typically required to meet a

*Tong (2009), Tong et al. (2007, 2008).

specification placing an upper limit on the fraction of SO_2 oxidized to SO_3. The mechanism for conversion of SO_2 to SO_3 is a cycle in which SO_2 is oxidized by a metal oxide, such as V_2O_5 or Fe_2O_3, serving as a catalyst, followed by regeneration of the active metal oxide by reaction with O_2. Writing the metal oxide in the generic form, M_xO_y:

$$SO_2(g) + M_xO_y(s) \rightarrow SO_3(g) + M_xO_{y-1}(s) \qquad \text{(Reaction 2.2)}$$

$$M_xO_{y-1}(s) + 1/2\ O_2(g) \rightarrow M_xO_y(s) \qquad \text{(Reaction 2.3)}$$

If an SCR catalyst is also to serve as a reactor for mercury oxidation, it must also promote reaction, according to a mechanism so far not well understood, between mercury and HCl, in which either the mercury, the HCl, or both, are adsorbed. Taking as an example the case in which mercury is adsorbed, but HCl is not:

$$Hg(0, ads) + HCl(g) \rightarrow HgCl(g) \qquad \text{(Reaction 2.4)}$$

This reaction is followed by addition of a second chlorine atom, possibly, but not necessarily, via a homogeneous reaction, for example:

$$HgCl(g) + 1/2\ Cl_2(g) \rightarrow HgCl_2(g) \qquad \text{(Reaction 2.5)}$$

In the face of this complex system of reactions, and the competition of at least some of the adsorbed species for similar surface sites, optimization of catalyst formulation and geometry and operating conditions to simultaneously maximize NO_X reduction, minimize SO_2 oxidation, and maximize mercury oxidation has not proven to be a simple problem. The purpose of the present work was to provide measurements of the behavior of this system that contribute to understanding the interactions among the three processes and improvement of the accuracy with which the performance of SCR, with respect to all three requirements, can be simulated. The ultimate goal is the identification of conditions that maximize the conversion of mercury from the elemental state to water-soluble mercuric chloride during SCR of NO_X by NH_3, while maintaining good NO_X reduction performance and minimizing the oxidation of SO_2 to SO_3.

2.2. Laboratory Experiments

Experiments to quantify catalyst performance were conducted in the Catalyst Test Facility at Southern Research Institute (SRI) by Giang Tong, Graduate Research Assistant in the Interdisciplinary Engineering Program at the University of Alabama at Birmingham (UAB) and by George Blankenship of SRI, under the direction of Peter Walsh of UAB and Thomas Gale of SRI. The experiments were performed in a flow reactor using a sample of commercial catalyst and simulated flue gases containing Hg, HCl, NO, NH_3, SO_2, CO, H_2O, CO_2, O_2, and N_2.

2.2.1. Southern Research Institute Catalyst Test Facility

The laboratory experiments were conducted in the Catalyst Test Facility at Southern Research Institute, shown in Figure 2.2.1. The facility has been described by Gale et al. (2006b), Tong (2009), and, briefly, by Tong et al. (2007). The catalyst sample

is housed in a quartz glass cell in 3-foot-long vertical tube furnace having an inside diameter of 3 inches. The tube furnace has separately controllable zones in which temperatures can be set at any level from ambient to 1200 ^{o}C. Catalyst samples up to 600 mm long and having cross sections up to 50 mm square or 70 mm in diameter can be tested. Provision has been made for introducing all of the following gases: nitrogen, oxygen, carbon dioxide, carbon monoxide, steam, sulfur dioxide, nitric oxide, ammonia, mercury, hydrogen chloride, and chlorine. The compositions of the inlet and outlet streams are monitored using continuous analyzers and a Fourier transform-infrared spectrometer. Mercury is determined by atomic fluorescence.

2.2.2. Quartz Cell, Flow System, and Gas Analysis

The heated sections of the reactor are made of quartz glass to minimize wall effects. The quartz glass cell housing the catalyst is shown in Figure 2.2.2. Quartz wool was wrapped around the catalyst and tightly packed into the gap between the outer surface of the catalyst and its quartz glass holder to minimize gas flow over the outer surface of the catalyst.

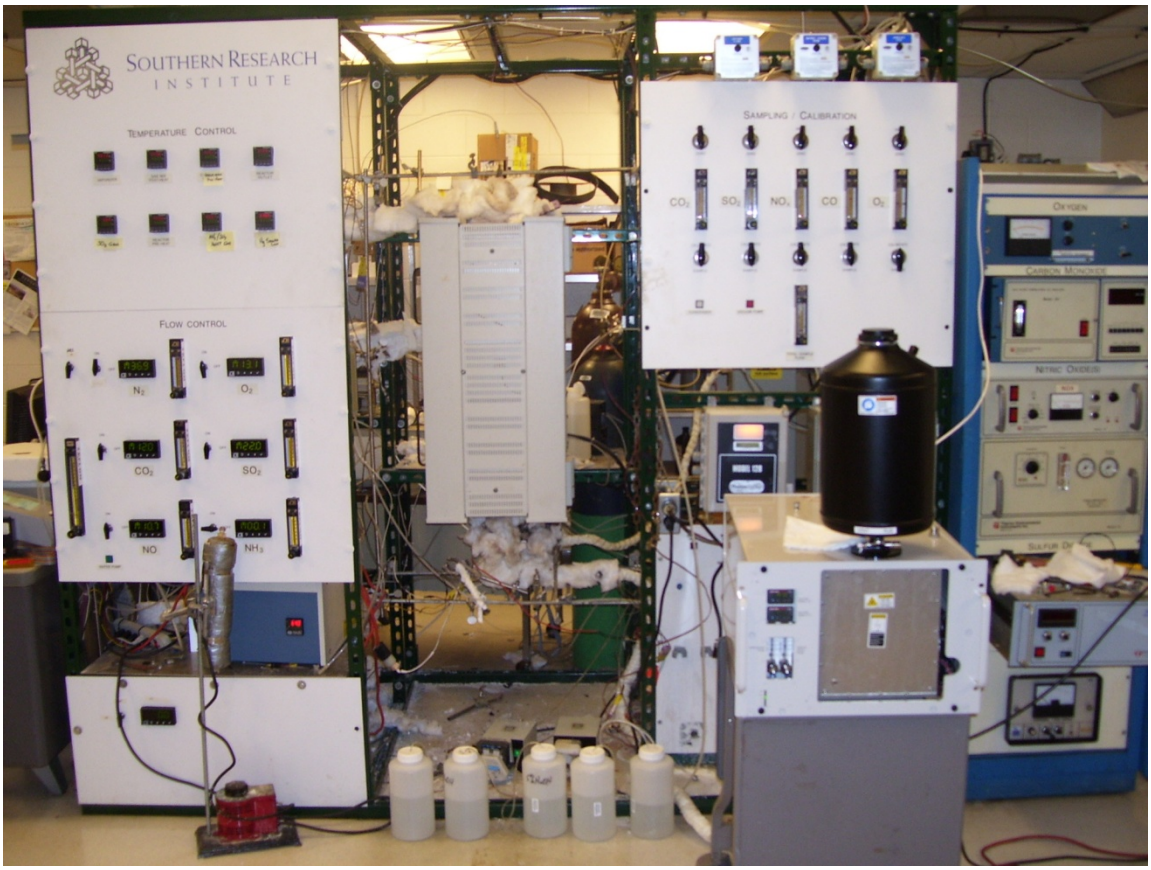

Figure 2.2.1. The Catalyst Test Facility at Southern Research Institute. The quartz glass cell housing the catalyst sample is in the vertical tube furnace just to the left of center in the photograph. Continuous gas analyzers are on the far right and the Fourier transform-infrared spectrometer is in the foreground on the right.

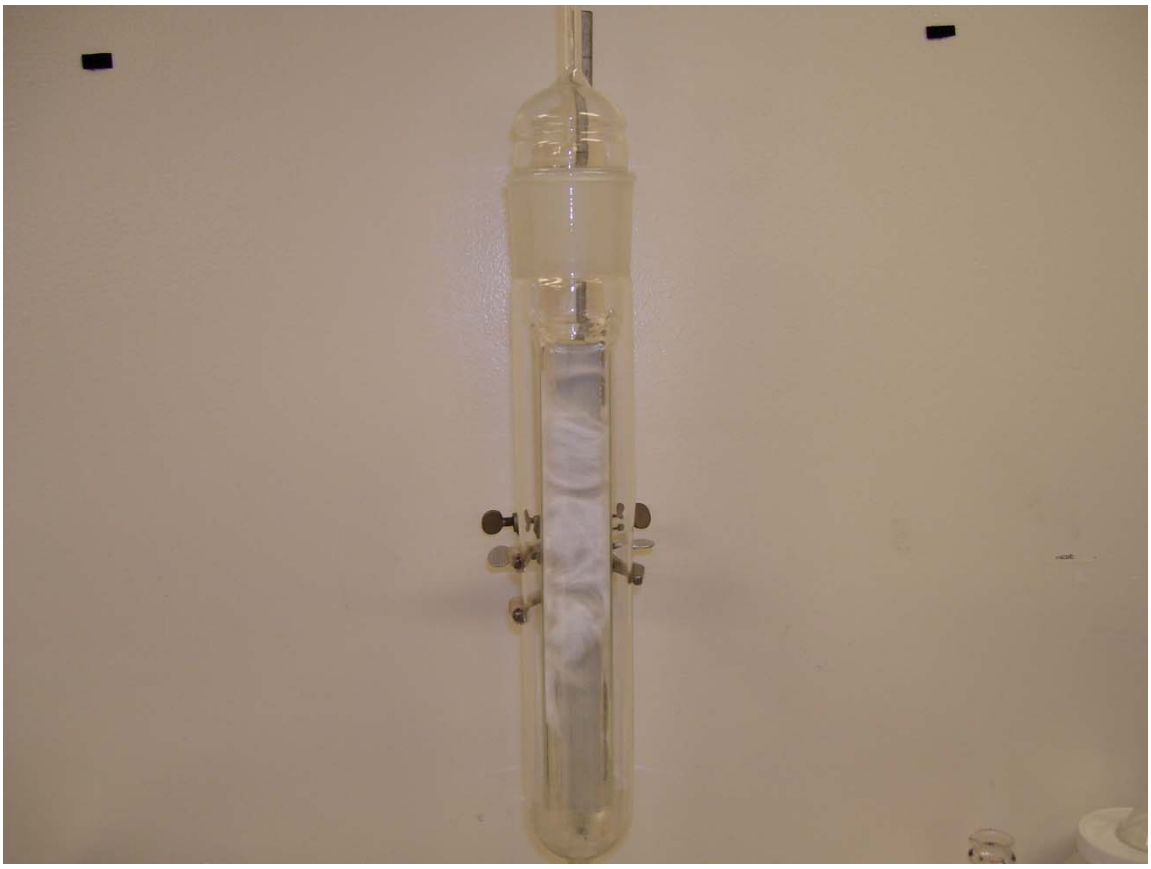

Figure 2.2.2. Quartz glass reactor cell with catalyst.

The simulated flue gas was prepared from compressed gas mixtures. Mass flow meters from Brooks Instrument (Hatfield, PA, 5850E Series) and Omega Engineering, Inc. (Stamford, CT, Models DMA-7104E, 7108E, 7102E, and 7101E) were used to control the flow rates of the individual components. The flow rates were monitored using an HP-34970A data acquisition system. The steam content of the gas mixture was controlled by feeding water through a Cole-Palmer Instrument Co. (Vernon Hills, IL) Model Masterflex C/L metering micro-pump.

Mercury was introduced using a PS Analytical Ltd. (Deerfield Beach, FL) Model 10.534 CavKit Mercury Calibration System, consisting of a reservoir containing an inert substrate impregnated with elemental mercury maintained at a constant temperature. The mercury reservoir supplies a stream of nitrogen saturated with elemental mercury at the temperature of the reservoir, diluted by additional nitrogen before mixing with the other gases. All gas contact surfaces between the mercury generator and reactor were made from Teflon or glass and heated to approximately 120 ºC using heating tape, to prevent vapor condensation and minimize adsorption of mercury. The simulated flue gas stream was mixed and heated in a quartz glass tube before entering the reactor.

The compositions of the inlet and outlet gas streams were determined using continuous gas analyzers and an MKS Instruments (Andover, MA) MultiGas 2030

Fourier transform-infrared (FT-IR) spectrometer. The sample line from the reactor to the spectrometer was heated to approximately 232 ^{o}C.

2.2.3. Catalyst and Test Conditions

A commercial-type square-cell monolithic V_2O_5-WO_3/TiO_2 SCR catalyst, generously provided by Cormetech, Inc. (Durham, NC), was used for all of the measurements presented in Section 2 of the report. A photograph of the catalyst sample is shown in Figure 2.2.3. The V_2O_5 loading of the catalyst was low (< 2 wt%), and the V_2O_5 was uniformly distributed through the thickness of the monolith in order to maintain high activity in the presence of erosion by particles in coal-fired installations. The TiO_2 support does not exhibit activity for mercury oxidation (Zhuang et al., 2000).

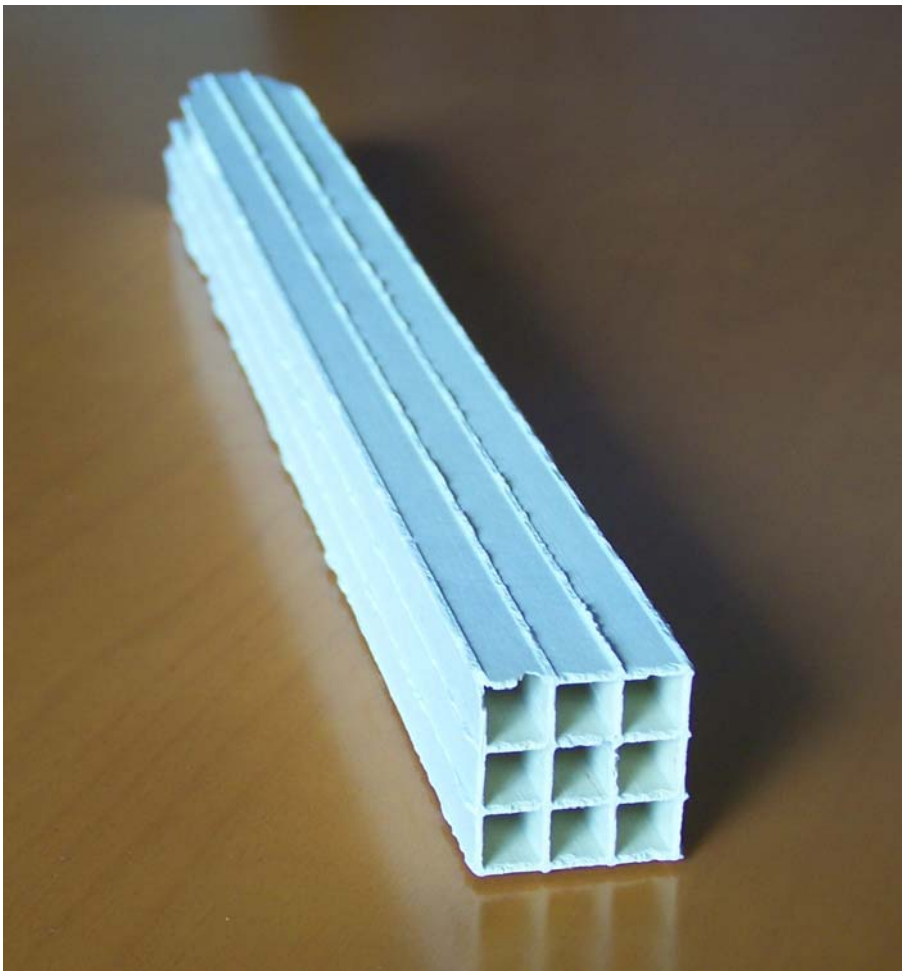

Figure 2.2.3. Test specimen of selective catalytic reduction (SCR) catalyst.

Properties of the catalyst and the ranges of conditions under which the measurements were made are given in Table 2.2.1. The gas composition is intended to be representative of an untreated flue gas from combustion of medium-sulfur (~ 1.3 wt%) bituminous coal. However, NO alone was used to represent NO_X, and no particulate matter (soot, unburned coal char, or fly ash) was present. The temperature of 378 ^{o}C is

near the midpoint of the catalyst manufacturer's suggested operating temperature range for coal-fired applications (316 to 427 ^{o}C). Temperature was measured using a K-type thermocouple inserted into the catalyst bed.

Table 2.2.1. SCR Catalyst Properties and Experimental Conditions.

Property or Condition	Value
Catalyst supplier	Cormetech, Inc.
Catalyst composition	V_2O_5-WO_3/TiO_2
Catalyst geometry	square-cell monolith
Catalyst cross-section	square, 25 x 25 mm
Catalyst channel open area	square, 7 x 7 mm
Catalyst wall thickness	1 mm
Catalyst length	305 mm*
Catalyst void volume	136.7 cm^3
Catalyst geometric surface/volume ratio	0.571 mm^{-1}
Total surface/volume ratio	3.23 mm^{-1}
Catalyst temperature	378 ^{o}C (+11, -25 ^{o}C)
Residence time in catalyst at 378 ^{o}C	0.53 s
Flue gas flow rate at 21°C, 1 atm	7 std. L/min
Synthetic flue gas composition (dry basis, other than H_2O):	
O_2	4 - 7 vol%
CO_2	14 - 16 vol%
H_2O	7 - 10 vol%
HCl	0 - 100 ppmv
SO_2	800 - 900 ppmv
NO	0 - 350 ppmv
NH_3	0 - 345 ppmv
CO	0 - 2000 ppmv
Hg(0) at 20°C, 1 atm	10,000 ng/m^3
N_2	balance

* The average length. The original length was 310 mm, but the outlet end was chipped, as can be seen in Figure 2.2.3.

2.2.4. Determination of Elemental and Total Mercury

Elemental mercury is collected and concentrated in a gold trap, then desorbed, and determined by cold vapor atomic fluorescence spectrometry (Tekran, Knoxville, TN, Model 2537A Mercury Vapour Analyzer). A heated sample line maintained at approximately 232 ^{o}C was used to transport the sample stream from the reactor outlet. The Tekran instrument was configured to provide an integrated mercury value every 150 seconds. Mercury analysis data from the Tekran instrument were downloaded to capture software via a RS232 serial port, and exported to a Microsoft Excel spreadsheet for analysis and plotting. Mercury concentrations are specified at a temperature of 20 ^{o}C, 1 atm pressure, in dry gas at a 5 ^{o}C dew point.

In order to determine the total mercury in a gas sample, oxidized mercury in the sample is first reduced to the elemental form. The conventional method for accomplishing the reduction is a wet chemical system using stannous ion [Sn(II)] as the reducing agent. This system suffers from a number of disadvantages, among which are its need for attention and maintenance by experienced operators and consumption of large quantities of reagents. A more serious problem is the noise introduced into the total mercury measurement by the accumulation of mercury in condensate just upstream from the stannous ion reduction system. Droplets of the condensate, containing dissolved mercury, periodically run down the wall of the inlet tube into the reduction system, causing noise and spikes in the concentration record (Merritt et al., 2005). The accumulation of mercury in condensate and release as solute in droplets of condensate having various sizes and concentrations of mercury add to the difficulty in accurately determining the average steady concentration of mercury under a given set of experimental conditions.

An alternative to the wet chemical reduction was developed at the Tennessee Valley Authority (TVA). The system is described in a U.S. Patent by Van Pelt and Meischen (1999) and in a publication by Meischen, Van Pelt, Zarate, and Stephens (2004). An evaluation of the system and comparison with the wet chemical reduction method were performed by SRI and documented by Merritt, McCain, and Cushing (2005).

In the TVA system, mercury reduction occurs entirely in the gas phase, avoiding the problem of accumulation and release of mercury via condensate. The reduction of mercury from the oxidized to elemental forms is accomplished by heating the gas sample to 750 ^{o}C in a quartz glass cell. Midway in its passage through the cell, still at 750 ^{o}C, hydrogen gas is added to react with oxygen in the sample. The flow rate of hydrogen required to just consume all of the oxygen is determined by analysis of the sample for O_2 at the outlet from the system. The removal of O_2 and its conversion to water vapor inhibit the reoxidation of elemental mercury by acid gases such as HCl (Van Pelt and Meischen, 1999; Meischen et al., 2004). The system was observed to perform well in TVA's own tests and in the evaluation by SRI. Field tests conducted by TVA at a 700 MW plant equipped with SCR and a scrubber gave total mercury measurements that were within 20% of those obtained using the Ontario Hydro method.

The TVA group generously shared their expertise and design criteria for the mercury reduction system with SRI, and provided to SRI two of the quartz glass cells that they had designed and fabricated. A mercury reduction system assembled at SRI using the design guidelines and a reaction cell provided by TVA is shown in Figure 2.2.4. Use of this system for reduction of oxidized mercury in the exit gas from the catalyst reactor eliminated the noise that had complicated the determination of total mercury and the identification of steady-state conditions in previous work.

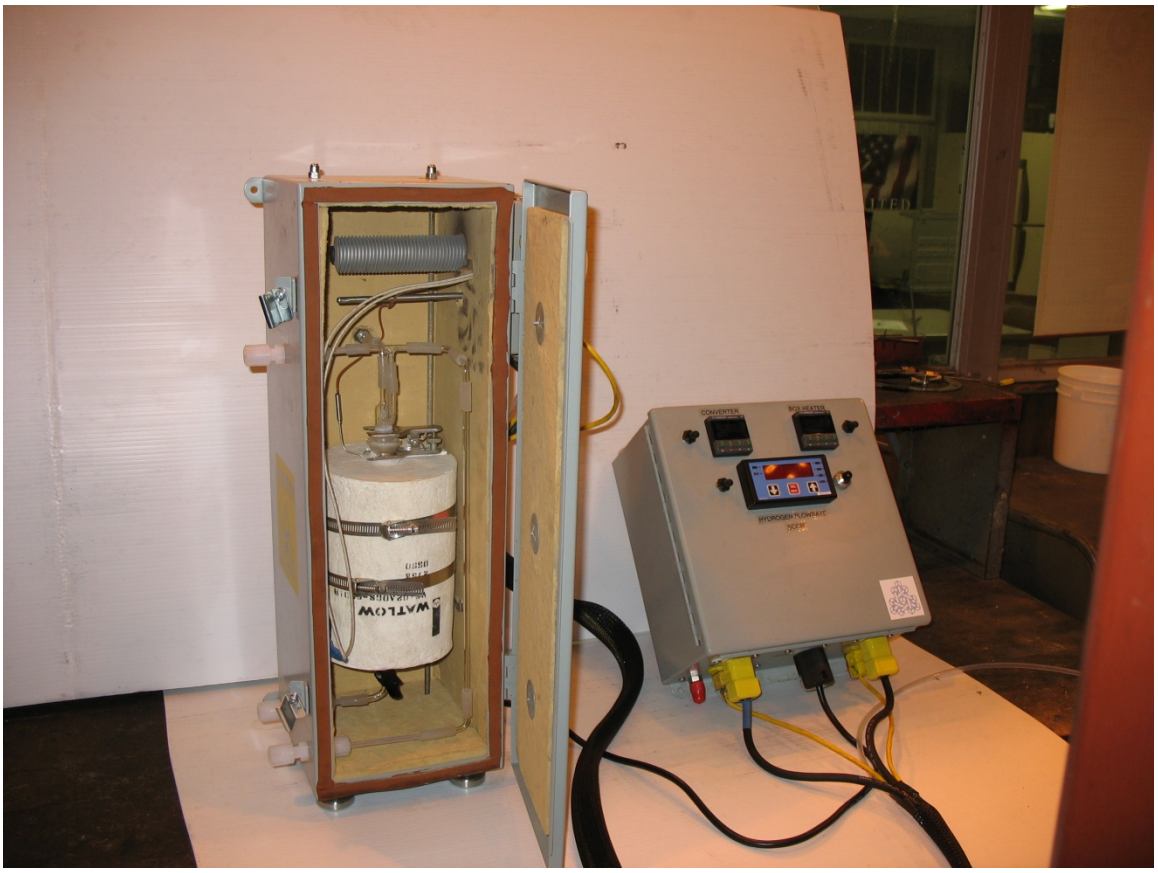

Photograph by J. Sammy O'Neal, SRI

Figure 2.2.4. System for reduction of mercury from the oxidized to the elemental state at 750 ^{o}C followed by introduction of hydrogen gas to consume oxygen and inhibit reoxidation of mercury on cooling (Van Pelt and Meischen, 1999; Meischen et al., 2004).

The TVA high-temperature system for reduction of oxidized mercury to elemental form and reaction of oxygen in the gas sample with hydrogen, to inhibit reoxidation of mercury on cooling, resulted in a marked improvement in the quality of total mercury measurements and a significant reduction in the time required to determine the distribution of mercury between elemental and oxidized states under a given set of catalyst conditions. All of the total mercury measurements presented in Section 2 of the report were obtained using the TVA mercury reduction system.

A portable O_2 analyzer with a micro fuel cell sensor (Teledyne Analytical Instruments, City of Industry, CA, Model 320P-D) was used to periodically check the O_2 concentration in the gas sample after addition of H_2, to ensure that enough hydrogen was being added to inhibit oxidation of elemental mercury. Maintaining unreacted O_2 at ≤ 0.5 vol% was sufficient. The O_2 analyzer is insensitive to flow rate and detects O_2 within $\pm$ 0.1 vol% from 0 to 100 vol%.

The total mercury measurements presented in Section 2 of the report are corrected for the change in mercury concentration resulting from the removal of O_2 from the gas sample by reaction with H_2, and removal of the product water vapor.

2.2.5. Determination of Sulfate

Total sulfate in the gas stream leaving the reactor was determined using a modified controlled condensation method, in which the sample is passed through a tube packed with glass wool at a temperature below the acid dew point. Sulfur trioxide formed by oxidation of SO_2 reacts with water vapor on cooling to form sulfuric acid, H_2SO_4. On reaching its dew point, sulfuric acid condenses, either directly on the glass fibers or as a mist. The SO_3 and H_2SO_4 may also react with ammonia to form ammonium bisulfate, NH_4HSO_4, present as a fine particulate aerosol in the cooled sample. Both acid mist and ammonium bisulfate particles are collected on the glass wool by filtration. Because the collection and analysis include both sulfuric acid and particulate bisulfate (and sulfate, if present) the results are reported as sulfate, rather than as sulfuric acid or SO_3. An advantage of the controlled condensation method is minimization of interference from SO_2, compared with methods using impingers to capture sulfuric acid and sulfates.

A flue gas sample (~ 14 L) was taken directly from the exit of the catalyst reactor into a tube loosely packed with glass wool, maintained at 79.5 ^{o}C by a heated water jacket, where sulfuric acid condenses and the acid and ammonium bisulfate and sulfate are trapped. The condenser was extracted with 10 mL of deionized water, followed by two 10 mL washes with isopropyl alcohol (IPA), pH adjusted by addition of 25 μL of 70% perchloric acid per liter of isopropyl alcohol. The water and alcohol washes were combined and diluted to 50 mL with isopropyl alcohol, then titrated with 0.01 N barium perchlorate standard solution to a thorin indicator end point, as described in EPA Method 6.

A titrant volume of only 0.3 mL resulted in a calculated sulfate concentration of 3.1 ppmv, equivalent to conversion of approximately 0.4% of the SO_2 at the reactor inlet to sulfate. Either a larger gas sample (> 14 L) should be extracted or a more dilute (< 0.01 N) standard barium perchlorate solution should be used, to better differentiate sulfate levels of only several parts per million.

2.2.6. Experimental Procedure

The procedure in a typical experiment was to first allow the reactor containing the catalyst sample to reach a steady temperature of 378 °C with only N_2 flowing, then introduce the other gas constituents, except mercury, HCl, and NH_3, at flow rates expected to give the desired composition according to the mass flow controllers, verified by measurements using the continuous monitors and FT-IR spectrometer at the outlet from the reactor. Elemental mercury vapor, in its nitrogen carrier gas, was then added to the flow through the reactor. The gas mixture containing HCl was then introduced, but with HCl maintained at a low level, and the system was run overnight at 378 ^{o}C in a conditioning mode, to allow the catalyst to reach steady state with respect to adsorbed mercury. On the following day, the concentration of HCl was increased to the proper value for the tests planned, NH_3 was introduced at the desired ratio to NO, the NO at the reactor outlet was allowed to reach its steady level, and the measurements of elemental and total mercury at the catalyst outlet were recorded until their steady-state distribution was identified.

An example of an experimental data set beginning at start up for preconditioning, to load or charge the catalyst with mercury, is shown in Figure 2.2.5. The measurements were made under the conditions given in Table 2.2.1, but in the absence of HCl, NO, NH_3, and CO. The figure shows the catalyst loading phase, a short period at steady state, an upset due to interruption of the CO_2 supply, and reestablishment of steady state after restoration of the CO_2 flow. Because no oxidizing agent is present, all of the mercury at the outlet from the SCR catalyst is in its elemental form at the steady state.

An example of total and elemental mercury measurements in the presence of HCl, NO, and NH_3 is shown in Figure 2.2.6. In this case, the raw data indicate that elemental mercury is approximately 36% of the total, so the fraction of mercury oxidized is approximately 64%, but total mercury measurements require correction for the volume fraction of O_2 removed by reaction with H_2 in the TVA thermal converter. Diversion of the flow to the controlled condensation apparatus, for determination of sulfate, upsets the flow to the mercury analyzer, as shown by the disturbance to the measurements at the far right in Figure 2.2.6, but the flow through the reactor remains the same.

After correction for O_2 removal, the fraction of mercury oxidized was calculated using the following equation, in which HgT and Hg0 are the average total (elemental + oxidized) and average elemental mercury concentrations, respectively:

$$\text{Fraction of Mercury Oxidized (\%)} = [(\text{HgT} - \text{Hg0})/\text{HgT}] \cdot 100 \qquad (2.1)$$

The standard deviation of the fraction of mercury oxidized, σ_{FrHgOx}, was calculated as follows, from the standard deviations of the HgT and Hg0 measurements, σ_{HgT} and σ_{Hg0}, respectively:

$$\sigma_{FrHgOx}\ (\%) = (\text{Hg0}/\text{HgT})[(\sigma_{HgT}/\text{HgT})^2 + (\sigma_{Hg0}/\text{Hg0})^2]^{1/2} \cdot 100 \qquad (2.2)$$

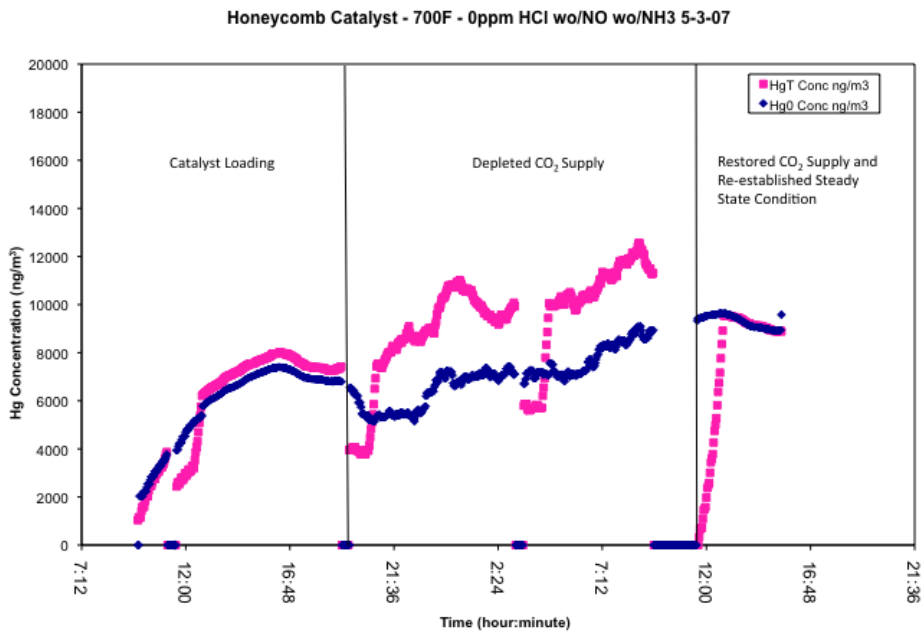

Figure 2.2.5. Mercury concentration measurements at the catalyst outlet during equilibration of mercury vapor with the catalyst, adjustment of flow rates, an upset condition, and arrival at steady state, in the absence of HCl, NO, NH_3, and CO. HgT = Total Hg, Hg0 = Elemental Hg. Because no oxidizing agent is present, all of the mercury is in its elemental form, HgT = Hg0, at steady state.

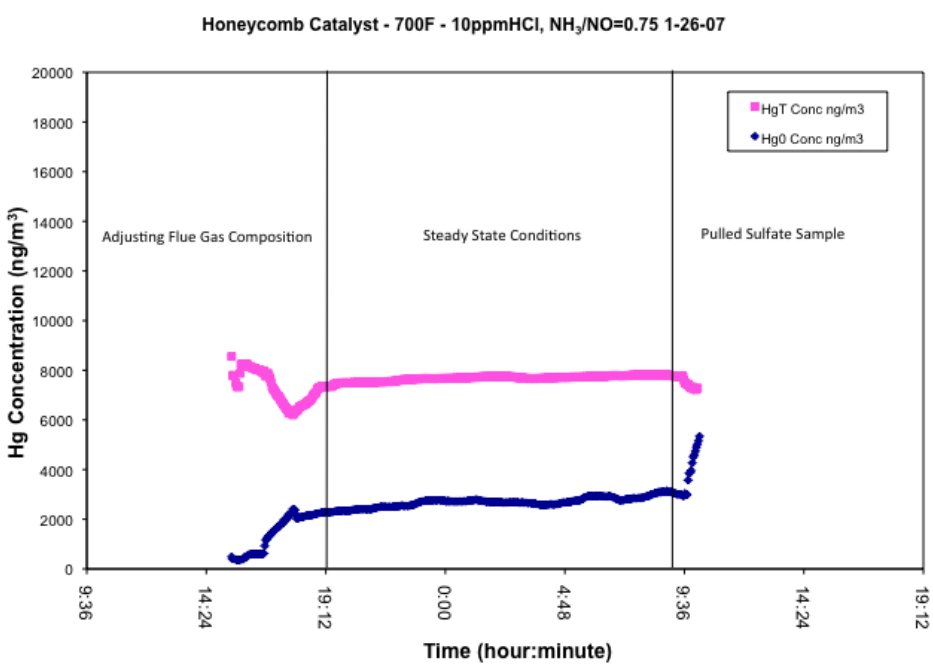

Figure 2.2.6. Example of mercury concentration measurements in the presence of HCl, NO, and NH_3. HgT = Total Hg, Hg0 = Elemental Hg. HCl = 10 ppmv, NH_3/NO at the catalyst inlet = 0.75. The raw data, at steady state, without correction for O_2 removal in the TVA thermal converter, indicate that approximately 36% of the mercury is in the elemental state, so approximately 64% is oxidized.

2.3. Experimental Results and Discussion

2.3.1. Program of Laboratory Measurements of SCR Performance

The laboratory experiments using the SCR catalyst fall into three groups: (1) measurements of the dependence of the extent of mercury oxidation in the catalyst on the HCl concentration in flue gas, in the absence of NO and NH_3, in the presence of NO, and in the presence of both NO and NH_3, (2) measurements of the dependence of both mercury and SO_2 oxidation on NH_3-to-NO ratio at two levels of HCl (1 and ~10.5 ppmv), and (3) measurements of the dependence of mercury and SO_2 oxidation on the CO content of flue gas at three levels of HCl (~2, ~11.5, and ~50 ppmv) and high NH_3-to-NO ratio (0.91 to 0.94). Two runs were also conducted using a reactor containing sea sand in place of the SCR catalyst, at low HCl levels and high NH_3-to-NO ratio, with and without CO. The entire set of experimental measurements of NO reduction, mercury oxidation, and sulfate formation is presented in Table 2.3.1.

2.3.2. Reactor Containing Sand

Two runs without SCR catalyst in the reactor were intended to demonstrate the absence of contributions from homogeneous gas-phase reactions or heterogeneous reactions on quartz glass to oxidation of mercury under the conditions of the laboratory experiments. Washed sea sand (Thermo Fisher Scientific Inc., Waltham, MA) was placed in the reactor in place of the SCR catalyst, to maintain the same gas residence time as in the catalyst sample. The gas composition data and mercury measurements are entered in the last two rows of Table 2.3.1. The first set of measurements was made in the presence of 1 ppmv HCl and NH_3/NO = 0.95, in the absence of CO, at 365 ^{o}C. The second set of measurements was made in the presence of 2.2 ppmv HCl, NH_3/NO = 0.91, and 102 ppmv CO, at 353 ^{o}C. Other conditions were as specified in Table 2.2.1.

In both cases, the observed average total mercury concentrations are actually less than the average concentrations of elemental mercury, resulting in apparent negative extents of mercury oxidation. Negative extents of mercury oxidation, which were sometimes observed, though rarely as much as -21.5%, may be attributed to adsorption of mercury on the surfaces of the mercury reduction system and its transfer lines, when those surfaces had not had sufficient time to equilibrate with mercury in the sample stream, causing the total mercury measurement to be lower than the elemental mercury measurement.

The measurements using the reactor containing sand were intended to show that there was no significant homogeneous oxidation of mercury during the gas residence time in the SCR catalyst and no significant heterogeneous oxidation of mercury on surfaces other than those of the SCR catalyst. However, as will be seen later, there was little oxidation of mercury even in the presence of the SCR catalyst, under the conditions during the tests with the reactor containing sand, because the HCl volume fraction was low and the NH_3/NO ratio relatively high, and because CO, present in one of the tests, was observed to suppress mercury oxidation. The conditions chosen for evaluation of

Table 2.3.1.[a]

Measurements of NO Reduction, Mercury Oxidation, and Sulfate Formation in the SCR Catalyst, as Functions of HCl, NO, NH_3-to-NO Ratio, and CO in the Simulated Flue Gas.

HCl inlet	NO inlet	NO inlet std. dev.	NH_3 inlet	NH_3/NO inlet	NO outlet	NO outlet std. dev.	NO Reduction	NO Reduction std. dev.	CO inlet	Elemental Hg measured[b]	Elemental Hg measured[b] std. dev.	Total Hg measured[b]	Total Hg measured[b] std. dev.	O_2 inlet	O_2 after reaction with H_2	Total Hg corrected[b,c]	Total Hg corrected[b,c] std. dev.	Fraction Hg Oxidized	Fraction Hg Oxidized std. dev.	SO_2 inlet	SO_2 inlet std. dev.	SO_4^{2-} outlet[e]	SO_4^{2-} outlet[e] std. dev.	SO_4^{2-}/SO_2	SO_4^{2-}/SO_2 std. dev.
ppmv	ppmv	ppmv	ppmv	mol/mol	ppmv	ppmv	%	%	ppmv	ng/m^3	ng/m^3	ng/m^3	ng/m^3	vol%	vol%	ng/m^3	ng/m^3	%	%	ppmv	ppmv	ppmv	ppmv	%	%
0 to 100 ppmv HCl, without NO, without NH_3, without CO																									
0	0	-	0	-	0	-	-	-	0	9210	334	9201	326	5.16[d]	0.21[d]	8746	310	-5.3	5.3	940	-	-	-	-	-
1	0	-	0	-	0	-	-	-	0	9054	87	9832	71	5.16[d]	0.21[d]	9345	67	3.1	1.2	856	-	-	-	-	-
2	0	-	0	-	0	-	-	-	0	8627	122	10001	141	5.16[d]	0.21[d]	9506	134	9.2	1.8	851	-	-	-	-	-
5	0	-	0	-	0	-	-	-	0	2635	109	7723	119	5.16[d]	0.21[d]	7341	113	64.1	1.6	817	-	-	-	-	-
10	0	-	0	-	0	-	-	-	0	1748	164	7958	126	5.16[d]	0.21[d]	7564	120	76.9	2.2	878	-	-	-	-	-
25	0	-	0	-	0	-	-	-	0	1045	164	7910	128	5.16[d]	0.21[d]	7518	122	86.1	2.2	867	-	-	-	-	-
50	0	-	0	-	0	-	-	-	0	778	189	8186	260	5.16[d]	0.21[d]	7781	247	90.0	2.4	860	-	-	-	-	-
100	0	-	0	-	0	-	-	-	0	734	200	8037	233	5.16[d]	0.21[d]	7639	221	90.4	2.6	861	-	-	-	-	-
0 to 100 ppmv HCl, 300 ppmv NO, without NH_3, without CO																									
0	300	-	0	0	312	-	-4	-	0	6429	204	7965	215	5.16[d]	0.21[d]	7571	204	15.1	3.5	930	-	-	-	-	-
1	300	-	0	0	314	-	-5	-	0	6700	169	8926	93	5.16[d]	0.21[d]	8484	88	21.0	2.2	869	-	-	-	-	-
2	300	-	0	0	314	-	-5	-	0	6220	108	9321	159	5.16[d]	0.21[d]	8860	151	29.8	1.7	853	-	-	-	-	-
5	300	-	0	0	310	-	-3	-	0	1317	174	9726	162	5.16[d]	0.21[d]	9245	154	85.8	1.9	913	-	-	-	-	-
10	300	-	0	0	311	-	-4	-	0	1056	169	9592	167	5.16[d]	0.21[d]	9117	159	88.4	1.9	906	-	-	-	-	-
25	300	-	0	0	310	-	-3	-	0	858	152	9587	156	5.16[d]	0.21[d]	9112	148	90.6	1.7	901	-	-	-	-	-
50	300	-	0	0	309	-	-3	-	0	884	165	9671	178	5.16[d]	0.21[d]	9192	169	90.4	1.8	883	-	-	-	-	-
100	300	-	0	0	306	-	-2	-	0	363	136	9489	170	5.16[d]	0.21[d]	9019	162	96.0	1.5	871	-	-	-	-	-
0 to 100 ppmv HCl, 350 and 369 ppmv NO, unspecified NH_3/NO, without CO																									
0	350	9	f	f	41	-	88	-	0	9788	321	8765	338	5.16[d]	0.21[d]	8331	321	-17.5	5.9	-	-	-	-	-	-
1	350	9	f	f	20	-	94	-	0	10881	232	10560	539	5.02	0.2	10051	513	-8.3	6.0	782	-	-	-	-	-
1	350	9	f	f	20	-	94	-	0	10439	196	10450	122	5.02	0.2	9946	116	-5.0	2.3	782	-	-	-	-	-
2	350	9	f	f	-	-	-	-	0	8303	197	10339	235	5.99	0.5	9771	222	15.0	2.8	782[h]	-	10.7	1.1	1.37	0.14[i]
3	350	9	f	f	-	-	-	-	0	9756	295	11620	326	5.01	0.26	11068	311	11.9	3.6	782[h]	-	9.9	0	1.3	-
4	350	9	f	f	-	-	-	-	0	6977	153	10949	187	5.16[d]	0.21[d]	10407	178	33.0	1.9	-	-	-	-	-	-
5	350	9	f	f	8.9	0.1	97.5	0.1	0	5158	212	9243	157	5.48	0.39	8773	149	41.2	2.6	827	-	-	-	-	-
8	350	9	f	f	10.6	0.2	97.0	0.1	0	4464	212	9693	189	5.28	0.088	9190	179	51.4	2.5	822	-	-	-	-	-
10	350	9	f	f	13.4	0.2	96.2	0.1	0	3984	288	10106	218	5.09	0.097	9601	207	58.5	3.1	815	-	-	-	-	-
10	350	9	f	f	13.4	0.2	96.2	0.1	0	4333	252	10706	524	5.33	0.2	10157	497	57.3	3.2	815	-	-	-	-	-
15	350	9	f	f	16.0	0.2	95.4	0.1	0	3149	153	9561	173	5.4	0.088	9053	164	65.2	1.8	820	-	-	-	-	-
20	350	9	f	f	20.6	0.2	94.1	0.2	0	3030	461	10004	272	5.23	0.14	9495	258	68.1	4.9	813	-	-	-	-	-
24	350	9	f	f	24.3	0.2	93.1	0.2	0	2181	191	9027	184	6.8	0.13	8425	172	74.1	2.3	799	-	-	-	-	-
50	350	9	f	f	35.7	0.4	89.8	0.3	0	1790	435	9320	144	4.93	0.08	8868	137	79.8	4.9	811	-	-	-	-	-
75	350	9	f	f	78.5	0.6	77.6	0.6	0	1641	191	8813	510	4.56	0.17	8426	488	80.5	2.5	805	-	-	-	-	-
75	350	9	f	f	78.5	-	78	-	0	1358	199	8561	181	4.56	0.17	8185	173	83.4	2.5	805	-	-	-	-	-
100	369	1	f	f	13.4	0.4	96.4	0.1	0	1182	248	7546	1114	5.16[d]	0.21[d]	7172	1059	83.5	4.2	-	-	-	-	-	-

Please see the notes at the end of the table.

Table 2.3.1 (continued).[a]
Measurements of NO Reduction, Mercury Oxidation, and Sulfate Formation in the SCR Catalyst, as Functions of HCl, NO, NH_3-to-NO Ratio, and CO in the Simulated Flue Gas.

HCl inlet	NO inlet	NO inlet std. dev.	NH_3 inlet	NH_3/NO inlet	NO outlet	NO outlet std. dev.	NO Reduction	NO Reduction std. dev.	CO inlet	Elemental Hg measured[b]	Elemental Hg measured[b] std. dev.	Total Hg measured[b]	Total Hg measured[b] std. dev.	O_2 inlet	O_2 after reaction with H_2	Total Hg corrected[b,c]	Total Hg corrected[b,c] std. dev.	Fraction Hg Oxidized	Fraction Hg Oxidized std. dev.	SO_2 inlet	SO_2 inlet std. dev.	SO_4^{2-} outlet[e]	SO_4^{2-} outlet[e] std. dev.	SO_4^{2-}/SO_2	SO_4^{2-}/SO_2 std. dev.
ppmv	ppmv	ppmv	ppmv	mol/mol	ppmv	ppmv	%	%	ppmv	ng/m^3	ng/m^3	ng/m^3	ng/m^3	vol%	vol%	ng/m^3	ng/m^3	%	%	ppmv	ppmv	ppmv	ppmv	%	%
1 ppmv HCl, 300 ppmv NO, 0 to 0.95 NH_3/NO, without CO																									
1	300	-	0	0	300	-	0	-	0	6853	363	11134	389	5.16[d]	0.21[d]	10583	370	35.2	4.1	877	-	10.8	0	1.23	-
1	300	-	60	0.20	254	-	15	-	0	7561	314	11517	455	4.48	0.09	11011	435	31.3	3.9	885	-	8.8	0	0.99	-
1	300	-	120	0.40	196	-	35	-	0	7503	184	10574	209	4.64	0.15	10099	200	25.7	2.3	882	-	8.1	0.4	0.92	0.05[i]
1	300	-	180	0.60	148	-	51	-	0	6455	189	8930	192	5.06	0.16	8492	183	24.0	2.8	871	-	8.0	0.4	0.92	0.05[i]
1	300	-	240	0.80	89	-	70	-	0	7261	120	9192	214	4.70	0.23	8781	204	17.3	2.4	876	-	7.2	0.7	0.82	0.08[i]
1	300	-	285	0.95	49	-	84	-	0	8141	179	9813	157	5.05	0.59	9375	150	13.2	2.4	873	-	6.7	0.7	0.77	0.08[i]
10 ppmv HCl, 300 and 345 ppmv NO, 0 to 1.15 NH_3/NO, without CO																									
10	300	-	0	0	300	-	0	-	0	832	159	8320	144	5.16[d]	0.21[d]	7908	137	89.5	2.0	838[g]	37[g]	7.3	0	0.87	0.04
10	345	-	0	0	345	-	0	-	0	1455	177	8603	392	5.16[d]	0.21[d]	8177	373	82.2	2.3	838[g]	37[g]	8.2	0	0.98	0.04
10	300	-	63	0.21	237	-	21	-	0	813	212	8352	148	5.16[d]	0.21[d]	7939	141	89.8	2.7	838[g]	37[g]	8.2	0	0.98	0.04
10	300	-	92	0.31	208	-	31	-	0	818	153	8473	162	5.16[d]	0.21[d]	8054	154	89.8	1.9	838[g]	37[g]	6.8	0	0.81	0.04
10	300	-	105	0.35	207	-	31	-	0	1143	138	8529	192	5.16[d]	0.21[d]	8107	182	85.9	1.7	838[g]	37[g]	6.0	0.6	0.72	0.08
10	300	-	161	0.54	161	-	46	-	0	832	144	8023	182	5.16[d]	0.21[d]	7626	173	89.1	1.9	838[g]	37[g]	6.2	0.4	0.74	0.06
10	300	-	195	0.65	105	-	65	-	0	882	207	7960	203	5.16[d]	0.21[d]	7566	193	88.3	2.8	838[g]	37[g]	5.7	0.3	0.68	0.05
10	300	-	200	0.67	91	-	70	-	0	1206	135	8299	176	5.16[d]	0.21[d]	7888	167	84.7	1.7	838[g]	37[g]	5.0	0	0.60	0.03
10	300	-	225	0.75	75	-	75	-	0	1320	134	8007	143	5.16[d]	0.21[d]	7611	136	82.7	1.8	838[g]	37[g]	4.5	0	0.54	0.02
10	300	-	285	0.95	56	-	81	-	0	1951	147	8435	211	5.16[d]	0.21[d]	8017	201	75.7	1.9	838[g]	37[g]	2.7	0	0.32	0.01
10	300	-	315	1.05	1.5	-	100	-	0	1989	119	8311	157	5.16[d]	0.21[d]	7900	149	74.8	1.6	838[g]	37[g]	3.4	0	0.41	0.02
10	300	-	345	1.15	2	-	99	-	0	2379	182	7734	401	5.16[d]	0.21[d]	7351	381	67.6	3.0	838[g]	37[g]	4.5	0	0.54	0.02
2 ppmv HCl, 329 ppmv NO, 0.93 NH_3/NO, 0 to 101 ppmv CO																									
1.9	329	3	306	0.93	-	-	-	-	0	7457	178	10332	289	5.16[d]	0.21[d]	9821	275	24.1	2.8	823	10	-	-	-	-
1.9	329	3	306	0.93	22.2	1.1	93.3	0.3	5	6829	123	8942	199	5.16[d]	0.21[d]	8499	189	19.7	2.3	813	7	5.7	0.4	0.70	0.05
1.9	329	3	305	0.93	22.6	0.8	93.1	0.3	7.5	7076	111	8660	96	5.16[d]	0.21[d]	8231	91	14.0	1.7	807	7	5.9	0	0.73	0.01
1.9	329	3	305	0.93	23.0	0.8	93.0	0.3	10.5	6907	109	8332	60	5.16[d]	0.21[d]	7920	57	12.8	1.5	799	7	5.9	0	0.74	0.01
2.2	329	3	302	0.92	26.4	1.0	92.0	0.3	25	6655	118	7689	153	5.16[d]	0.21[d]	7308	145	8.9	2.4	807	14	6.2	0.4	0.77	0.05
2.1	329	3	309	0.94	19.1	0.6	94.2	0.2	52	7811	198	8294	249	5.16[d]	0.21[d]	7883	237	0.9	3.9	805	6	-	-	-	-
2.2	329	3	307	0.93	21.2	0.7	93.6	0.2	101	7976	187	8066	146	5.16[d]	0.21[d]	7667	139	-4.0	3.1	800	7	7.0	0.8	0.9	0.1

Please see the notes at the end of the table.

Table 2.3.1 (continued).[a]
Measurements of NO Reduction, Mercury Oxidation, and Sulfate Formation in the SCR Catalyst, as Functions of HCl, NO, NH_3-to-NO Ratio, and CO in the Simulated Flue Gas.

HCl inlet	NO inlet	NO inlet std. dev.	NH_3 inlet	NH_3/NO inlet	NO outlet	NO outlet std. dev.	NO Reduction	NO Reduction std. dev.	CO inlet	Elemental Hg measured[b]	Elemental Hg measured[b] std. dev.	Total Hg measured[b]	Total Hg measured[b] std. dev.	O_2 inlet	O_2 after reaction with H_2	Total Hg corrected[b,c]	Total Hg corrected[b,c] std. dev.	Fraction Hg Oxidized	Fraction Hg Oxidized std. dev.	SO_2 inlet	SO_2 inlet std. dev.	SO_4^{2-} outlet[e]	SO_4^{2-} outlet[e] std. dev.	SO_4^{2-}/SO_2	SO_4^{2-}/SO_2 std. dev.
ppmv	ppmv	ppmv	ppmv	mol/mol	ppmv	ppmv	%	%	ppmv	ng/m^3	ng/m^3	ng/m^3	ng/m^3	vol%	vol%	ng/m^3	ng/m^3	%	%	ppmv	ppmv	ppmv	ppmv	%	%
11 to 12 ppmv HCl, 313 ppmv NO, 0.91 NH_3/NO, 0 to 2001 ppmv CO																									
11	313	2	285	0.91	18.0	0.4	94.2	0.1	0	2529	149	8112	111	5.16[d]	0.21[d]	7710	106	67.2	2.0	810	4	-	-	-	-
11	313	2	285	0.91	18.0	0.4	94.2	0.1	0	2392	138	7986	89	5.16[d]	0.21[d]	7591	85	68.5	1.9	810	4	-	-	-	-
11	313	2	285	0.91	18.0	0.4	94.2	0.1	0	2447	147	8127	108	5.16[d]	0.21[d]	7725	103	68.3	1.9	810	4	-	-	-	-
11	313	2	285	0.91	18.0	0.4	94.2	0.1	0	2459	167	8384	106	5.16[d]	0.21[d]	7969	101	69.1	2.1	810	4	-	-	-	-
11	313	2	285	0.91	18.0	0.4	94.2	0.1	0	2522	181	10442	152	5.16[d]	0.21[d]	9925	144	74.6	1.9	810	4	-	-	-	-
11.5	313	2	285	0.91	18.1	0.4	94.2	0.1	4	3173	425	8703	308	5.0	0.51	8312	294	61.8	5.3	787	4	-	-	-	-
11.5	313	2	285	0.91	18.1	0.4	94.2	0.1	4	3209	219	8664	102	5.0	0.51	8275	97	61.2	2.7	787	4	-	-	-	-
11	313	2	285	0.91	18.8	0.3	94.0	0.1	19	3627	115	8460	84	5.27	0.15	8027	80	54.8	1.5	805	3	-	-	-	-
11	313	2	285	0.91	18.8	0.3	94.0	0.1	19	3083	188	8349	93	5.27	0.15	7922	88	61.1	2.4	805	3	5.2	0.4	0.65	0.05
12.1	313	2	285	0.91	18.2	0.2	94.2	0.1	50	3766	108	8938	90	5.41	0.01	8455	85	55.5	1.4	838	2	-	-	-	-
12.1	313	2	285	0.91	18.2	0.2	94.2	0.1	50	3571	185	8071	122	5.41	0.01	7635	115	53.2	2.5	838	2	6.4	0.4	0.76	0.05
11.5	313	2	285	0.91	17.8	0.2	94.3	0.1	118	4038	183	8422	122	5.4	0.2	7984	116	49.4	2.4	811	2	-	-	-	-
11.4	313	2	285	0.91	16.3	0.9	94.8	0.3	263	4723	163	8223	166	5.2	0.2	7812	158	39.5	2.4	825	7	-	-	-	-
11.4	313	2	285	0.91	16.3	0.9	94.8	0.3	263	4844	148	8722	113	5.2	0.2	8286	107	41.5	1.9	825	7	-	-	-	-
11.7	313	2	285	0.91	16.9	1.0	94.6	0.3	511	5546	152	8815	123	5.2	0.2	8374	117	33.8	2.0	819	8	-	-	-	-
11.6	313	2	285	0.91	17.3	1.1	94.5	0.4	1013	6579	141	8847	72	5.16[d]	0.21[d]	8409	68	21.8	1.8	824	9	-	-	-	-
11.6	313	2	285	0.91	17.3	1.1	94.5	0.4	1013	6641	200	8869	59	5.16[d]	0.21[d]	8430	56	21.2	2.4	824	9	10.8	0	1.31	0.01
11.6	313	2	285	0.91	18.4	2.0	94.1	0.6	2001	8106	159	9356	106	5.16[d]	0.21[d]	8893	101	8.8	2.1	820	11	-	-	-	-
11.6	313	2	285	0.91	18.4	2.0	94.1	0.6	2001	7918	163	9261	79	5.16[d]	0.21[d]	8803	75	10.0	2.0	820	11	9.7	1.5	1.2	0.2
50 ppmv HCl, 313 ppmv NO, 0.91 NH_3/NO, 5 to 2053 ppmv CO																									
49	313	2	285	0.91	21.5	0.9	93.1	0.3	5	1425	305	8333	150	5.16[d]	0.21[d]	7921	143	82.0	3.9	830	9	6.4	0	0.77	0.01
49	313	2	285	0.91	21.8	1.1	93.0	0.4	114	1553	286	8389	211	5.16[d]	0.21[d]	7974	201	80.5	3.6	832	10	-	-	-	-
50	313	2	285	0.91	21.2	1.0	93.2	0.3	254	1571	147	8296	191	5.16[d]	0.21[d]	7885	182	80.1	1.9	825	6	7.0	0	0.85	0.01
49	313	2	285	0.91	21.1	0.8	93.3	0.3	511	1771	150	8503	125	5.16[d]	0.21[d]	8082	119	78.1	1.9	820	10	7.8	0.4	0.95	0.05
50	313	2	285	0.91	21.6	0.7	93.1	0.2	1043	2134	146	8441	330	5.16[d]	0.21[d]	8023	314	73.4	2.1	831	8	7.8	0.4	0.94	0.05
49	313	2	285	0.91	21.1	0.6	93.3	0.2	2053	2389	219	8603	307	5.16[d]	0.21[d]	8177	292	70.8	2.9	828	9	8.0	0	0.97	0.01
Reactor containing washed sea sand																									
2.2	329	3	300	0.91	292	5	11	2	102	7459	145	6458	155	5.16[d]	0.21[d]	6138	147	-21.5	3.8	806	24	5.9	0	0.73	0.02
1	300	-	285	0.95	-	-	-	-	0	8894	206	8536	76	5.16[d]	0.21[d]	8113	72	-9.6	2.7	-	-	-	-	-	-

Please see the notes for the table on the following page.

Notes for Table 2.3.1.

a. Some reevaluation of data and correction of typographical errors have been done since the publication of this work by Tong (2009). Where there are differences between the present report and the earlier publication, values should be taken from the present report.
b. Mercury concentrations at 20 ^{o}C, 1 atm pressure, and dry (5 ^{o}C dew point).
c. Total mercury measurements corrected for removal of oxygen by reaction with hydrogen in the TVA thermal converter.
d. Oxygen was not measured during these runs. The values assigned are the averages of the oxygen mole fractions in the simulated flue gas and after reaction with H_2 in the thermal mercury converter during the runs when they were measured.
e. The average and standard deviation are based on titration of two separate controlled condensation samples.
f. Data from the mass flow controller, from which to calculate NH_3 at the inlet, are not available for these runs. At the start of the series, the flow rate of the gas mixture containing NH_3 was adjusted, in the presence of 1 ppmv HCl, to give 20 ppmv NO at the catalyst outlet, therefore NH_3 at the inlet must have been at least 330 ppmv and the NH_3/NO ratio at least 0.94. The NH_3/NO ratio was expected to remain fixed during all of the runs from 0 to 75 ppmv HCl, but it must have reached at least 0.975 to give the observed NO removal in the presence of 5 ppmv HCl. The flow system was restarted for the last run, at 100 ppmv HCl, and the conditions during that run are even less well defined, but the NH_3/NO ratio must have been at least 0.964.
g. Runs conducted prior to implementation of FT-IR to monitor SO_2. An average inlet SO_2 concentration of 838 ppmv and standard deviation of 37 ppmv were estimated from subsequent FT-IR measurements under similar conditions.
h. Assumed to be the same as in the previous two runs, under similar conditions.
i. Standard deviation based only on the contribution from the standard deviation of the SO_4^{2-} measurements.

possible contributions to mercury oxidation from homogeneous reactions or from relatively inert quartz glass and sand surfaces were therefore unable to provide any evidence for the presence or absence of such effects.

2.3.3. Dependence of Mercury Oxidation on HCl

Because the expected form of oxidized mercury in flue gas at low temperatures is $HgCl_2$ (Senior et al., 2000a, 2000b; Dajnak et al., 2003; Presto and Granite, 2006), one of the most important influences on mercury oxidation is the concentration of HCl (Yudovich and Ketris, 2005). Hall et al. (1991) and Ghorishi (1998) both showed shifts in mercury speciation towards its oxidized form when HCl and NO_X were present in flue gas. Srivastava et al. (2003) found Hg(0) to be the predominant mercury species at the exit of the SCR catalyst during tests with Powder River Basin coal, when there was no HCl in the flue gas.

The extent of mercury oxidation over the SCR catalyst was examined in the presence of 0 to 100 ppmv of HCl, covering the range from low-chlorine Powder River Basin subbituminous coals to moderate-chlorine bituminous coals. Measurements in the absence of NO and NH_3, in the presence of NO and absence of NH_3, and in the presence of both NO and NH_3 (NH_3/NO ~ 0.8 to 1 mol/mol) are compared in Figure 2.3.1. As shown in the figure, the extent of mercury oxidation is highly sensitive to the concentration of HCl at low levels of HCl (Eswaran and Stenger, 2005), and is suppressed in the presence of NH_3 (Machalek et al., 2003; Niksa and Fujiwara, 2005b; Senior, 2006; Gale et al., 2006b), because ammonia competes with at least one of the reactants (Hg, HCl) for surface sites toward the entrance to the monolith, before the NH_3 is consumed by reaction with NO and where it is still present at significant concentration (Niksa and Fujiwara, 2005b). Of the three conditions shown in Figure 2.3.1, the extent of mercury oxidation is most variable in the presence of both NO and NH_3 at NH_3/NO ratios near stoichiometric (Figure 2.3.1c, NH_3/NO ~ 0.8 to 1), when small changes in conditions, such as the inlet levels of NO and NH_3, can cause large changes in the concentration of unreacted NH_3 toward the catalyst exit.

The steep rise in mercury oxidation at low HCl volume fractions is in contrast to the behavior predicted by Niksa and Fujiwara (2005b) in the presence of both NO and NH_3. In a square honeycomb catalyst at 364 ^{o}C, at an NH_3/NO ratio of 0.9 and space velocity of 3930 h^{-1}, those authors' calculations showed that the fraction of mercury oxidized at the exit from the catalyst increased approximately linearly from 0 at low HCl volume fractions, to only 14% of mercury oxidized in the presence of 25 ppmv HCl.

Figure 2.3.1 also shows that the extent of mercury oxidation was higher in the presence of 300 ppmv NO, without NH_3, than in the absence of both NO and NH_3, for all volume fractions of HCl, consistent with the findings by Hall et al. (1991) and Ghorishi (1998). It appears that NO is able to serve as an oxidizing agent for mercury or, possibly that, when NH_3 is absent, NO removes residual strongly-bound NH_3 left on the catalyst from previous tests, freeing active sites on the catalyst for mercury oxidation (G. A. Blankenship, personal communication, 2007).

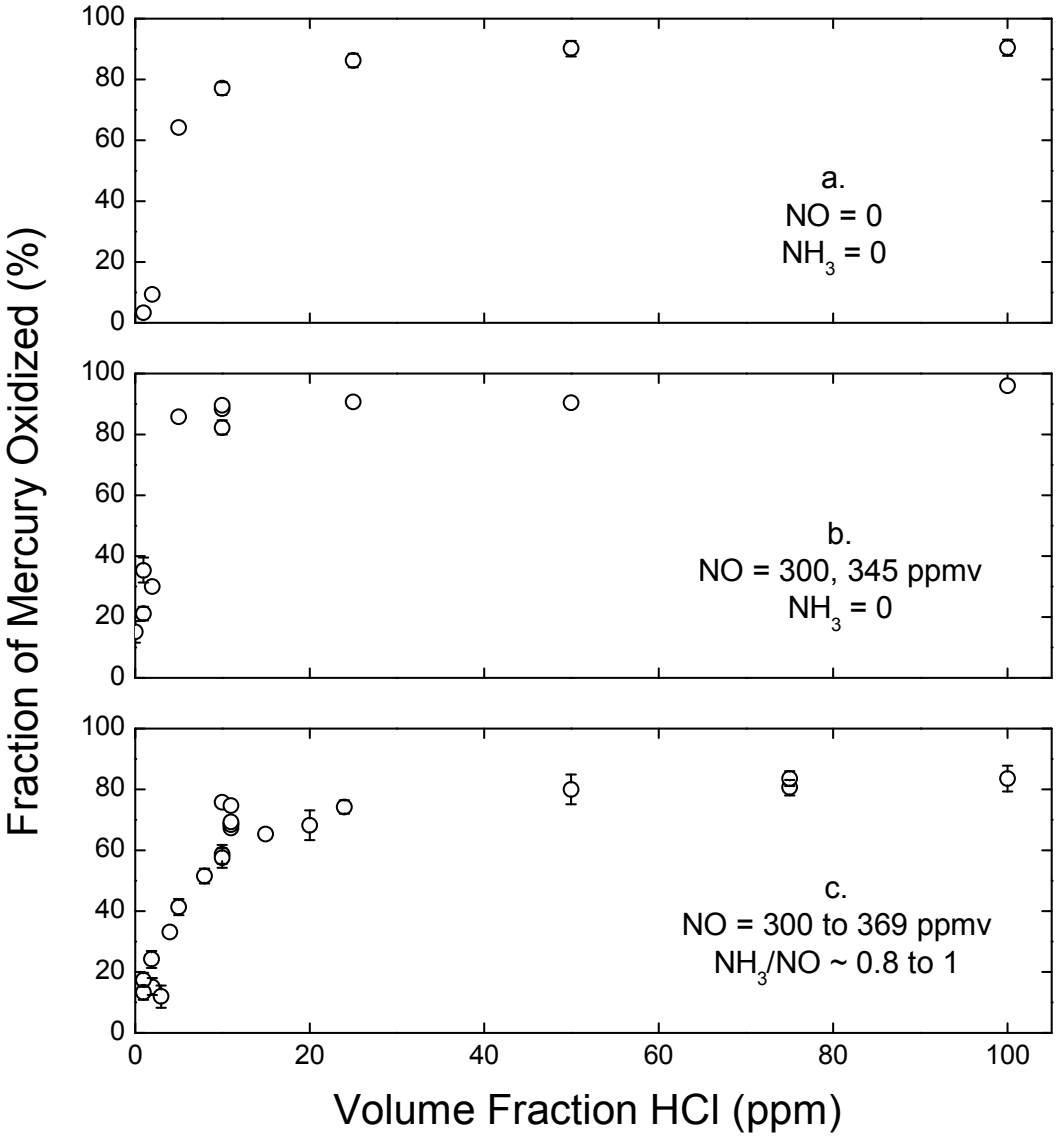

Figure 2.3.1. Dependence of mercury oxidation in the square channel monolithic catalyst on the volume fraction of HCl, in the presence and absence of NO and NH_3, and absence of CO. Conditions as specified in Table 2.2.1 and:

a. Without NO and NH_3.
b. With 300 or 345 ppmv NO, but without NH_3.
c. With 300 to 369 ppmv NO and NH_3/NO ratio at the catalyst inlet from ~0.8 to ~1.

2.3.4. Interaction between Mercury Oxidation and NO Reduction

Measurements of the fraction of mercury oxidized, as a function of the ratio of NH_3 to NO at the catalyst inlet, at two levels of HCl (1 and 10-11 ppmv), in the presence of 300 to 345 ppmv NO at the catalyst inlet and absence of CO, are shown in Figure 2.3.2. As seen by comparison of the measurements at the two HCl levels, mercury oxidation has a strong dependence on HCl over the entire range of NH_3/NO ratio, at these low HCl concentrations. In the presence of the higher concentration of HCl, the effect of increasing the NH_3/NO ratio is small, until the ratio approaches and exceeds stoichiometric, when excess ammonia is present throughout the length of the catalyst and competes for surface sites with mercury, HCl, or both, over the entire length of the

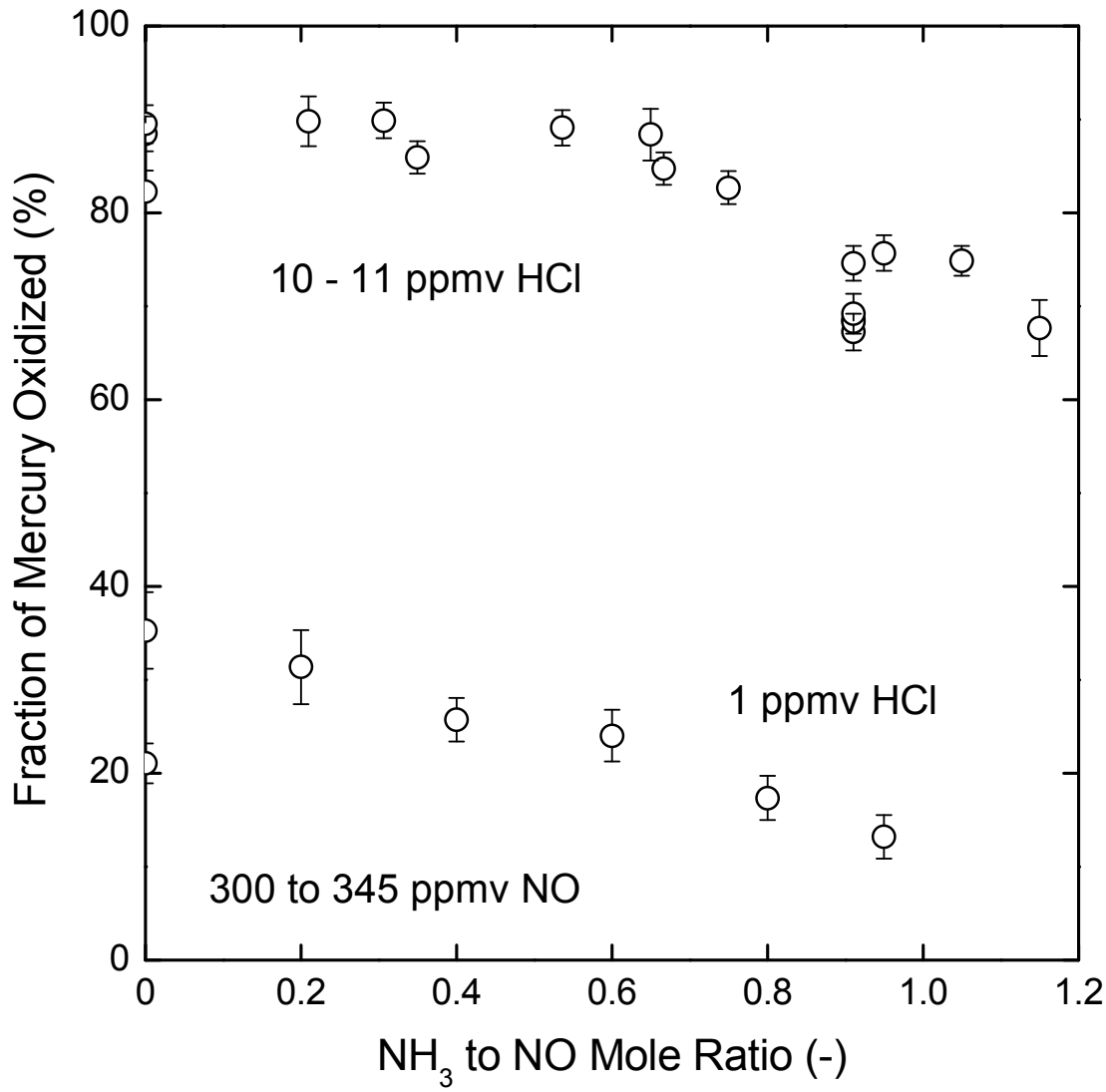

Figure 2.3.2. Dependence of mercury oxidation in the square channel monolithic catalyst on NH_3/NO ratio at the catalyst inlet, in the presence of 1 ppmv HCl and 10 to 11 ppmv HCl, with 300 to 345 ppmv NO at the catalyst inlet, in the absence of CO, and with other conditions as specified in Table 2.2.1.

catalyst channels (Niksa and Fujiwara, 2005b). Ammonia may also reduce $HgCl_2$ to Hg(0) by the following homogeneous reaction (Pritchard, 2008):

$$HgCl_2 + NH_3 + \tfrac{1}{4}O_2 \rightarrow Hg(0) + 2HCl + \tfrac{1}{2}N_2 + \tfrac{1}{2}H_2O \qquad \text{(Reaction 2.6)}$$

In the presence of the lower concentration of HCl, the decrease in extent of mercury oxidation with increasing NH_3/NO ratio is more significant, consistent with the predictions of Niksa and Fujiwara (2005b) and Senior (2006). NH_3/NO ratios larger than 0.95 were not examined under the lower HCl condition, but the fraction of mercury oxidized at NH_3/NO = 0.95 was less than 20%. Experimental work by Gale et al. (2006b) also showed that the addition of ammonia hindered mercury oxidation at low HCl levels (~2 ppmv), yet had little impact on mercury oxidation at higher HCl concentrations, consistent with the data shown in Figures 2.3.1 and 2.3.2.

2.3.5. Inhibition of Mercury Oxidation by Carbon Monoxide

The possibility that CO in flue gas might interact with Cl adsorbed on SCR catalysts, and the need for examination of the effect of CO on mercury oxidation, were discussed by Presto et al. (2006) and Presto and Granite (2006). Dependence of the extent of mercury oxidation on CO mole fraction, in the presence of 1.9-2.2, 11-12, and 49-50 ppmv HCl, 313 and 329 ppmv NO, and NH_3/NO = 0.91 to 0.94, was measured over the range from 0 to ~2000 ppmv CO, with the results shown in Figure 2.3.3. As seen in the figure, CO has little effect on mercury oxidation in the presence of 50 ppmv HCl. At that HCl level, an increase in CO from 5 to 250 ppmv resulted in no significant decrease in the extent of mercury oxidation, and an increase in CO from 5 to 2053 ppmv was required to reduce the extent of mercury oxidation from 82 ± 4% to 71 ± 3%. However, the presence of CO clearly inhibits mercury oxidation at the lower levels of HCl, under the conditions investigated.

The data in Figure 2.3.3 are shown on an expanded CO scale in Figure 2.3.4, to better illustrate the dependence of mercury oxidation on CO over the practical range of CO in flue gas. In the presence of 2 ppmv HCl, a level expected in combustion products from some Power River Basin subbituminous coals, an increase in CO from 0 to 50 ppmv reduced the extent of mercury oxidation from 24 ± 3 to 1 ± 4%. A level of 100 ppmv of CO was sufficient to completely suppress mercury oxidation when only 2 ppmv of HCl were present. In the presence of 11-12 ppmv HCl, increasing CO from 0 to ~120 ppmv reduced mercury oxidation from ~70% to 50%. Variation in the CO content of flue gas when burning low-chlorine coals, such as those from the Power River Basin, is thus another possible source of variability and uncertainty in the extent of mercury oxidation in SCR, in addition to the high sensitivity of mercury oxidation to HCl itself, at low HCl.

It is interesting to compare these observations on the effect of CO in SCR with the predictions by Niksa et al. (2002), though under completely different circumstances, not in SCR, that increasing CO may promote mercury oxidation in flue gas by increasing the Cl atom concentration in the gas phase. Niksa and coworkers predicted an increase from 28 to 54% in the extent of mercury oxidation on increasing CO from 1 to 100 ppmv in the

combustion products, including unburned carbon and fly ash, from laboratory-scale coal flames, based upon their homogenous and heterogeneous reaction mechanism.

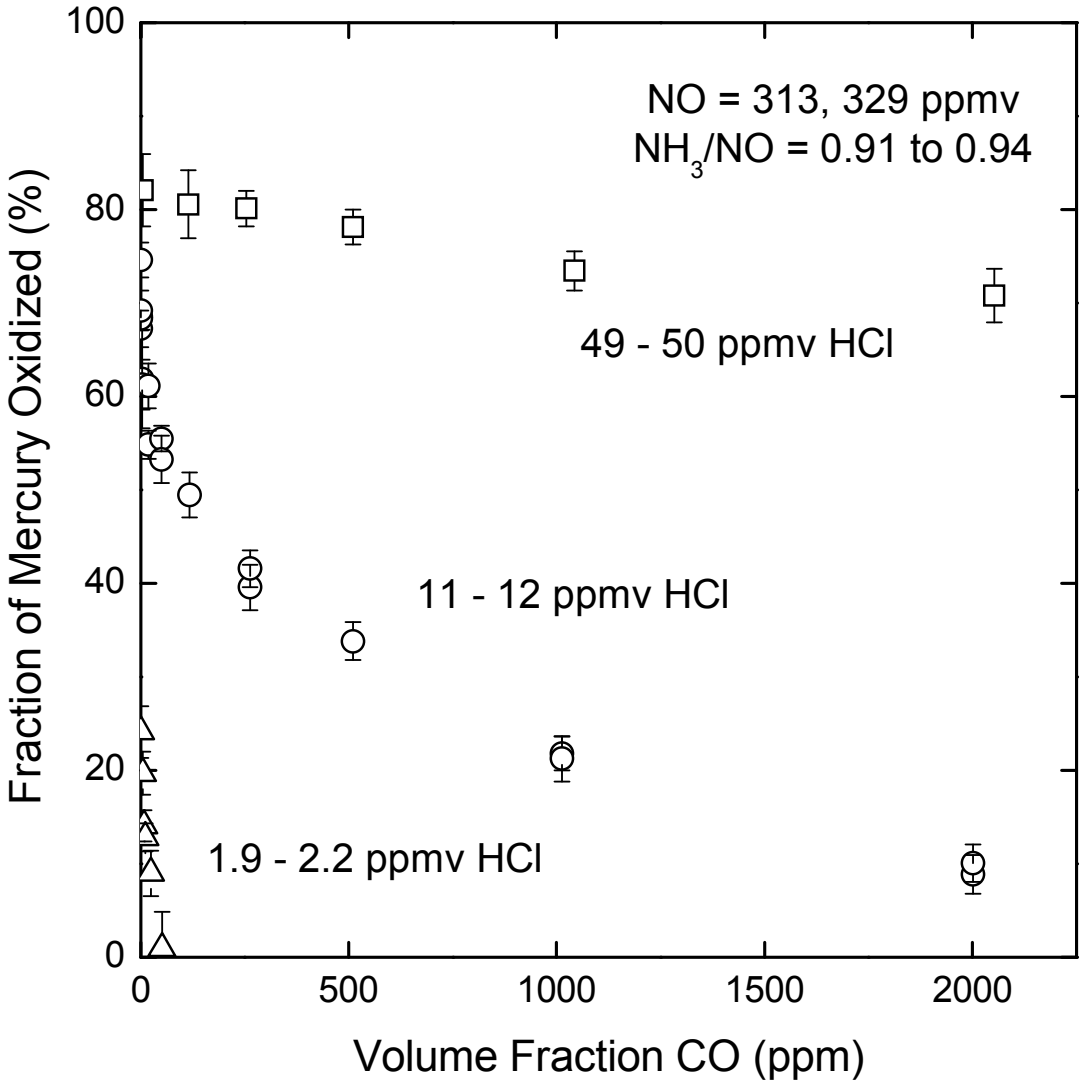

Figure 2.3.3. Dependence of mercury oxidation in the square channel monolithic catalyst on the volume fractions of CO and HCl, in the presence of 313 and 329 ppmv NO and NH_3/NO ratio from 0.91 to 0.94 at the catalyst inlet, with other conditions as specified in Table 2.2.1.

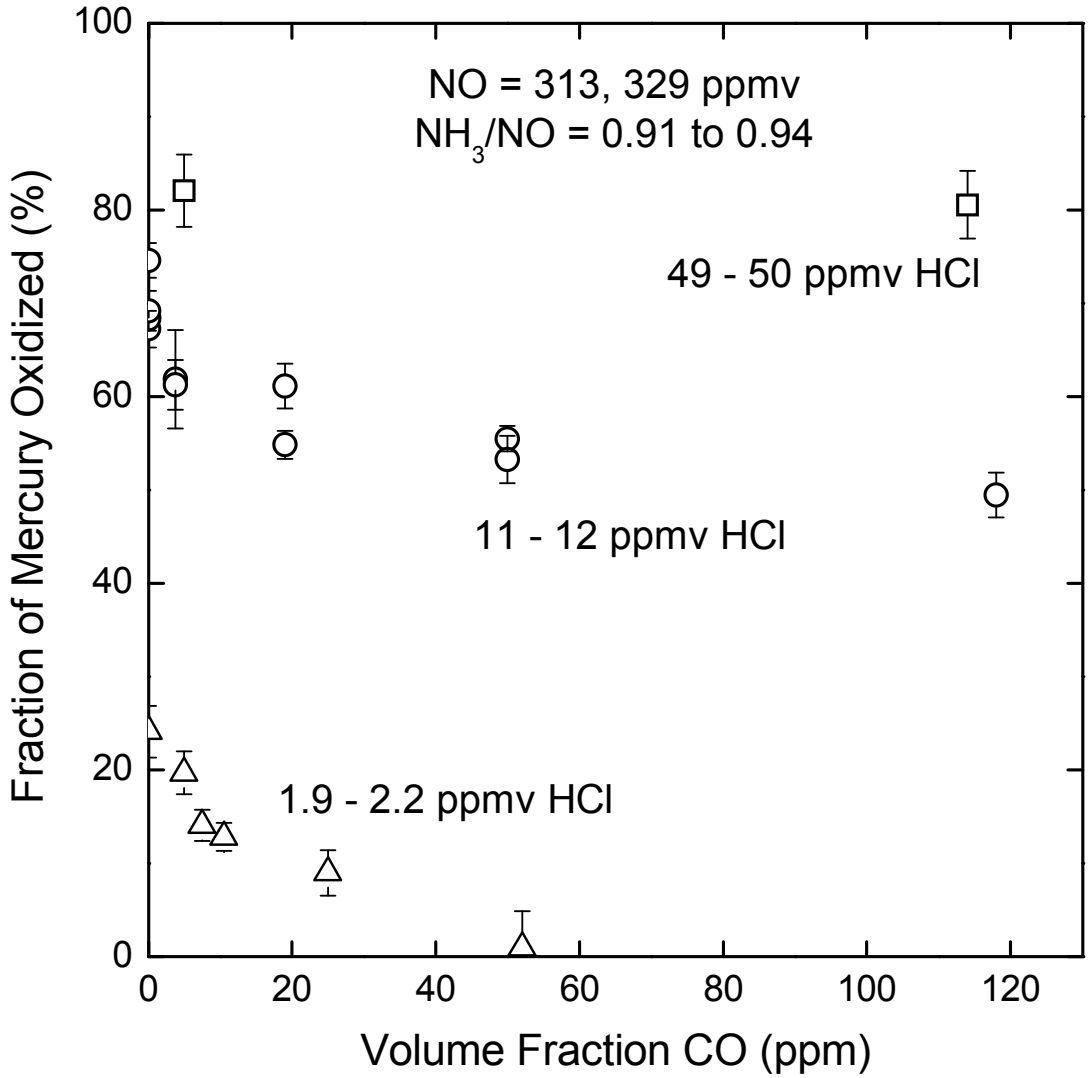

Figure 2.3.4. Dependence of mercury oxidation in the square channel monolithic catalyst on the volume fractions of CO and HCl, in the presence of 313 and 329 ppmv NO and NH_3/NO ratio from 0.91 to 0.94 at the catalyst inlet, with other conditions as specified in Table 2.2.1. The data are from Figure 2.3.3, shown on an expanded CO scale, corresponding to the practical range of CO in flue gas.

2.3.6. Sulfate Formation

Vanadium pentoxide is the catalyst of choice for oxidation of SO_2 to SO_3 in the manufacture of sulfuric acid, so the vanadium oxide in catalysts for NO_X reduction also serves as a catalyst for the oxidation of SO_2 to SO_3. To be useful in emission control applications, for oxidation of mercury or reduction of NO_X, a catalyst should not promote excessive oxidation of SO_2. Sulfates (SO_3, H_2SO_4, HSO_4^-, and SO_4^{2-}) were determined by the controlled condensation method described in Section 2.2.5, downstream from the reactor, under some of the conditions at which mercury oxidation was measured. The quartz wool filter used for controlled condensation and collection of sulfuric acid also

collects any NH_4HSO_4 and $(NH_4)_2SO_4$ aerosol formed by reaction of SO_3 with ammonia. The data on SO_2 in the feed, measurements of total sulfate at the catalyst outlet, and the conversion of SO_2 to sulfate are included in Table 2.3.1.

Measurements of the fraction of SO_2 converted to sulfate are shown in Figure 2.3.5 vs. HCl, in Figure 2.3.6 vs. NH_3/NO ratio, and in Figure 2.3.7 vs. CO. Many of the sulfate measurements were made in conjunction with examination of the effect of CO on mercury oxidation. As can be seen in the three figures, determination of the dependence of SO_2 oxidation on the three variables, HCl, NH_3/NO, and CO, is undermined by the high degree of scatter in the data.

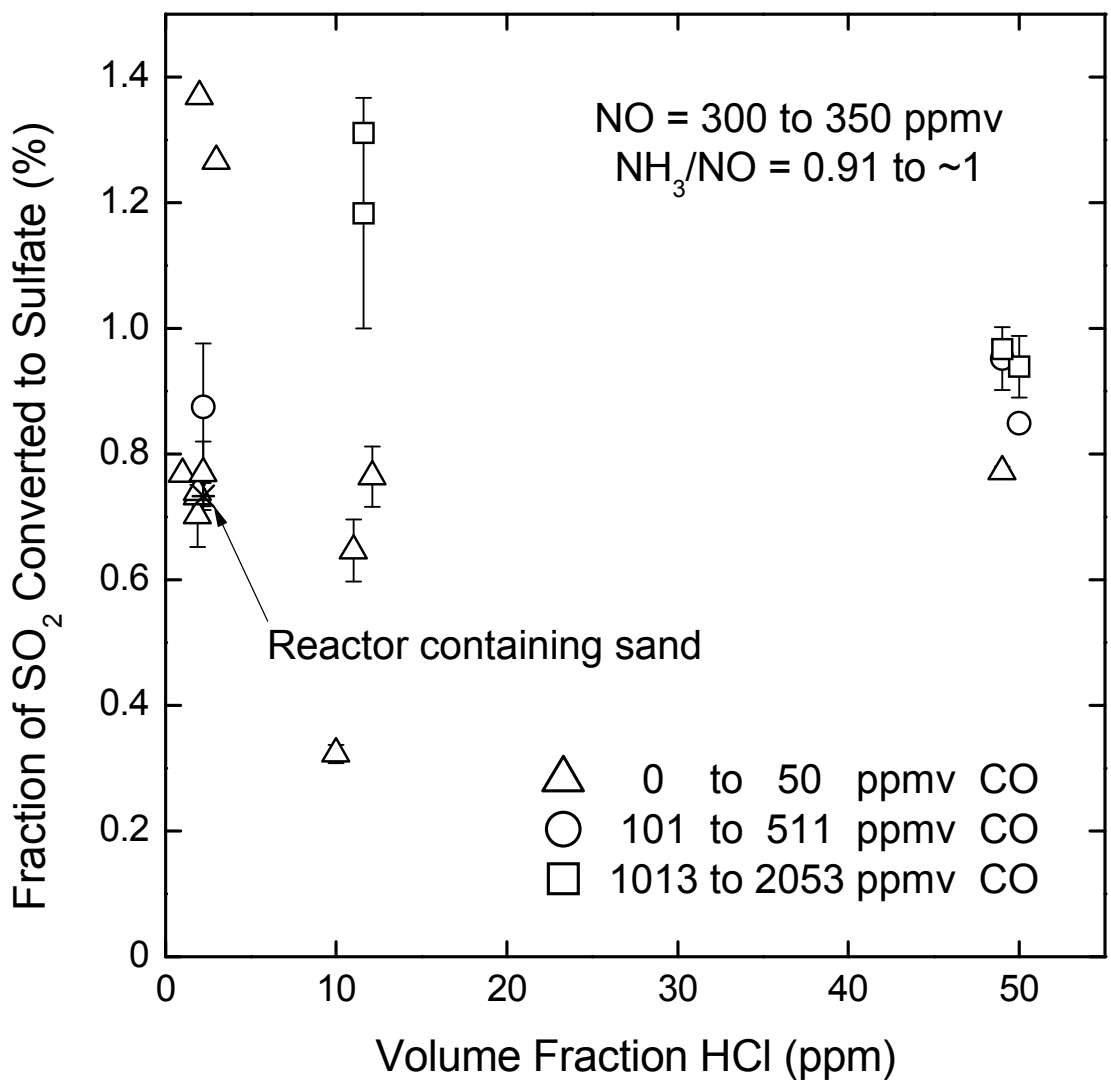

Figure 2.3.5. Dependence of SO_2 oxidation to sulfate in the square channel monolithic catalyst, and in the reactor containing sea sand, on HCl, in the presence of 300 to 350 ppmv NO and NH_3/NO ratio from 0.91 to ~1 at the inlet to the reactor, and CO in the ranges 0 to 50, 101 to 511, and 1013 to 2053 ppmv, with other conditions as specified in Table 2.2.1.

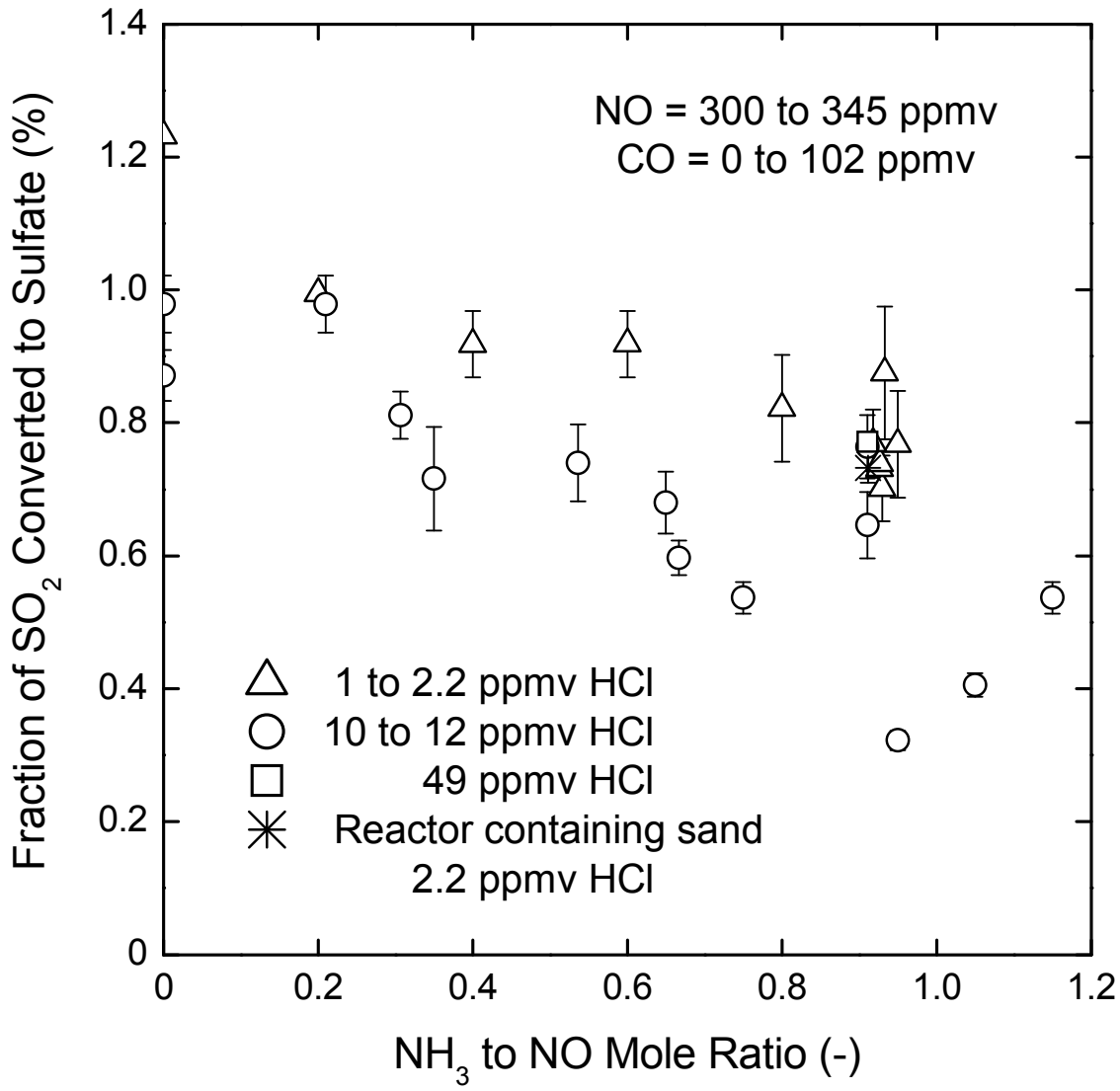

Figure 2.3.6. Dependence of SO_2 oxidation to sulfate in the square channel monolithic catalyst, and in the reactor containing sea sand, on NH_3/NO ratio at the inlet to the reactor, in the presence of 300 to 345 ppmv NO at the inlet, 0 to 102 ppmv CO, and HCl in the ranges 1 to 2.2, 10 to 12, and 49 ppmv, with other conditions as specified in Table 2.2.1.

Inspection of Figures 2.3.5, 2.3.6, and 2.3.7 shows that the conversion of SO_2 to sulfate in the presence of the SCR catalyst was similar, under many of the conditions investigated, to its conversion in the presence of the sea sand (symbol ✱ in the figures) used as the filler to maintain the same gas residence time in the "inert" reactor as in the SCR catalyst. One cannot tell, therefore, whether the SCR catalyst and sea sand are equally active as heterogeneous catalysts, whether SO_2 is oxidized by homogeneous

reactions in both cases, or whether SO_2 is oxidized by a combination of homogeneous and heterogeneous reactions. The sea sand is expected to contain some iron and, though its total surface area is low, it has high external surface area per unit of gas volume in the void space among the sand grains, so is expected to have some catalytic activity for oxidation of SO_2 to SO_3.

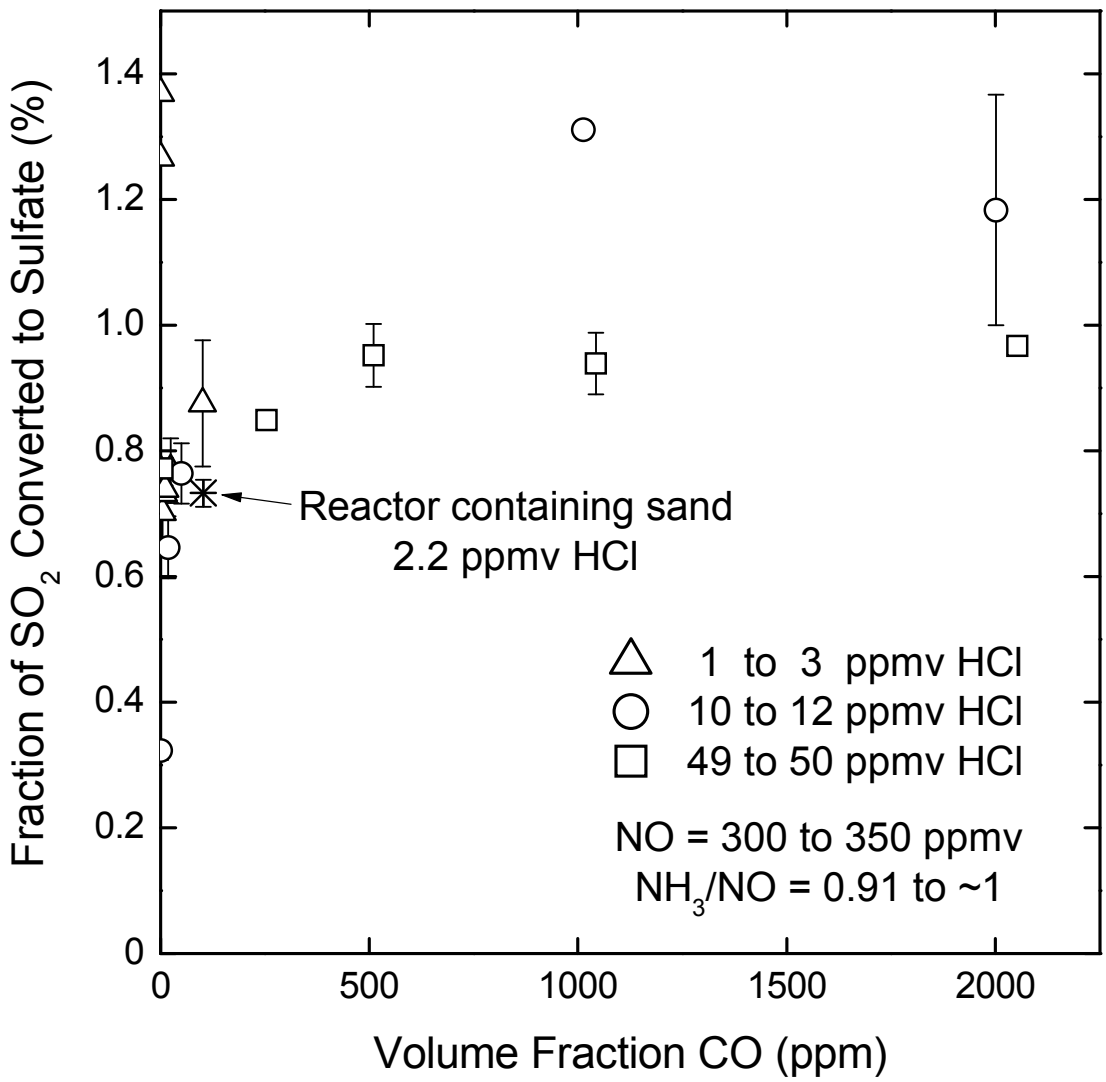

Figure 2.3.7. Dependence of SO_2 oxidation to sulfate in the square channel monolithic catalyst, and in the reactor containing sea sand, on CO, in the presence of 300 to 350 ppmv NO and NH_3/NO ratio from 0.91 to ~1 at the inlet to the reactor, and HCl in the ranges 1 to 3, 10 to 12, and 49 to 50 ppmv, with other conditions as specified in Table 2.2.1.

The data in Figure 2.3.5, showing the measurements of sulfate formation as a function of HCl, fall into three groups, according to the level of HCl. The averages and standard deviations of the measurements in the three groups are given in Table 2.3.2.

Table 2.3.2.
Averages and Standard Deviations of the Measurements of
SO_2 Conversion to Sulfate, Shown in Figure 2.3.5.

HCl (ppmv)	Average SO_4^{2-}/SO_2 (%)	Std. Deviation (%)
1 to 3	0.90*	0.26*
10 to 12	0.85	0.40
49 to 50	0.90	0.08

* Not including the measurement using the reactor containing sand.

The similarity of the average ratios of sulfate to SO_2 shown in the table suggests that there is no dependence of SO_2 oxidation to sulfate in the SCR catalyst on HCl, or that the dependence, if it exists, cannot be determined from these data.

In contrast to the conclusion above, regarding lack of dependence of SO_2 oxidation on HCl, the measurements shown in Figure 2.3.6 suggest that conversion of SO_2 to sulfate decreases both with increasing NH_3/NO ratio and with increasing HCl, with the exception of the measurement in the presence of 49 ppmv HCl at NH_3/NO = 0.91 (square symbol in the cluster of points at the right). Promotion of SO_2 oxidation in the complete absence of NH_3, and the decline in SO_2 oxidation with increasing NH_3/NO ratio, are both consistent with observations reported by Svachula et al. (1993) and Gale et al. (2006b). The sulfate measurements in the presence of 10 ppmv HCl, in the range of NH_3/NO ratio from 0.75 to 1.15, are close to the detection limit of the controlled condensation procedure (Section 2.2.5).

Dependence of the extent of SO_2 oxidation on CO mole fraction, over the range from 0 to ~2000 ppmv, is shown in Figure 2.3.7, in the presence of 1-3, 10-12, and 49-50 ppmv HCl, 300 to 350 ppmv NO, and NH_3/NO ratio from 0.91 to ~1. These data suggest that SO_2 oxidation increases with increasing CO, but the trend is not clear at low HCl levels (1 to 3 ppmv), where the measurements are very scattered and limited to the range of CO from 0 to 102 ppmv.

The tentative conclusions that may be drawn from the data shown in Figures 2.3.5, 2.3.6, and 2.3.7 are that sulfate formation decreased with increasing NH_3/NO ratio, may have been promoted by CO, and occurred to similar extents in the SCR catalyst and in the reactor containing sea sand. A dependence, or lack of dependence, of sulfate formation on HCl could not be established with any certainty.

2.4. Model for Reactions in the SCR Catalyst

2.4.1. Nitric Oxide Reduction and Mercury Oxidation

A model describing catalytic oxidation of mercury by HCl during NO reduction by ammonia in the absence of CO was based upon the work of Niksa and Fujiwara (2005b) and Senior (2006). Both adopted an Eley-Rideal mechanism for the Hg-HCl reaction. Niksa and Fujiwara assumed that HCl is adsorbed on the catalyst and reacts with gas-phase mercury, while Senior assumed that adsorbed mercury reacts with gas-phase HCl. Both assumed that gas-phase NO_X reacts with adsorbed NH_3.

In the present model, mercury, HCl, and NH_3 are all assumed to be adsorbed on the catalyst surface. Mercury oxidation then occurs by reaction of two adsorbed species. Although both NH_3 and HCl are adsorbed, they do not compete with each other for the same surface sites, but both compete for sites with elemental mercury. The fraction of surface occupied by mercury was assumed to be small. The flow through a catalyst channel was described as laminar and fully developed, with a one-dimensional treatment of diffusion and reaction at the catalyst wall. Pore diffusion in the catalyst wall, considered by Senior (2006), was neglected, and the ratios of effective to geometric surface area were incorporated in the rate coefficients. The pseudo-steady-state rate equation was integrated step-by-step from the entrance to exit of a catalyst channel.

The following transport and reaction steps for NO + NH_3 and Hg(0) + HCl were derived from the mechanisms of Niksa and Fujiwara (2005b) and Senior (2006) ("ads" indicates a species adsorbed on the catalyst surface):

NO Reduction by NH_3:

NH_3 (g) $\rightarrow$ NH_3 (ads)	diffusion	(Reaction 2.7)
NO (g) + NH_3 (ads) + 1/4 O_2 $\rightarrow$ N_2 (g) + 3/2 H_2O (g)	reaction	(Reaction 2.8)

Mercury Oxidation by HCl:

Hg(0) (g) $\rightarrow$ Hg(0) (ads)	diffusion	(Reaction 2.9)
HCl (g) $\rightarrow$ HCl (ads)	HCl in excess	(Reaction 2.10)
Hg(0) (ads) + HCl (ads) $\rightarrow$ HgCl (ads or g)	reaction	(Reaction 2.11)
HgCl (ads or g) + HCl (ads or g) $\rightarrow$ $HgCl_2$ (g)	reaction (fast)	(Reaction 2.12)

There are five adjustable parameters in the model: the reaction rate coefficients for NO + NH_3 and Hg(0) + HCl, and the adsorption equilibrium constants for NH_3, Hg(0), and HCl at the temperature of the catalyst. As in the experiments, temperature dependence was not investigated. The values chosen for the adjustable parameters are given in Table 2.4.1, along with those describing SO_2 oxidation, to be discussed in Section 2.4.3. The best fit to the mercury measurements was obtained with a small value

of the HCl adsorption equilibrium constant, suggesting that HCl is only weakly adsorbed. The C++ code for the radial diffusion and heterogeneous reaction model is listed in the Appendix.

Table 2.4.1.
Reaction Rate Coefficients and Adsorption Equilibrium Constants in the Radial Diffusion and Heterogeneous Reaction Model.

Reaction	Reaction Rate Coefficient	Adsorption Equilibrium Constant (m^3/kmol)
NH_3 (g) → NH_3 (ads)	-	3×10^6
Hg(0) (g) → Hg(0) (ads)	-	7.5×10^5
HCl (g) → HCl (ads), competing with Hg(0)	-	7.5
HCl (g) → HCl (ads), competing with SO_2	-	5×10^6
SO_2 (g) → SO_2 (ads)	-	1.5×10^{-7}
SO_3 (g) → SO_3 (ads)	-	5.7×10^6
H_2O (g) → H_2O (ads)	-	0
NO (g) + NH_3 (ads) + 1/4 O_2 (excess) → N_2 (g) + 3/2 H_2O (g)	0.05 m/s	-
Hg(0) (ads) + HCl (ads) → HgCl (ads or g)	0.014 kmol/(m^2 s)	-
HgCl (ads or g) + HCl (ads or g) → $HgCl_2$ (g)	fast	-
$(V_2\text{-}SO_3\text{-}SO_2)_{ox} \rightarrow (V_2\text{-}SO_3)_{red} + SO_3$*	$k_{red}C_{tot} = 4.2 \times 10^{-5}$ kmol/(m^3 s)	-
$(V_2\text{-}SO_3)_{red} + 1/2O_2$ (g) → $(V_2\text{-}SO_3)_{ox}$*	$k_{ox}C_{tot} = 4.2 \times 10^{-5}$ $kmol^{1/2}/(m^{3/2}$ s)	-

* Svachula et al. (1993). The total concentration of active surface sites, C_{tot}, is here incorporated in the rate coefficient.

The reaction rate coefficients and equilibrium constants were adjusted to fit the measurements of the fraction of mercury oxidized versus NH_3/NO ratio in the presence of 1 and 10-11 ppmv HCl, from Figure 2.3.2. A comparison of the calculated values with the measurements is shown in Figure 2.4.1. The proposed mechanism successfully reproduces qualitative features of both the HCl and NH_3/NO ratio dependence of mercury oxidation. The decline in extent of mercury oxidation as the NH_3/NO ratio approaches and exceeds stoichiometric is captured with accuracy commensurate with the reproducibility of the experimental measurements.

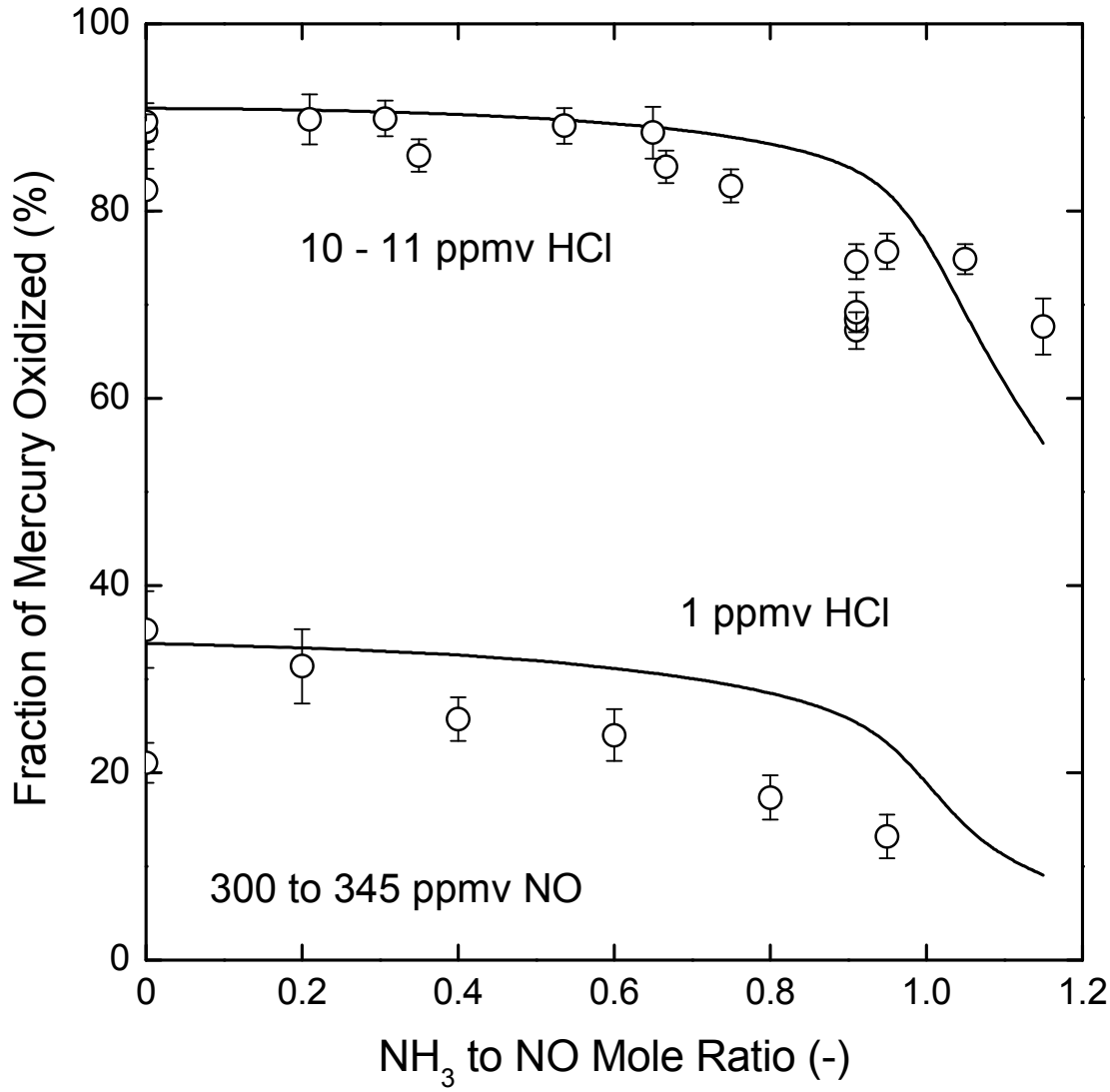

Figure 2.4.1. Comparison of calculated and measured dependence of mercury oxidation in the square channel monolithic catalyst on NH_3/NO ratio at the catalyst inlet. The calculations were done for 1 and 10 ppmv HCl and 300 ppmv NO at the catalyst inlet. The measurements were made in the presence of 1 ppmv HCl and 10 to 11 ppmv HCl, with 300 to 345 ppmv NO at the catalyst inlet, in the absence of CO, and with other conditions as specified in Table 2.2.1.

The dependence of mercury oxidation on HCl, over the entire range investigated (0 to 100 ppmv HCl), in the presence of 300 to 369 ppmv NO and NH_3/NO ratio from ~0.8 to ~1 at the catalyst inlet is shown in Figure 2.3.1c. The data from that figure are replotted on a larger scale in Figure 2.4.2 and compared with a calculation using the parameters adjusted to fit the measurements in Figure 2.4.1. At NH_3/NO ratios in the range from ~0.8 to ~1, the calculation overestimates the fraction of mercury oxidized at all levels of HCl investigated. Returning to Figure 2.4.1, we see that the overestimate of oxidized mercury, in the range of NH_3/NO ratio from 0.8 to 1, is a consequence of trying

to obtain the best overall fit to the measurements, including those at higher and lower NH_3/NO ratios. Trials using other values of the adjustable parameters showed that, while it was relatively easy to fit the mercury measurements more accurately at HCl levels below about 10 ppmv (though at the expense of the fit to the NH_3/NO trends in Figure 2.4.1), it was not possible, using the current model, to reproduce the low values of mercury oxidation (80 to 85%) observed at high HCl levels. The overall agreement with the measurements could be improved by introducing different types of surface sites, or a distribution of adsorption coefficients for each adsorbed species, at the cost of increasing the number of adjustable parameters.

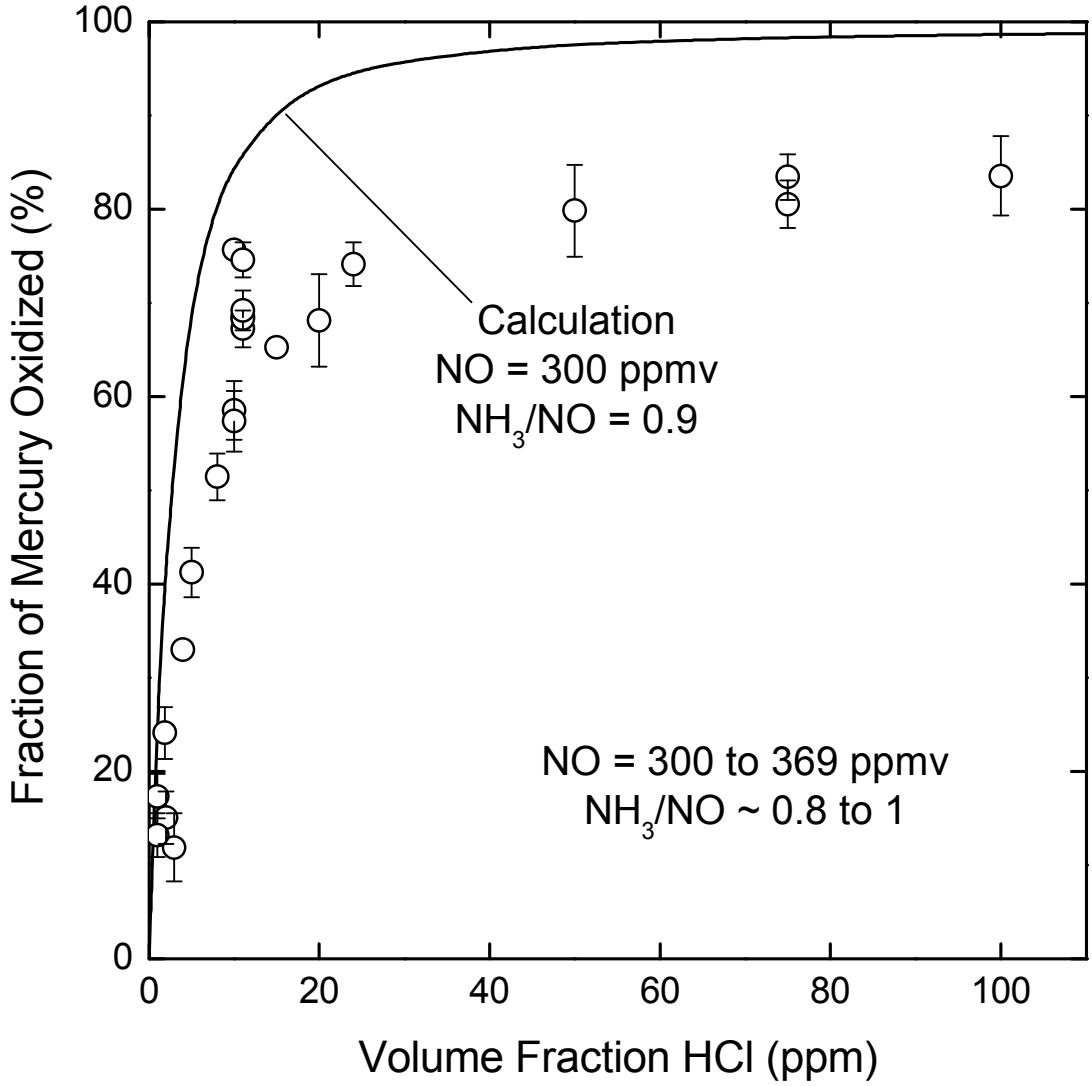

Figure 2.4.2. Comparison of calculated and measured dependence of mercury oxidation in the square channel monolithic catalyst on the volume fraction of HCl. The calculation was done for 300 ppmv NO and NH_3/NO ratio of 0.9 at the catalyst inlet. The measurements were made in the presence of 300 to 369 ppmv NO and NH_3/NO ratio from ~0.8 to ~1 at the catalyst inlet, in the absence of CO, and with other conditions as specified in Table 2.2.1.

2.4.2. Inhibition of Mercury Oxidation by Carbon Monoxide

Some possible explanations for the inhibition of mercury oxidation by CO, as shown in Figures 2.3.3 and 2.3.4, are:

1. CO competes with mercury for active sites.

2. CO reduces HgCl (ads) or $HgCl_2$ (ads) while the mercurous or mercuric chloride is still on the surface of the catalyst. For example (the species S* represents an active site on the catalyst):

   Hg(0) (g) + S* = Hg(0) (ads) (Reaction 2.13)

   Hg(0) (ads) + HCl (g or ads) = HgCl (ads) (Reaction 2.14)

   HgCl (ads) + CO (g) = Hg(0) (ads) + ClCO (g) (Reaction 2.15)

   HgCl (ads) = HgCl (g) + S* (Reaction 2.16)

   HgCl (g) + HCl (g) = $HgCl_2$ (g) + H (g) (Reaction 2.17)

3. CO destroys HgCl (g) or $HgCl_2$ (g) via homogeneous reaction after desorption of the mercurous or mercuric chloride from the catalyst surface.

None of these mechanisms, in conjunction with the current model for mercury oxidation by HCl and NO reduction by NH_3, was able to explain why the effect of CO diminishes as the HCl concentration increases. For example, calculations of the inhibition of mercury oxidation by CO, based on the third mechanism, above, in which CO reacts with, and destroys, HgCl(g) or $HgCl_2$(g) after desorption of the mercurous or mercuric chloride from the catalyst surface, are compared with the measurements from Figure 2.3.4, in Figure 2.4.3. The values of the adjustable parameters used in these calculations are very different from those given in Table 2.4.1, having been readjusted in an attempt to reproduce the measurements, but, even with wide adjustment of the parameters, the model was not able to capture the dependence of mercury oxidation on both CO and HCl.

Calculations to examine the possible effect of CO on homogeneous oxidation of mercury were performed by Balaji Krishnakumar in Joseph J. Helble's research group at Dartmouth College (B. Krishnakumar and J. J. Helble, personal communication, 2008). Dr. Krishnakumar is now with Niksa Energy Associates, Belmont, CA. The calculations were performed using the semi-empirical 8-step mechanism for homogeneous reactions of mercury and chlorine species that has evolved from work by Widmer et al. (2000), Niksa et al. (2001), Qiu et al. (2003), Niksa and Fujiwara (2005a), and Krishnakumar and Helble (2007). The calculations were performed for a simulated flue gas from an Ohio bituminous coal (130 ppmv HCl) using both a constant quench rate and a full-scale industrial boiler post-flame temperature profile.

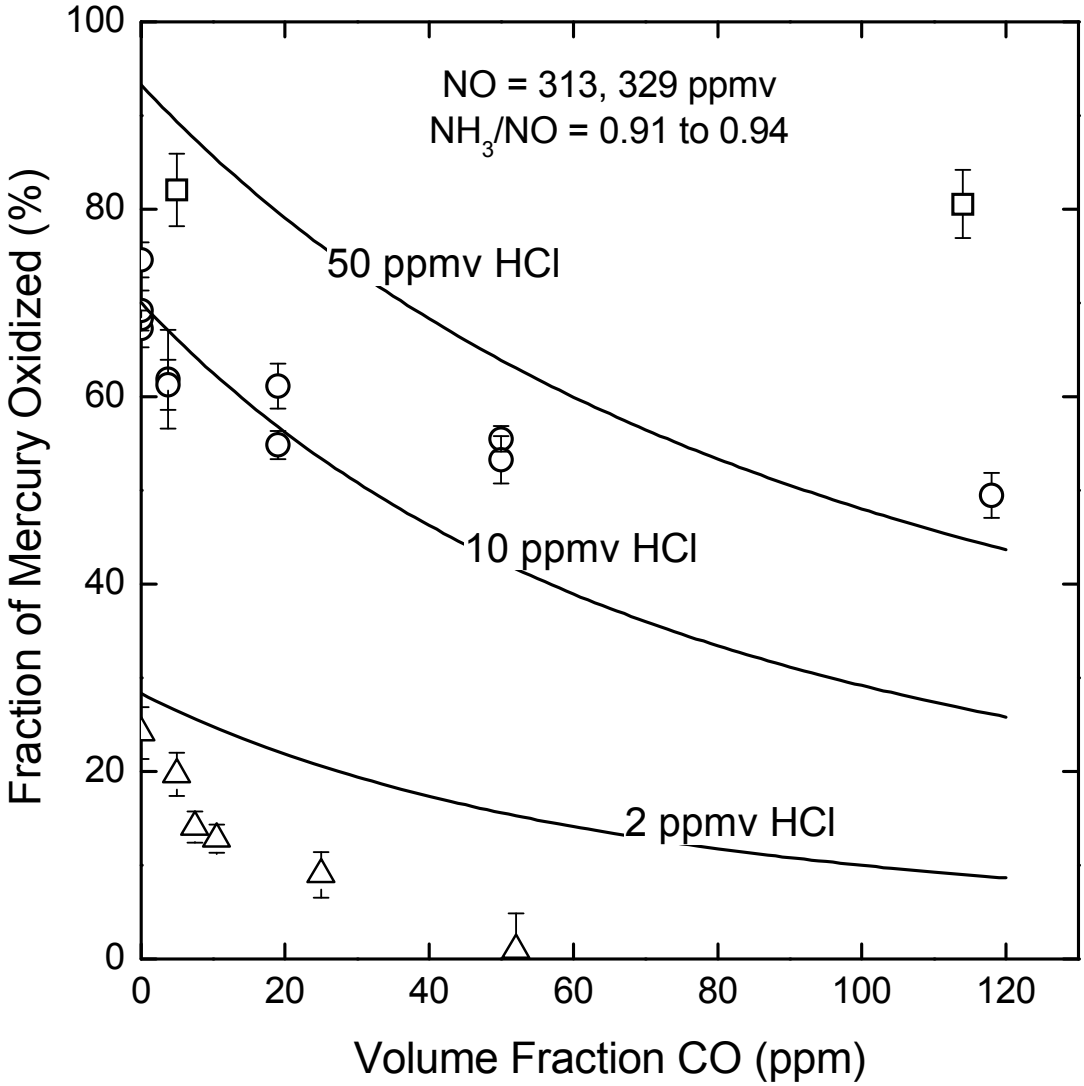

Figure 2.4.3. Comparison of calculated and measured dependence of mercury oxidation in the square channel monolithic catalyst on the volume fractions of CO and HCl. The calculations (solid curves) were done for 2, 10, and 50 ppmv HCl, and 320 ppmv NO and NH_3/NO ratio of 0.925 at the catalyst inlet. The measurements were made in the presence of 313 and 329 ppmv NO and NH_3/NO ratio from 0.91 to 0.94 at the catalyst inlet. The HCl levels corresponding to the symbols representing the measurements are: open triangles, 1.9 to 2.2 ppmv; open circles, 11 to 12 ppmv; and open squares, 49 to 50 ppmv. Other conditions are as specified in Table 2.2.1.

In the constant quench rate analysis, the flue gas was first cooled from 1177 to 367 ^{o}C in 1.5 seconds, then held at the final temperature for 2 seconds, simulating the convection heat transfer section of a boiler followed by SCR. The CO level was varied from 1.5 to 1500 ppmv. Homogeneous mercury oxidation was predicted to begin below 477 ^{o}C and continue during the 2 seconds of residence time under SCR conditions. The model predicted that approximately 11% of the mercury would be oxidized, increasing to 12% at 1500 ppmv CO. A similar calculation was performed for the full-scale industrial

boiler temperature profile from the furnace exit to the stack, with the flue gas held at 367 ^{o}C for 2 seconds, as in SCR. In this case, an increase in CO concentration from 1.5 to 1500 ppmv also had little effect on the extent of mercury oxidation. A third case, in which the calculation was begun at 377 ^{o}C and held at that temperature for 2 seconds, showed an increase of 3% in the extent of mercury oxidation over the range of CO from 1.5 to 1500 ppmv. Therefore, based on the simulations of the homogeneous system by Dr. Krishnakumar, CO is not expected to have a significant effect on the gas-phase oxidation of mercury over the entire post-combustion temperature range in coal-fired electric utility boilers, from the furnace exit to the stack (1177 to 77 ^{o}C), consistent with the experimental measurements reported by Kramlich and Castiglone (2004). The effect of CO, in the homogeneous system, is expected to be a slight promotion of mercury oxidation, rather than the inhibition of mercury oxidation observed in the present experiments with SCR catalyst. An explanation for the effect of CO on mercury oxidation in the SCR catalyst remains for future work.

2.4.3. Sulfur Dioxide Oxidation to Sulfate

Sulfate formation was treated using the rate expression for SO_3 formation in SCR by Svachula et al. (1993), which describes the dependence of the rate on all of the species, SO_2, O_2, SO_3, H_2O, NO_X, and NH_3. However, the empirical factor introduced by these authors to account for the promotion of SO_2 oxidation by NO_X was not included. An effect of HCl was added to the rate expression of Svachula et al. by assuming that it competes with SO_2 for active sites. This required a much larger adsorption coefficient for HCl than was used to describe the competition of HCl with Hg(0) for sites. Values of the parameters used to describe SO_2 oxidation are given in Table 2.4.1. The model for SO_3 formation is included in the C++ program listed in the Appendix.

Calculations of SO_3 formation are compared with the measurements of sulfate versus NH_3/NO ratio and HCl, from Figure 2.3.6, in Figure 2.4.4. The calculations were performed for 1 and 10 ppmv HCl in the presence of 300 ppmv NO and 877 ppmv SO_2 at the catalyst inlet, with no influence from CO. The calculated dependence of SO_3 formation on NH_3/NO ratio is in satisfactory agreement with the measurements of sulfate at both the intermediate (10 to 12 ppmv) and low (1 to 2.2 ppmv) HCl levels, with the exception of the measurements at high NH_3/NO ratio in the presence of 10 to 12 ppmv HCl, near the detection limit of the controlled condensation procedure, and the measurements at NH_3/NO = 0, where the promotion of SO_3 formation by NO is greatest, a component of the rate expression of Svachula et al. (1993) not included in the calculations. We also note: (1) that sulfate formation in the reactor containing sand is approximately the same as sulfate formation in the SCR catalyst in the presence of NH_3/NO at the catalyst inlet from 0.91 to 0.95 and HCl from 1 to 2.2 ppmv, and (2) that the single measurement at 49 ppmv HCl (open square symbol at the upper right) does not follow the trend established by the measurements at 1 to 2.2 and 10 to 12 ppmv HCl (sulfate formation decreasing with increasing HCl). Interpretation of the sulfate data and comparisons with the model are complicated by the uncertainties regarding the effect of HCl on sulfate formation and the contribution of the SCR catalyst to sulfate formation, discussed in Section 2.3.6.

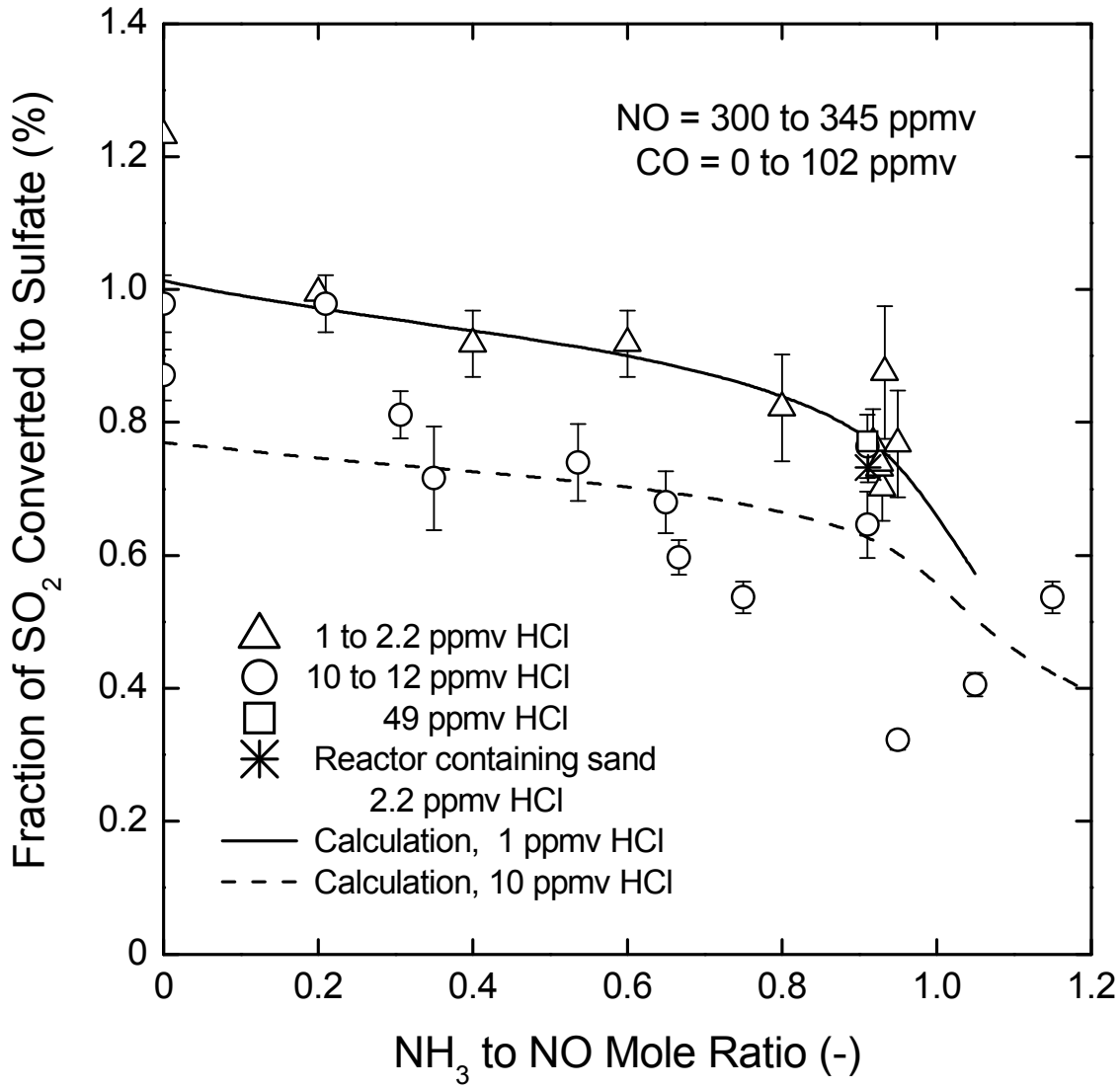

Figure 2.4.4. Comparison of calculated and measured dependence of SO_2 oxidation to sulfate in the square channel monolithic catalyst on NH_3/NO ratio at the inlet to the reactor and the volume fraction of HCl. The calculations were done for 1 ppmv HCl (solid curve), 10 ppmv HCl (dashed curve), and 300 ppmv NO at the catalyst inlet. The model makes no attempt to account for an effect of CO. The measurements were made in the SCR catalyst and in the reactor containing sea sand, in the presence of 300 to 345 ppmv NO at the inlet to the reactor, 0 to 102 ppmv CO, and HCl in the ranges 1 to 2.2, 10 to 12, and 49 ppmv, with other conditions as specified in Table 2.2.1.

The uncertainty regarding the dependence of sulfate formation on HCl is underscored by comparison of a calculation with the measurements of sulfate versus HCl, shown in Figure 2.4.5. The measurements are from Figure 2.3.5. The calculation shows the behavior of the model for SO_3 formation over the range of HCl from 0 to 55 ppmv, using the values of the parameters adjusted to fit the measurements in Figure 2.4.4. As shown in Figure 2.4.5, extrapolation to higher HCl levels, of the trend established by

fitting the measurements at 1 to 2.2 and 10 to 12 ppmv HCl (Figure 2.4.4), underestimates the fraction of SO_2 converted to sulfate in the presence of 49 to 50 ppmv HCl.

Effects, if they exist, of CO (Figure 2.3.7) and HCl on SO_2 oxidation, remain to be established in future work. Ability to account for such interactions, when they are present, would improve our ability to anticipate the effects of changes in coal and operating conditions on the contribution of SCR to sulfate formation.

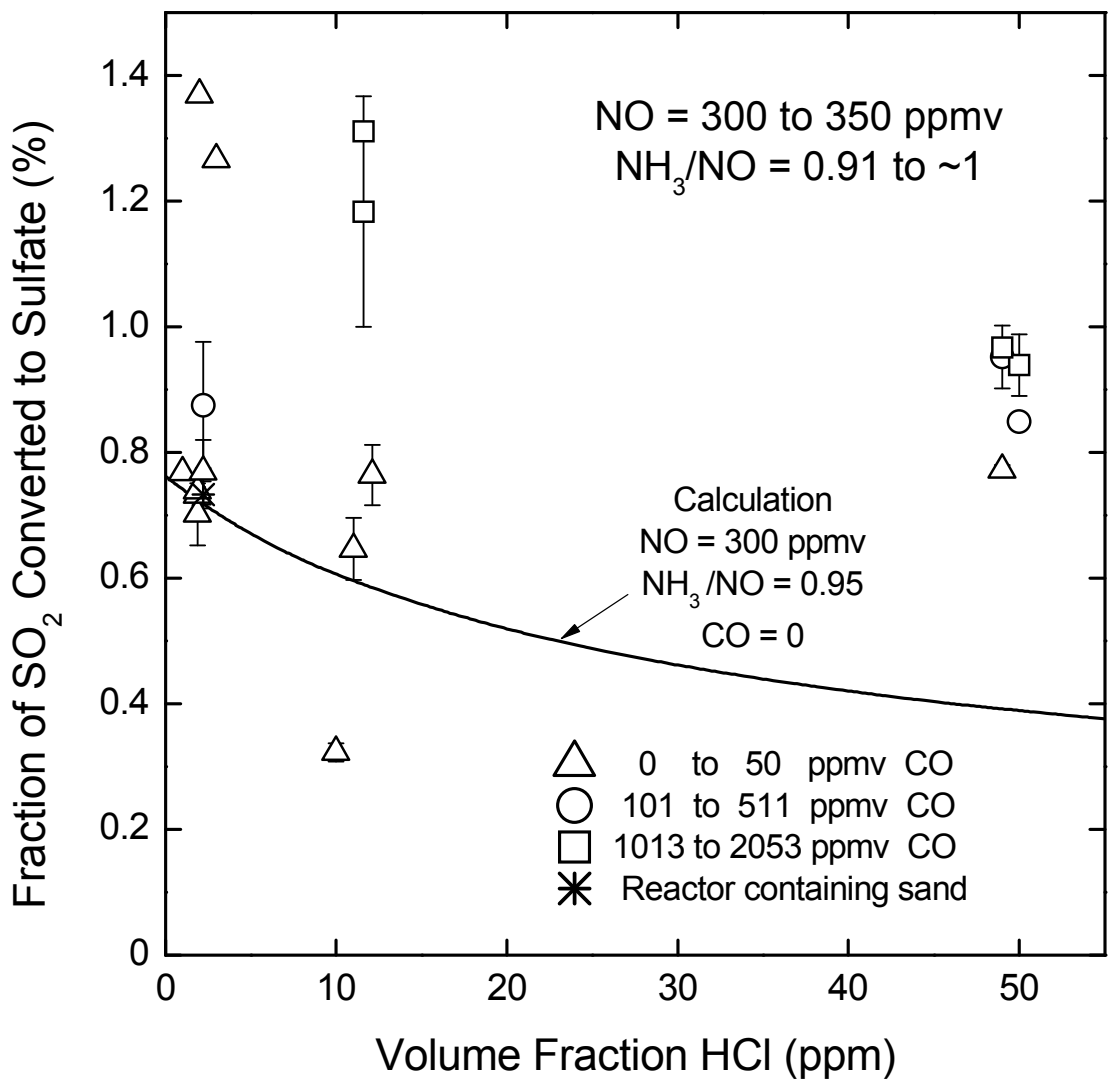

Figure 2.4.5. Comparison of calculated and measured dependence of SO_2 oxidation to sulfate in the square channel monolithic catalyst on the volume fraction of HCl. The calculation (solid curve) was done for 300 ppmv NO and NH_3/NO ratio of 0.95 at the catalyst inlet. The model makes no attempt to account for an effect of CO. The measurements were made in the SCR catalyst and in the reactor containing sea sand, in the presence of 300 to 350 ppmv NO and NH_3/NO ratio from 0.91 to ~1 at the inlet to the reactor, and CO in the ranges 0 to 50, 101 to 511, and 1013 to 2053 ppmv, with other conditions as specified in Table 2.2.1.

3. Mercury Oxidation and Adsorption by Unburned Carbon and Fly Ash*

Thomas K. Gale
Southern Research Institute

Neelesh S. Bhopatkar and Heng Ban†
University of Alabama at Birmingham

3.1. Pilot-Scale Experiments

The Combustion Research Facility (CRF), owned by the Southern Company and operated by Southern Research Institute, is located on the Birmingham, Alabama, campus of Southern Research Institute. The facility is designed for a firing rate of 1 MW(thermal) (3.4 million Btu/h) of natural gas or coal.

The CRF is designed to reproduce the conditions, including the temperature-time profile, in the flow in a full-scale electric utility boiler and its convection section, from the burners to particulate collection devices (Gale, 2005). The CRF has the full complement of equipment to crush, grind, and fire coal using methods similar to those employed at full-scale power plants and produces flue gas, fly ash, and unburned carbon having the same composition and subject to the same temperature history. A semi-continuous mercury monitor, equipped for spike and recovery calibration procedures, was used to obtain gas-phase elemental and total mercury measurements, with less than 5% uncertainty in most of the measured values (Gale, 2006).

Unburned carbon (UBC) in fly ash is known to be an important factor determining mercury oxidation and adsorption in flue gas from coal-fired boilers (Senior et al., 2000b; Fujiwara et al., 2002; Niksa et al., 2002; Gale, 2005, 2006; Niksa and Fujiwara, 2005a; Senior and Johnson, 2005; Kolker et al., 2006; Senior et al., 2006; Gale et al., 2006a, 2008). The complex role of calcium in mercury oxidation and removal has been observed in experiments and tests with Powder River Basin (PRB) coals and ash, calcium-based sorbents, and blends of PRB coals with Eastern and Western bituminous coals (Sjostrom et al., 1997, 2004; Galbreath et al., 1998; Ghorishi and Gullett, 1998; Ghorishi and Sedman, 1998; Singer et al., 2001; Ghorishi et al., 2002; Gale, 2002, 2005, 2006; Starns et al., 2002; Lissianski et al., 2003; Gale et al., 2006a, 2008). In the pilot-scale experiments at SRI (Gale, 2005, 2006), mercury speciation and capture data were

---

* Gale (2005, 2006), Gale et al. (2005, 2006a, 2008), Bhopatkar et al. (2005), Bhopatkar (2006).

† Present address for Heng Ban: Department of Mechanical and Aerospace Engineering, Utah State University, Logan, UT 84322

obtained while firing three different bituminous coals and blends of the bituminous coals with Powder River Basin coal, the focus being on moderate-to-low chlorine and moderate-to-low sulfur fuels. Most of the measurements were taken at the baghouse. The data showed that UBC is the dominant parameter affecting the mercury species distribution as long as sufficient chlorine was present, in agreement with Niksa and Fujiwara (2005a). A synergistic effect of coal blending was found to enhance Hg removal across the baghouse (Gale, 2005, 2006; Gale et al., 2006a, 2008). Increasing UBC, either by blending bituminous and PRB coals, or through combustion modifications, enhanced the oxidation and removal of mercury.

3.2. Experiments with Bituminous Coals

Oxidation of mercury and removal of mercury across the baghouse in the SRI Combustion Research Facility were investigated while firing three high volatile bituminous coals: Blacksville hvAb, Choctaw America hvAb, and Galatia hvBb. The Galatia and Choctaw America coals were each run at a single set of conditions, while the Blacksville coal was run with different amounts of unburned carbon suspended in the flue gas. The variation in unburned carbon was achieved by varying excess air. The unburned carbon concentrations, as weight fractions in the fly ash, and flue gas compositions during these experiments are given in Table 3.2.1.

Table 3.2.1.
Unburned Carbon in Fly Ash and Flue Gas Compositions
during the SRI Experiments with Bituminous Coals (Gale, 2006).
(Except for O_2 itself, the gas composition is corrected to 3 vol% O_2.)

Run No.	Coal Type*	UBC (%)	HCl ppmv	SO_3 ppmv	NO_X ppmv	SO_2 ppmv	CO ppmv	CO_2 (vol%)	H_2O (vol%)	O_2 (vol%)
1	GA	0.34	250	0.5	698	973	99	16.6	6.8	7.3
2	BL	0.57	54	12.0	635	1731	79	16.4	6.6	8.0
3	BL	0.35	54	13.5	654	1660	79	16.4	12.9	7.9
4	BL	7.32	54	3.2	212	1760	106	16.7	15.0	4.9
5	BL	7.71	54	5.0	222	1771	107	16.6	8.1	5.4
6	CA	6.77	12	2.5	457	605	98	17.0	7.2	8.0

* BL: Blacksville hvAb Coal.
CA: Choctaw America hvAb Coal.
GA: Galatia hvBb Coal.

During the experiments with Blacksville and Galatia coals, the oxidation and removal of mercury were examined under two different flue gas quench rate conditions, beginning at the location in the convection section where the temperature of the flue gas was between 482 and 427 ^{o}C (900-800 ^{o}F). Just downstream from that point, the quench rates were:

Normal quench rate condition: 482 to 503 ^{o}C/s (899 to 938 ^{o}F/s)

High quench rate condition: 615 to 625 ^{o}C/s (1139 to 1157 ^{o}F/s)

The temperature-time histories of flue gas in the convection section of the CRF under the two conditions are shown in Figure 3.2.1. The difference in temperature histories began at 2 seconds into the convection section, where the gas temperature was approximately 455 ^{o}C (850 ^{o}F).

Mercury samples were collected at two locations, at both quench rates, and with two levels of unburned carbon while firing the Blackville coal, providing observations of the effects of unburned carbon, temperature, and temperature history. Samples were collected at two locations at the normal quench rate and low unburned carbon while firing the Galatia coal, and only one sample was taken at the ESP inlet (lower temperature location) at the normal quench rate with high unburned carbon while firing the Choctaw America coal. The fraction of total mercury appearing in the oxidized state and fraction of total mercury adsorbed on fly ash and unburned carbon in each of these cases are given in Table 3.2.2.

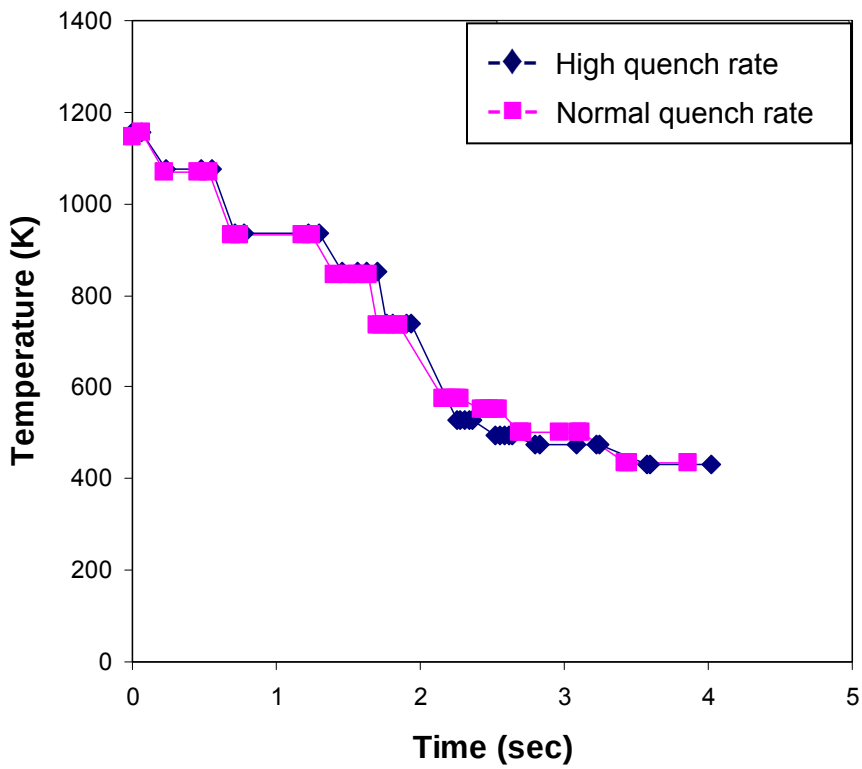

Figure 3.2.1. The temperature-time histories of flue gas in the convection section of the SRI Combustion Research Facility under the high and normal quench rate conditions, while firing the bituminous coals (Gale, 2006).

Table 3.2.2.
Fraction of Total Mercury in the Oxidized State and Fraction of Total Mercury Adsorbed on Fly Ash and Unburned Carbon at Different Quench Rates and Temperatures during the SRI Experiments with Bituminous Coals (Gale, 2006).

Run No.	Coal	Quench Rate °C/s (°F/s)	Temperature °C (°F)	- - - Mercury (%) - - - Oxidation	Removal	Temperature °C (°F)	- - - Mercury (%) - - - Oxidation	Removal
1	Galatia	494 (922)	286 (547)	19	0	163 (325)	46	0
2	Blacksville	503 (938)	279 (535)	34	0	163 (325)	38	0
3	Blacksville	615 (1139)	222 (431)	24	6	159 (318)	27	5.6
4	Blacksville	625 (1157)	177 (351)	18	15	142 (288)	39	29.4
5	Blacksville	482 (899)	288 (550)	45	11	164 (328)	55	26.4
6	Choctaw America*	476 (889)	--	--	--	>163 (>325)*	57*	0*

* Measurement at ESP inlet.

3.3. Experiments with Blends of Bituminous and Powder River Basin Coals

Another series of experiments was conducted in the SRI Combustion Research Facility using blends of Powder River Basin coal with bituminous coals (Gale, 2005). The bituminous coals were the Blacksville and Choctaw America hvAb coals fired in the experiments described above. The purpose in blending the coals was to systematically vary unburned carbon, the ratio of unburned carbon to calcium, and the chlorine concentration in the flue gas. The unburned carbon in ash, calcium oxide in ash, and gaseous species volume fractions in the flue gas during the tests using the coal blends are given in Table 3.3.1.

Table 3.3.1.
Unburned Carbon in Fly Ash, Calcium Oxide in Ash, and Flue Gas Compositions during the SRI Experiments Firing Blends of PRB Coal with Bituminous Coals (Gale, 2005).
(Gas compositions are the actual volume fractions.)

Run No.	UBC (wt%)	CaO (wt%)	HCl ppmv	NO_X ppmv	SO_2 ppmv	CO ppmv	CO_2 (vol%)	H_2O (vol%)	O_2 (vol%)
12	0.72	22.2	13.0	177.2	603.3	63.1	12.0	6.0	7.8
13	0.72	22.2	13.0	170.6	615.4	63.3	12.5	6.0	7.6
14	0.95	21.6	13.0	143.9	661.0	69.1	12.7	6.0	7.3
15	1.45	21.3	13.0	128.5	702.0	80.1	13.0	6.0	7.4
16	0.33	21.7	8.0	122.2	494.2	58.8	14.3	7.1	6.2
17	0.47	22.8	8.0	188.2	510.5	55.3	12.9	7.1	7.6
21	0.34	25.2	2.6	153.4	365.7	55.8	12.3	6.8	7.6
22	0.57	25.0	2.6	114.2	401.9	61.3	13.9	6.8	6.2
24	0.52	22.2	15.0	333.9	688.8	67.9	12.4	6.0	7.4

The distribution of mercury between elemental and oxidized states and fraction of mercury adsorbed on fly ash and unburned carbon were measured at the inlet to the baghouse. Measurements were made under two conditions of gas temperature at that location: 138 and 169 ^{o}C (280 and 337 ^{o}F). The temperature-time histories of flue gas in the convection section of the CRF under the two conditions are shown in Figure 3.3.1.

The fraction of total mercury present in the oxidized state and fraction of total mercury adsorbed on fly ash and unburned carbon at the inlet to the baghouse for each combination of coal blend and conditions are given in Table 3.3.2. Only one of the runs listed in Tables 3.3.1 and 3.3.2 was conducted at the higher baghouse temperature: Run No. 13.

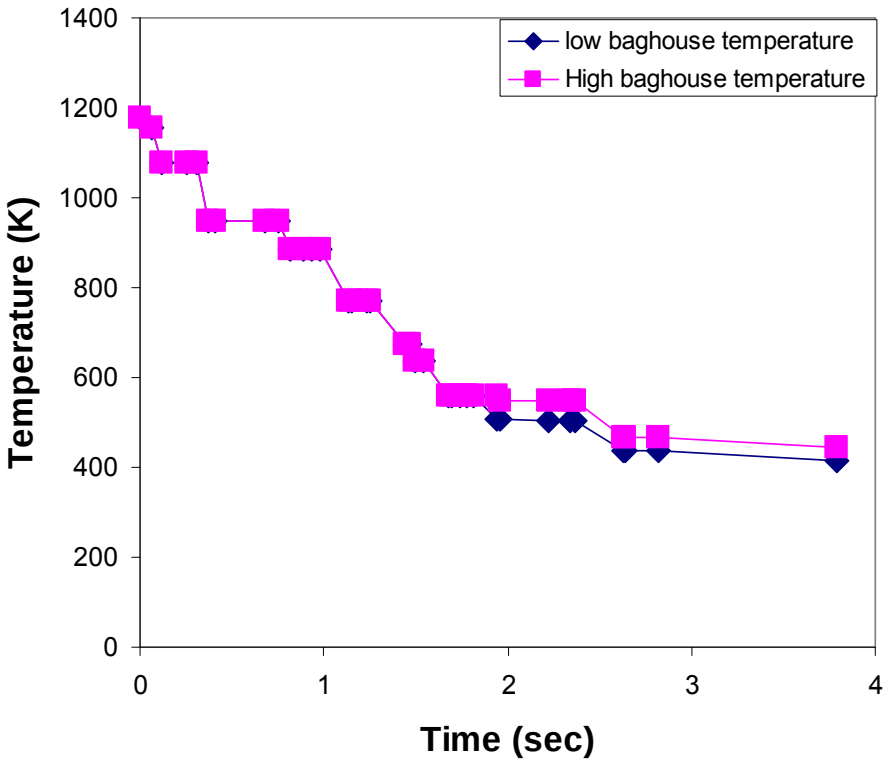

Figure 3.3.1. The temperature-time histories of flue gas in the convection section of the SRI Combustion Research Facility under the high and low baghouse temperature conditions, while firing the blends of PRB coal with bituminous coals (Gale, 2005).

Table 3.3.2.
Fraction of Total Mercury in the Oxidized State and Fraction of Total Mercury Adsorbed on Fly Ash and Unburned Carbon at the Inlet to the Baghouse during the SRI Experiments with Blends of PRB Coal with Bituminous Coals (Gale, 2005).

Run No.	Coal Blend* wt%	Temperature at Baghouse Inlet °C (°F)	Hg Oxidation (%)	Hg Removal (%)
12	80%PRB/20%BL	138 (280)	41.3	18.6
13	80%PRB/20%BL	169 (337)	43.9	11.4
14	80%PRB/20%BL	138 (280)	36.2	2.3
15	80%PRB/20%BL	138 (280)	39.1	17.4
16	90%PRB/10%BL	138 (280)	47.1	4.3
17	90%PRB/10%BL	138 (280)	38.5	8.6
21	90%PRB/10%CA	138 (280)	36.5	10.6
22	90%PRB/10%CA	138 (280)	39.9	12.2
24	60%PRB/40%BL†	138 (280)	52.6	22.4

* BL: Blacksville hvAb Coal. CA: Choctaw America hvAb Coal.
† Only fired for a few hours. The ash composition was influenced by residue from the previous run. The actual ash composition was approximately 80%PRB/20%BL.

3.4. Mechanism and Kinetics of Mercury Oxidation and Adsorption

The CHEMKIN 4.0.2 (Kee et al., 2005; Reaction Design, 2005, 2006) software package for integration of the coupled differential equations describing a chemical/physical reaction mechanism, was used to model the mercury oxidation and removal results obtained in the SRI Combustion Research Facility, while firing the bituminous coals (Gale, 2006) and blends of Powder River Basin coal with bituminous coals (Gale, 2005), described above. The data set under consideration consists of measurements while firing three bituminous coals (Galatia, Blacksville, and Choctaw America), with flue gas subjected to two thermal histories (normal and high gas quench rates); and three unburned carbon levels (low, < 1% UBC; medium, 1% < UBC < 7%; and high, > 7% UBC). Blends of Blackville and Choctaw America coals with Powder River Basin coal provided systematic variation of the chlorine and unburned carbon contents of flue gas, and the CaO to unburned carbon ratio.

A mechanism consisting of nine homogeneous and heterogeneous reactions for mercury oxidation and removal was developed to interpret the data. The model includes chlorination of carbon sites by reaction with HCl(g) to form the adsorbed species, HCl(C) (the "C" in parentheses is intended to indicate adsorption on solid carbon surface); reaction of elemental vapor phase mercury, Hg(g), with the chlorinated sites to form adsorbed mercurous chloride, HgCl(C); and desorption of HgCl(C) back to the flue gas as HgCl(g). The presence of calcium oxide, CaO(s), enhances mercury removal by stabilizing the HgCl(C) formed on the carbon surface and by reaction of HgCl(g) with CaO(s) to form HgCl(CaO).

The complete mechanism consists of the following reactions:

$$HCl(g) + C(s) = Cl(C) + H(C) \qquad \text{(Reaction 3.1)}$$

$$2\,Cl(C) = Cl_2(g) + 2\,C(s) \qquad \text{(Reaction 3.2)}$$

$$Hg(g) + Cl(C) = HgCl(C) \qquad \text{(Reaction 3.3)}$$

$$HgCl(C) = HgCl(g) + C(s) \qquad \text{(Reaction 3.4)}$$

$$Hg(g) + Cl(g) = HgCl(g) \qquad \text{(Reaction 3.5)}$$

$$Hg(g) + Cl_2(g) = HgCl(g) + Cl(g) \qquad \text{(Reaction 3.6)}$$

$$HgCl(g) + Cl_2(g) = HgCl_2(g) + Cl(g) \qquad \text{(Reaction 3.7)}$$

$$HgCl_2(g) + C(s) = HgCl(C) + Cl(g) \qquad \text{(Reaction 3.8)}$$

$$HgCl(g) + CaO(s) = HgCl(CaO) \qquad \text{(Reaction 3.9)}$$

Reaction (3.1) describes the adsorption of HCl(g) on carbon sites to form chlorinated carbon sites. Reaction (3.2) accounts for the loss of chlorinated sites by formation and desorption of chlorine, $Cl_2(g)$, from the carbon surface. Reaction (3.3) describes the reaction of elemental vapor-phase mercury, Hg(g), with chlorinated carbon sites forming adsorbed HgCl(C). Reaction (3.4) is the desorption of partially oxidized mercurous chloride, HgCl(g), from the carbon surface. The formation and accumulation of mercury on the carbon surfaces as HgCl(C) accounts for the adsorption and removal of mercury from the gas by unburned carbon at low temperatures. Reactions (3.5) and (3.6) describe the oxidation of vapor phase elemental mercury, Hg(g), via chlorine species such as Cl(g) and $Cl_2(g)$ in the gas phase. Reaction (3.8) accounts for readsorption of fully oxidized mercuric chloride, $HgCl_2(g)$, onto open carbon sites.

The experimental data suggested that calcium enhances mercury capture by stabilizing mercury adsorbed onto carbon surfaces, or by reacting with HgCl(g) vapor after its desorption from carbon surface, but prior to its conversion to $HgCl_2(g)$. These mechanisms, proposed by Gale (2005), account for the effect of calcium on mercury removal. Reaction (3.9) describes the reaction of calcium oxide, CaO(s), with gas-phase HgCl(g), the route chosen for stabilization of adsorbed mercury and enhancement of mercury removal by calcium in the present work.

The unknown pre-exponential factors, temperature exponents, and activation energies in Arrhenius-type rate coefficients for Reactions (3.1-3.9) were found by coupling the Simplex Centroid (Nelder and Mead, 1965) FORTRAN code with the CHEMKIN Release 4.0.2 software (Kee et al., 2005; Reaction Design, 2005, 2006) and minimizing the differences between the experimental results and the values calculated using the model. The values of the parameters providing the best agreement between the model and measurements are given in Table 3.4.1.

Table 3.4.1.
Arrhenius Parameters for Rate Coefficients of Mercury and Chlorine Reactions in Products of Combustion of the Bituminous Coals and Coal Blends.
Rate coefficients of the form: $k = AT^{\beta}e^{-E_a/RT}$

Reaction	A (*)	β	E_a (cal/mol)
3.1. $HCl(g) + C(s) = Cl(C) + H(C)$	59100	0	- 1130
3.2. $Cl(C) + Cl(C) = Cl_2(g) + 2\,C(s)$	0.2×10^{17}	0	- 1990
3.3. $Hg(g) + Cl(C) = HgCl(C)$	1.2×10^{17}	0	1000
3.4. $HgCl(C) = HgCl(g) + C(s)$	200	0	974.0
3.5. $HgCl_2(g) + C(s) = HgCl(C) + Cl(g)$	710	0	- 13692.4
3.6. $HgCl(g) + CaO(s) = HgCl(CaO)$	0.54×10^{10}	0	- 1000
3.7. $Hg(g) + Cl(g) = HgCl(g)$	9.0×10^{15}	0	0
3.8. $Hg(g) + Cl_2(g) = HgCl(g) + Cl(g)$	1.39×10^{14}	0	34000
3.9. $HgCl(g) + Cl_2(g) = HgCl_2(g) + Cl(g)$	1.39×10^{14}	0	1000

* cm, s, mol units depending on whether homogeneous or heterogeneous.
(C) species adsorbed on unburned carbon
(CaO) species adsorbed or reacted with CaO
(g) gaseous species
(s) solid species

3.5. Comparison of the Model with the Pilot-Scale Measurements

The chemical mechanism, with the adjusted values of the Arrhenius parameters, was successful in reproducing, qualitatively, important features of the experimental observations, as shown in Figure 3.5.1. The measured values of HCl (in ppmv), extent of mercury oxidation (%), and mercury removal (%) by adsorption on fly ash and unburned carbon are shown in Figure 3.5.1a, at the top. The measured values of HCl are repeated in Figure 3.5.1b, at the bottom, along with the simulation results for mercury oxidation and removal.

We may conclude from Figure 3.5.1 that change in HCl volume fraction had relatively weak influence on mercury oxidation or removal, over the range shown (10 to 190 ppmv HCl). On the other hand, there is a clear correlation in the experimental data (Figure 3.5.1a) between unburned carbon and mercury removal, but only a weak correlation between unburned carbon and the extent of mercury oxidation. The simulation (Figure 3.5.1b) captures the effect of unburned carbon on mercury removal quite well, but overestimates the influence of unburned carbon on the extent of mercury oxidation.

Comparison of simulation results with experimental measurements for all of the bituminous coal runs listed in Tables 3.2.1 and 3.2.2 is shown in Figure 3.5.2. Simulations of all of the PRB-bituminous coal blend tests listed in Tables 3.3.1 and 3.3.2 are compared with experiment in Figure 3.5.3.

Referring to Figure 3.5.2, we see that the removal of mercury by fly ash and unburned carbon in the flue gas from combustion of the bituminous coals, at both high and low temperatures, is reproduced quite accurately by the simulation (magenta triangle and blue square symbols). The extent of mercury oxidation, on the other hand, is not so well explained. This is because of oversensitivity of the oxidation process in the model to the concentration of unburned carbon.

Referring now to Figure 3.5.3, showing the comparison for the coal blends, we see that mercury removal (blue diamond symbols) is approximately reproduced, with removal for only two runs greatly overpredicted. The effect on mercury removal here is due primarily to the increase in mercury capture in the presence of calcium, represented in the model by Reaction (3.9).

The model is evidently unable to account properly for the principal factor controlling mercury oxidation in the flue gas from combustion of the coal blends (Figure 3.5.3, magenta square symbols), again primarily because of oversensitivity to unburned carbon. The four cases whose extents of mercury oxidation are greatly underpredicted by the model (four points near the bottom center in Figure 3.5.3) are the cases having the lowest unburned carbon and lowest HCl volume fractions (Run No's 16, 17, 21, and 22 in Tables 3.3.1 and 3.3.2).

A subsequent series of experiments at pilot scale, again in the CRF at Southern Research Institute but under a separate project, was conducted with blends of PRB with Eastern and Western bituminous coals, covering the range of blend composition from 100% PRB to 100% bituminous coal (Gale, Lani, and Offen, 2008). The mercury removal measurements at the inlet and exit from the ESP were fit using an empirical expression containing six terms: linear and quadratic terms in the UBC concentration in flue gas, linear and quadratic terms in the CaO concentration in flue gas, a term containing the product of UBC and CaO concentrations, and a constant. The two variables, UBC and CaO concentration, five coefficients, and the constant were sufficient to reproduce the measurements at the inlet and exit from the ESP while firing the PRB-Western bituminous coal blends and at the exit from the ESP while firing the PRB-

Eastern bituminous coal blends, with R^2 values from 0.74 to 0.89 for the least-squares multiple regression analysis (Gale, Lani, and Offen, 2008). The UBC and CaO concentrations alone were therefore able to explain both the effect of UBC and the synergistic effect between UBC and CaO in ash on mercury removal at the entrance and exit from the ESP, under the low chlorine (2 to 50 ppmv HCl) and low SO_3 conditions investigated.

a. Experimental

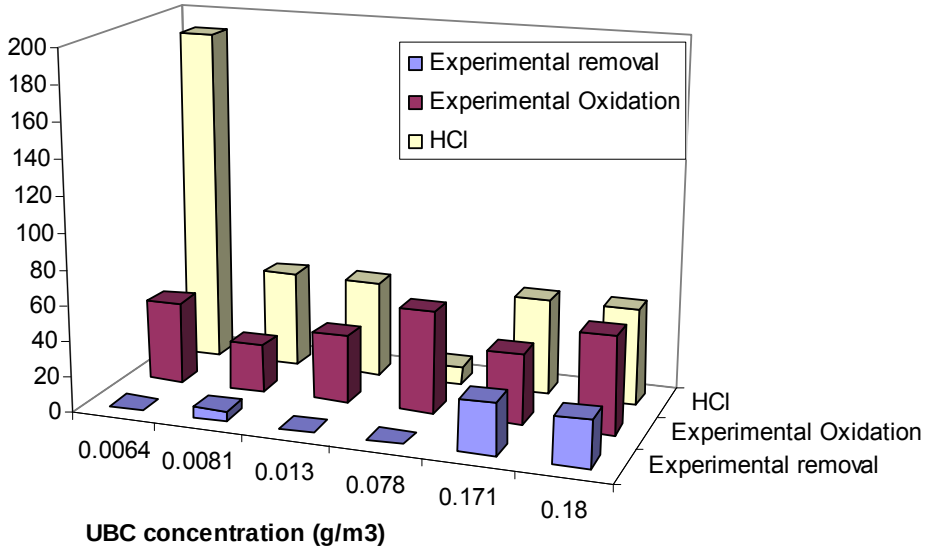

b. Simulation

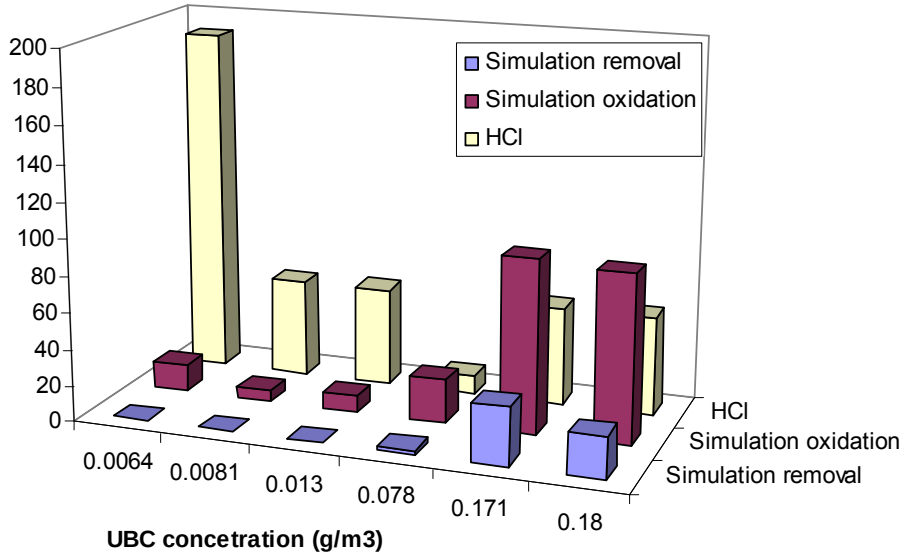

Figure 3.5.1. Comparison of experimental and simulated relationships between unburned carbon (UBC, g/m^3), HCl volume fraction (ppm), mercury oxidation (%), and mercury removal (%) (Bhopatkar, 2006). a. Experimental. b. Simulation.

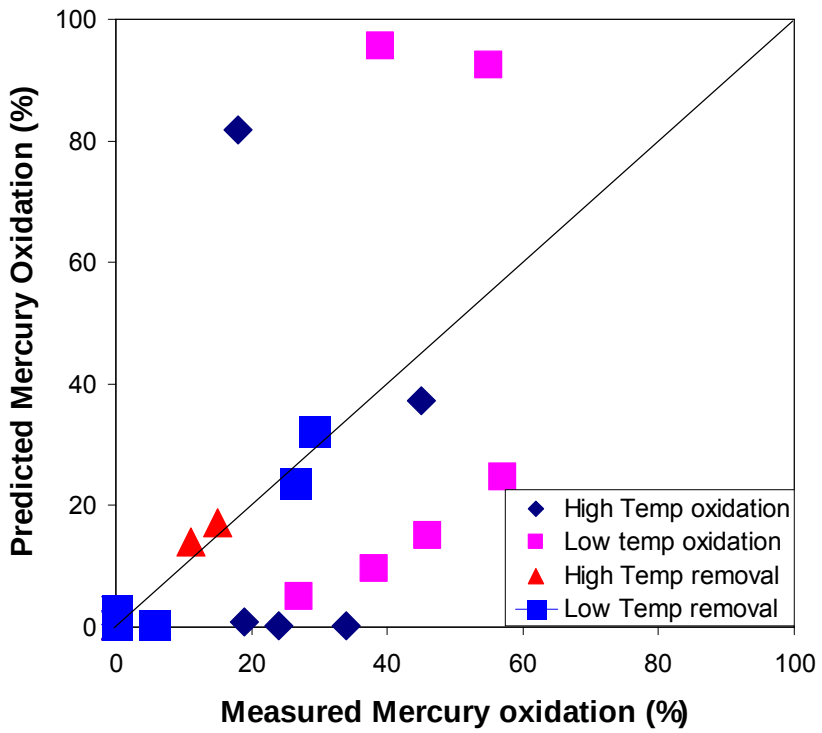

Figure 3.5.2. Comparison of the simulation of mercury oxidation and removal with experimental measurements while firing the bituminous coals (Bhopatkar, 2006).

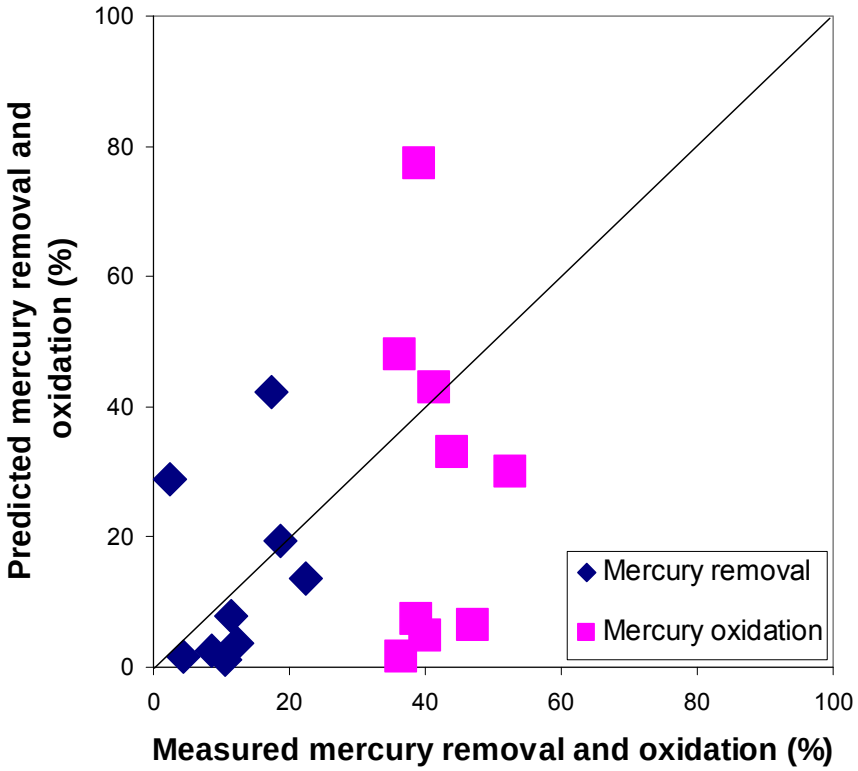

Figure 3.5.3. Comparison of the simulation of mercury oxidation and removal with experimental measurements while firing the blends of PRB coal with bituminous coals (Bhopatkar, 2006).

4. Toward the Development of Combined Catalysts and Sorbents for Low Temperature Oxidation and Removal of Mercury from Flue Gas

Conrad W. Ingram, Selasi Blavo, Tesfamariam Mehreteab, Victor Banjoko, and Yohannes Ghirmazion
Clark Atlanta University

4.1. Introduction

Thermally stable and cost effective catalyst/adsorbents are sought to provide the basis for a technology for simultaneous oxidation and removal of elemental and oxidized mercury from flue gas. Pinto and Smirniotis (2006) have shown that Mn/TiO_2 SCR-type catalysts, combined with thermally stable, thiol-functionalized silicas, are promising candidates for simultaneous reduction of NO_X by CO, adsorption of oxidized mercury, and oxidation and removal of elemental mercury from flue gas at temperatures below 200 ^oC. Improved performance with respect to oxidation and capture of elemental mercury and increased tolerance to SO_2 are goals in the second phase of the research and development program undertaken by Pinto and Smirniotis.

The present research project included an investigation of methods by which to prepare combined catalyst/sorbent systems for removal of mercury, based on surfactant-templated nanoporous silicas containing a transition metal and an organic functionality. High thermal stability and high capacity to oxidize and capture mercury are the primary performance objectives. Our proposed materials are based on the highly ordered, high surface area (~ 1000 m^2/g), thermally stable, surfactant-templated nanoporous (> 2 nm) family of silicates and aluminosilicates, namely, MCM-41 (Mobil Composition of Matter; Kresge et al., 1992), MSU (Michigan State University; Bagshaw et al., 1995) and SBA-15 (University of California, Santa Barbara; Zhao et al., 1998) depicted in Figure 4.1.1, that were developed in the 1990's. They have demonstrated great potential for applications as sorbents, catalysts, and catalyst supports.

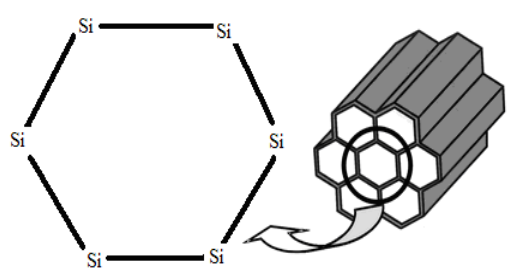

Figure 4.1.1. The hexagonal pore structure of MCM-41 and SBA-15 nanoporous silicas.

The object of this work is to create crystalline or highly ordered multifunctional nanoporous organosilicates, by simultaneously introducing organic and metal ion functionalities within the pore structure of these materials that can oxidize elemental mercury and adsorb the resulting oxidized mercury simultaneously. We expect that some metal-containing organosilicates will combine several desirable properties in one material: high thermal and mechanical stability, imparted by the silicate content, and flexible and tunable surface properties resulting from the incorporation of various metal ions and organic functionalities within the framework.

The introduction of organic functionalities to form our proposed metal-containing nanoporous materials is accomplished by directly co-condensing the organoalkoxysilane precursors with the main silica source, typically a siloxane (e.g. tetraethylorthosilicate, TEOS, $(C_2H_5O)_4Si$).

4.2. Synthesis of the Catalysts/Sorbents

Surfactant templated mesoporous organic-inorganic organosilicates were synthesized according to the methods of Burleigh et al. (2004). The organosilicate precursors were:

3-aminopropyltriethoxysilane (APTES),
mercaptopropyltrimethoxysilane (MPTMS),
3-chloropropyltrimethoxysilane (CPTMS), and
tetraethylorthosilicate (TEOS).

Cetyltrimethylammonium bromide ($C_{16}H_{33}N(CH_3)_3Br$, CTMABr) was the surfactant used for all samples. Mixtures of the reactants were stirred at room temperature and/or 100 ^oC for several hours. The white precipitates were recovered by filtration followed by repeated washing with deionized water. The surfactant was removed from the mesostructured materials by repeated extraction in ethanol/acid (1 M HCl) at 70 ^oC.

4.2.1. Synthesis of SBA-15

A 4 g aliquot of Pluronic-123 surfactant (as template), 10 g of TEOS, and 98.8 g of water were mixed to give a final mixture having the following molar composition: $1SiO_2$:0.013Pluronic-123:$70H_2O$. The pH of the mixture was adjusted to 2 with HCl. The mixture was stirred for 12 h at 35 ^oC, then heated in a sealed high-density polyethylene bottle under static conditions at 100 ^oC for 24 h. The solid was recovered by filtration, washed with deionized water, dried, and calcined at 550 ^oC in flowing dry air for up to 14 h.

4.2.2. Synthesis of MCM-41

A 6.71 g aliquot of CTMABr, 360 mL of water, and 1.41g of NaOH were mixed at 40 ^oC for 30-40 min. 30 mL of TEOS were added and the mixture stirred for 3 days at room temperature. The molar ratio of the reaction mixture was 1TEOS:0.12CTMABr:0.23NaOH:$130H_2O$. The resulting precipitate was filtered, washed with deionized water, dried at room temperature, and calcined at 500 ^oC for 5 h.

4.2.3. Synthesis of MCM-41 Containing Transition Metal, Manganese

In a flask, 1.3 g of titanium butoxide were dissolved in 39.2 g of isopropanol under nitrogen atmosphere. In a second flask, 20.8 gm of TEOS were dissolved in 15.7 g of isopropanol. The titanium-containing mixture was slowly mixed into the second flask, followed by addition of 9.6 g of 40 wt% tetraethylammonium hydroxide (TEAOH). The Si/Ti mole ratio in the synthesis mixture was 25. After stirring the mixture for 20 min, 47 g of CTMABr (25 wt% solution) and 44 g of water were added with further stirring for 1 h. The mixture was then heated at 100 °C for 3 days. The resulting precipitate was filtered, washed with deionized water, dried at room temperature, and calcined at 500 °C for 12 h.

4.2.4. Synthesis of MCM-41 Containing Transition Metal, Titanium

A 0.80 g aliquot of CTMABr, and 43 mL of NaOH were mixed. A 0.3968 g aliquot of manganese acetate and 1.5 g of TEOS were mixed at 40 °C for 3 days at room temperature. The resulting precipitate was filtered, washed with deionized water, dried at room temperature, and calcined at 500 °C for 5 h.

4.2.5. Synthesis of MCM-41 Containing Transition Metals, Titanium and Vanadium

A 5.94 g aliquot of titanium butoxide was dissolved in 39.2 g of isopropanol under nitrogen atmosphere. In a second flask, 41.6 g of TEOS was dissolved in 15.7 g of isopropanol. The titanium-containing mixture was slowly mixed into the second flask, followed by the addition of 9.6 g of 40 wt% tetraethylammonium hydroxide. After stirring for 20 min, 18.9 g of CTMABr (25 wt% solution) were added, followed by addition of 0.33 g of vanadium sulfate and 87 mL of water. The mixture was then heated at 100 °C for 3 days. The molar composition of the reaction mixture was TEOS:0.1Ti:0.26CTMABr:0.26TEAOH:23H_2O:0.01V. The resulting precipitate was filtered, washed with deionized water, dried at room temperature, and calcined at 500 °C for 12 h.

4.2.6. Synthesis of MCM-41 Containing Amino Organic Functionality as Pendant

A 3.13 g aliquot of CTMABr, 167 mL of water, and 0.66 g of NaOH were mixed at 40 °C for 1 h. 3.16 g of 3-aminopropyltriethoxysilane (APTES) and 12.5 mL of TEOS were added to the mixture, which was stirred for 3 days at room temperature. The mole ratio of the reaction mixture was 0.9TEOS:0.12CTMABr:0.23NaOH:130H_2O:0.2APTES. The mixture was filtered, and the precipitate washed with deionized water and dried at room temperature. The CTMABr was extracted from the sample by refluxing in 250 mL of acidified ethanol for 6 h at 70 °C.

4.2.7. Synthesis of MCM-41 Containing CPTMS Organic Functionality as Pendant

A 3.06 g aliquot of CTMABr, 164 mL of water, and 0.64 g of NaOH were mixed at 40 °C for 1 h. A 3.00 g aliquot of CPTMS and 12.3 mL of TEOS were added to the

mixture, which was stirred for 3 days at room temperature. The molar ratio of the synthesis mixture was 1TEOS:0.12CTMABr:0.23NaOH:130H_2O:0.2CPTMS. The mixture was filtered, the precipitate washed with deionized water and dried at room temperature. The sample was extracted with 250 mL of acidic ethanol for 6 h at 70 ^oC.

4.2.8. Synthesis of MCM-41 Containing Mercapto Organic Functionality as Pendant

A 3.0 g aliquot of CTMABr, 169 mL of water, and 0.66 g of NaOH were mixed at 40 ^oC for 1 h. 3.16 g of MPTMS and 12.6 mL of TEOS were added to the mixture. The molar ratios of the components of the synthesis mixture were 1TEOS:0.12CTMABr:0.23NaOH:130H_2O:0.2MPTMS. The mixture was stirred for 3 days at room temperature, filtered with deionized water, dried at room temperature, and calcined at 500 ^oC for 5 h. The sample was extracted with 250 mL of acidic ethanol for 6 h at 70 ^oC.

4.2.9. Synthesis of MCM-41 Containing Transition Metal, Manganese, and Amino Organic Functionality as Pendant

A 3.13 g aliquot of CTMABr, 167 mL of water, and 0.66 g of NaOH were mixed at 40 ^oC for 1 h. A 3.16 g aliquot of APTES, 12.5 mL of TEOS, and 1.53 g of manganese acetate were added and the mixture stirred for 3 days at room temperature. The molar ratios of the components of the synthesis mixture were 1TEOS:0.12CTMABr:0.23NaOH:130H_2O:0.2APTES:0.1Mn. The mixture was filtered, washed with deionized water, dried at room temperature, and extracted with 250 mL ethanol for 6 h at 70 ^oC.

4.2.10. Synthesis of MCM-41 Containing Transition Metal, Manganese, and CPTMS Organic Functionality as Pendant

A 3.06 g aliquot of CTMABr, 164 mL of water, and 0.64 g of NaOH were mixed at 40 ^oC for 1 h. A 3.00 g aliquot of CPTMS, 12.2 mL of TEOS, and 1.48 g of manganese acetate were added to the mixture, which was then stirred for 3 days at room temperature. The molar ratios of the components of the synthesis mixture were 1TEOS:0.12CTMABr:0.23NaOH:130H_2O:0.2CPTMS:0.1Mn. The resulting precipitate was filtered, washed with deionized water, dried at room temperature, and extracted with 250 mL ethanol for 6 h at 70 ^oC.

4.2.11. Synthesis of MCM-41 Containing Transition Metal, Manganese, and MPTMS Organic Functionality as Pendant

A 3.0 g aliquot of CTMABr, 169 mL of water, and 0.66 g of NaOH were mixed at 40 ^oC for 1 h. A 3.16 g aliquot of MPTMS, 12.6 mL of TEOS, and 1.55 g of manganese acetate were added to the mixture, which was then stirred for 3 days at room temperature. The molar ratios of the components of the synthesis mixture were 1TEOS:0.12CTMABr:0.23NaOH:130H_2O:0.2MPTMS:0.1Mn. The resulting precipitate

was filtered, washed with deionized water, dried at room temperature, and extracted with 250 mL ethanol for 6 h at 70 ^{o}C.

4.2.12. Synthesis of Nano-Zeolite Y

191 g of aluminum isopropoxide and 1608 g of water were mixed for 30 min and 2.63 g NaOH were added. 815.3 g of tetramethylammonium hydroxide were then added and left to react for 20 min, followed by addition of 389 g of TEOS. The mixture was left for 12 h until a clear solution was obtained. The mixture was then transferred to an oven at 100 ^{o}C for three days, the precipitate separated using a high speed centrifuge at 21,000 rpm for 2 h, and the solid dried at 100 ^{o}C.

4.3. Characterization of the Catalysts/Sorbents

Samples of the catalysts/sorbents that were synthesized are shown in Figure 4.3.1.

Figure 4.3.1. The catalysts/sorbents synthesized.

4.3.1. X-ray Diffraction

X-ray powder diffraction (XRD) measurements were recorded on a Philips X'PERT diffractometer with a Cu K_{α} anode, voltage 40 kV, and current of 45 mA. Scanning was done at 2θ angles from 1 to 10° with step size of 0.02^{o}, step time of 10 s, and slit width of 1/2°.

The X-ray diffraction patterns of the samples are presented below. Purely siliceous MCM-41 showed expected diffraction features that are characterized by a peak of relatively high intensity at a 2θ angle of ~ 2.0^{o} and smaller peaks between 2θ angles of 3 to 5°, all attributed to the hexagonally arranged two-dimensional pore structure of the material (Figure 4.3.2). Titanium-containing MCM-41 also showed similar features

(Figure 4.3.3). These peaks were absent in materials containing manganese or containing combinations of transition metal and organic functionalities (Figures 4.3.4 to 4.3.8). The absence of the characteristic peaks may have resulted from a high degree of disorder in the matrices.

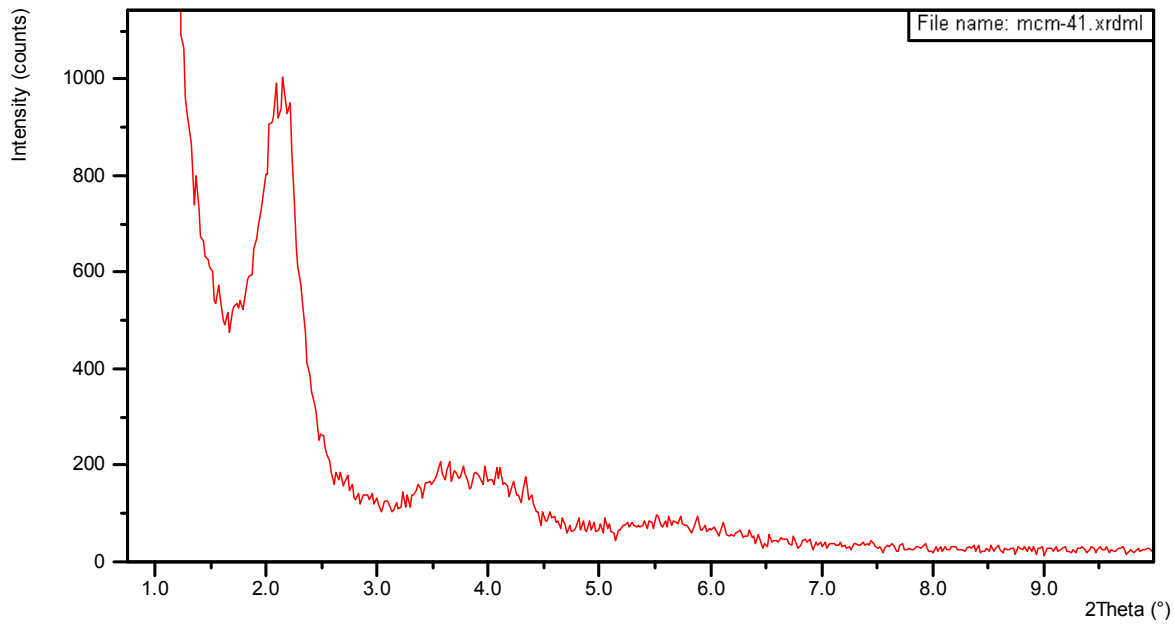

Figure 4.3.2. X-ray diffraction pattern of MCM-41.

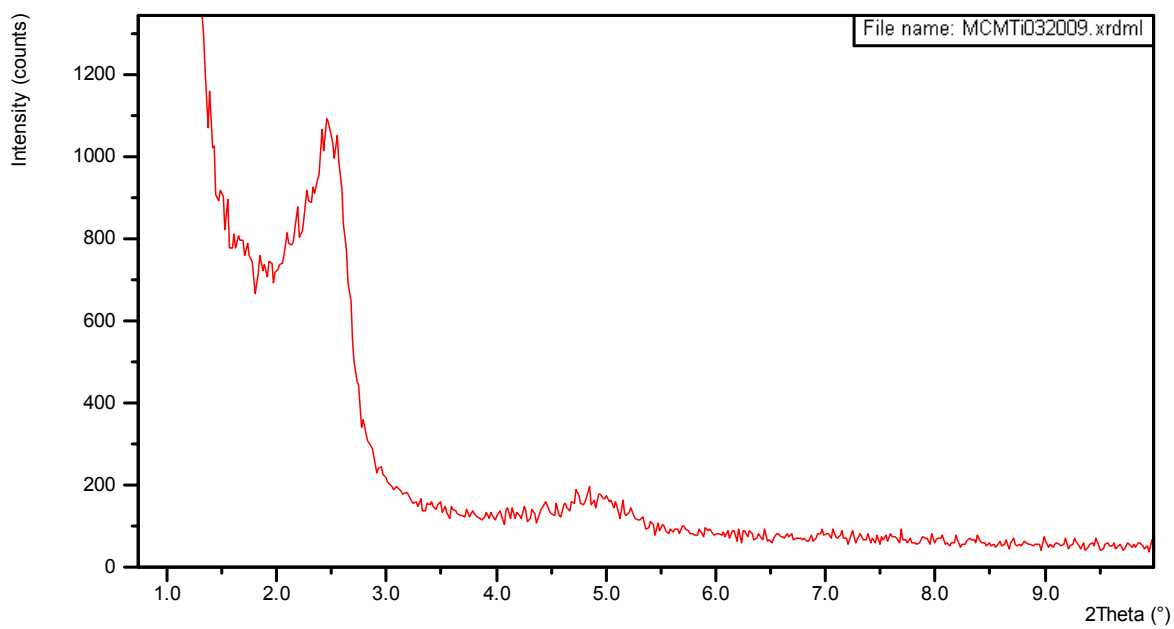

Figure 4.3.3. X-ray diffraction pattern of MCM-41 containing titanium.

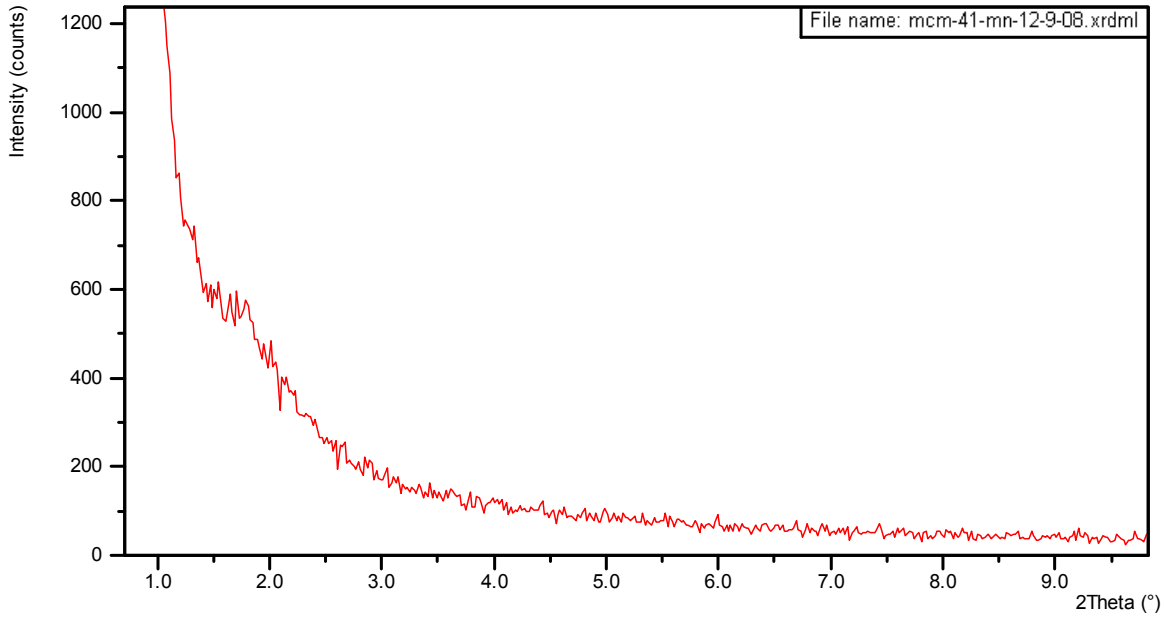

Figure 4.3.4. X-ray diffraction pattern of MCM-41 containing manganese.

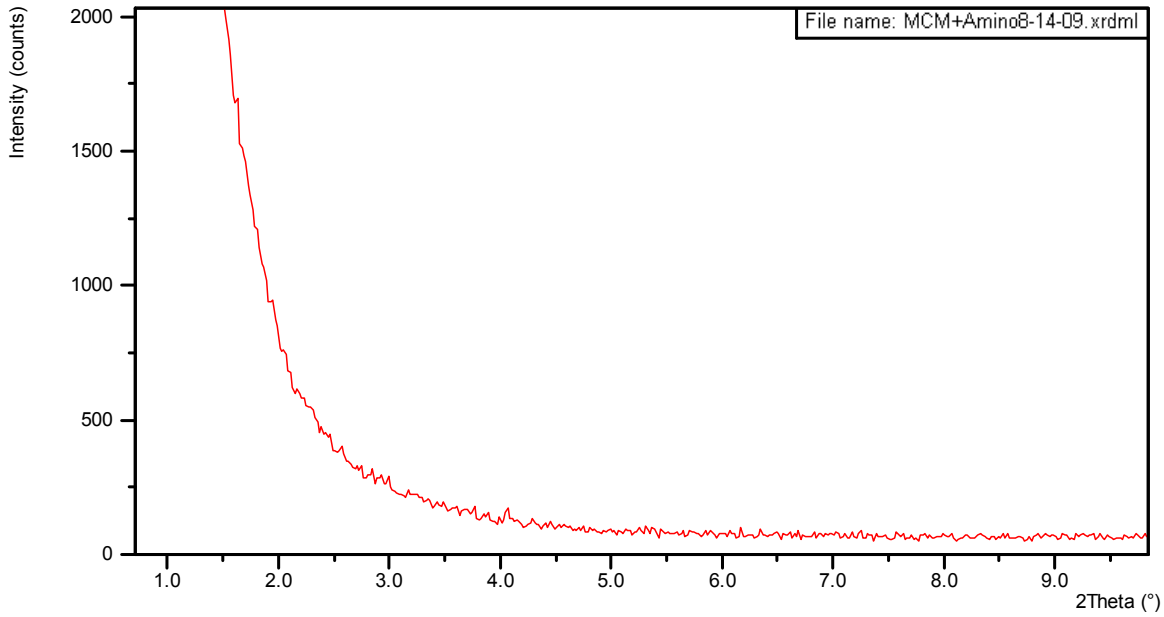

Figure 4.3.5. X-ray diffraction pattern of MCM-41 containing APTES organic functionality as pendant.

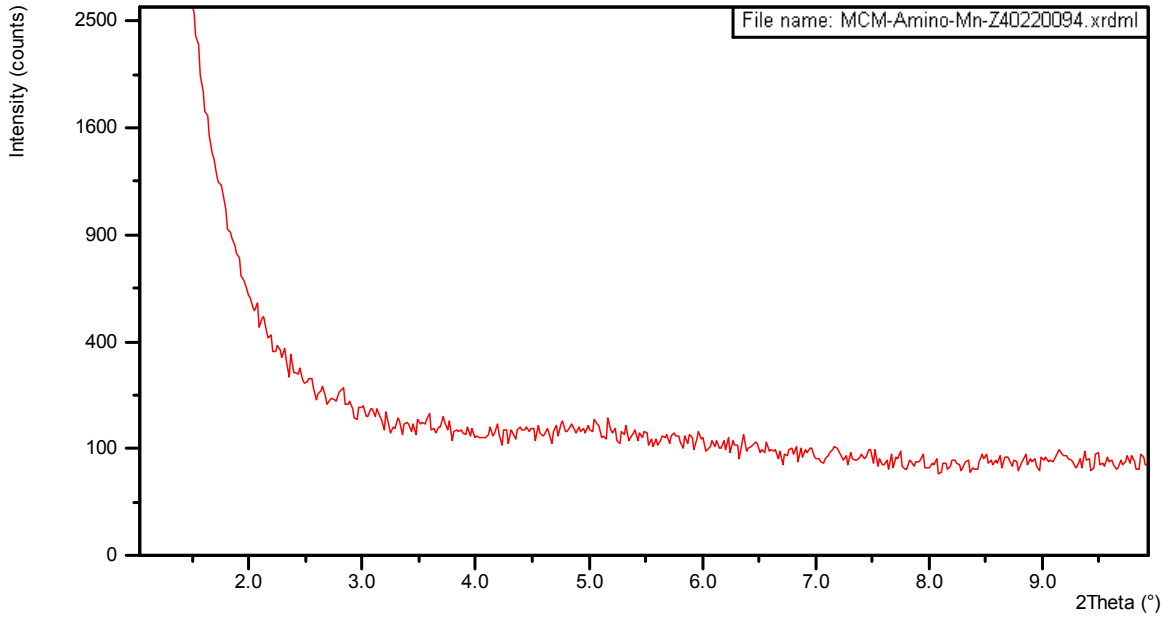

Figure 4.3.6. X-ray diffraction pattern of MCM-41 containing manganese and amino functionality as pendant.

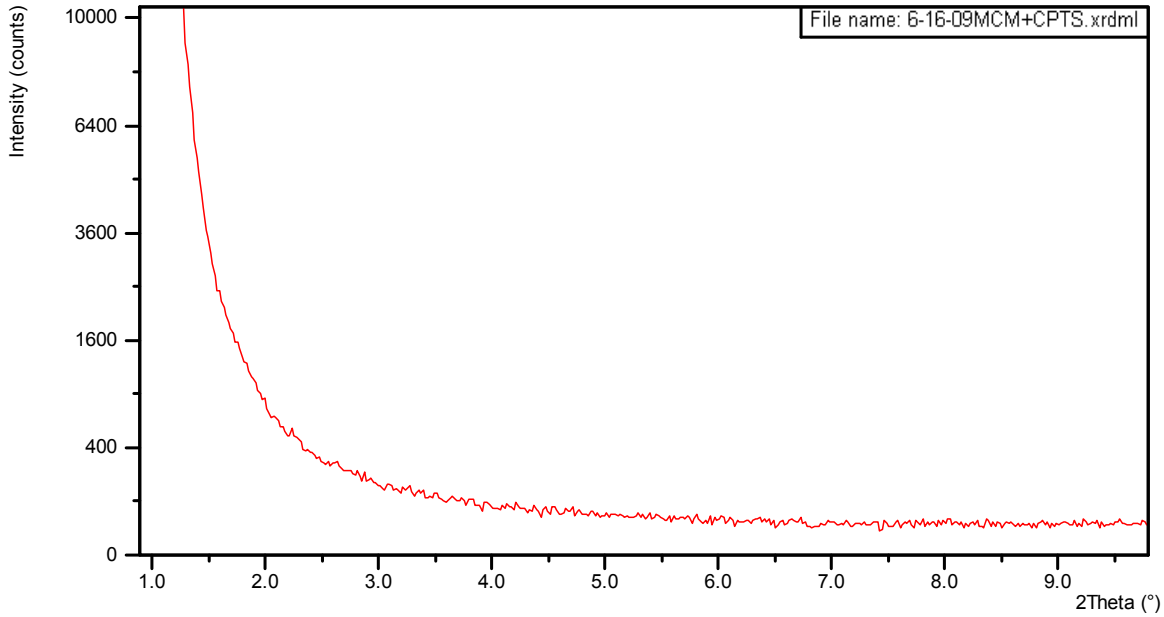

Figure 4.3.7. X-ray diffraction pattern of MCM-41 containing CPTMS organic functionality as pendant.

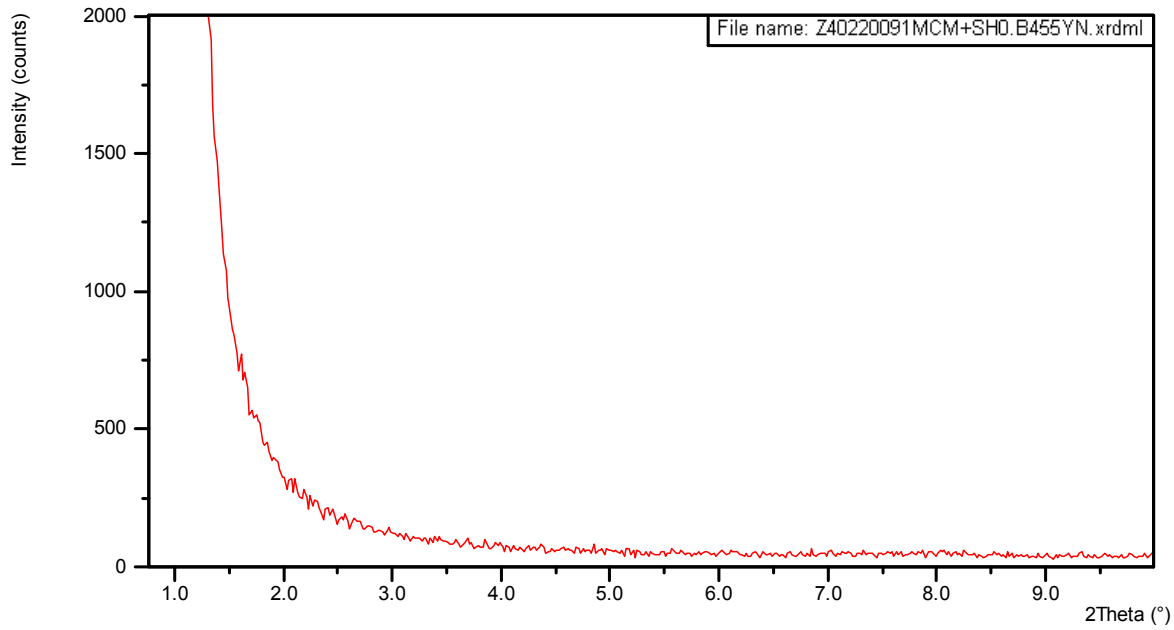

Figure 4.3.8. X-ray diffraction pattern of MCM-41 containing mercapto (−SH) organic functionality as pendant.

4.3.2. BET Surface Area and Pore Size Analyses

Multiple-point BET surface area and pore size analyses were conducted on a Micromeretics ASAP 2020 porosimeter. Samples were degassed under N_2 for 2 h at 200 ^{o}C and adsorption measurements were performed at 77 K with nitrogen adsorbate. The materials all show mesoporous (> 2 nm) pore size distributions, having median pore sizes from 3.3 to 5.7 nm. The surface areas ranged from 642 m^2/g for purely siliceous SBA-15 to 135 m^2/g for the mercapto-functionalized MCM-41 (Figures 4.3.9 to 4.3.12).

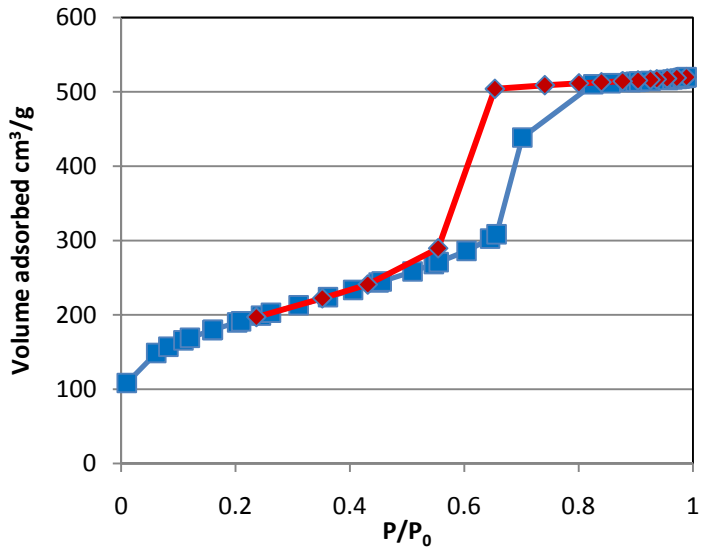

Figure 4.3.9. Nitrogen adsorption/desorption isotherms of SBA-15 sample. Pore size 5.44 nm, pore volume 0.62 cm^3/g, and surface area 642 m^2/g.

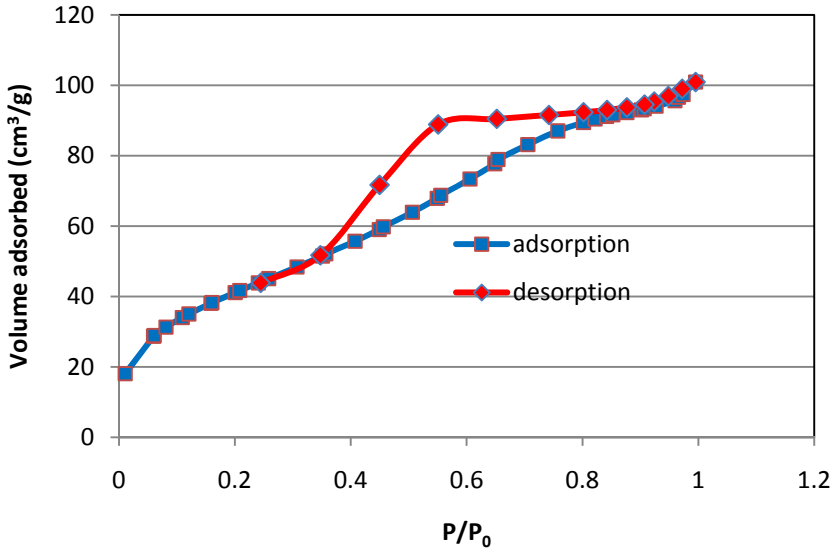

Figure 4.3.10. Nitrogen adsorption/desorption isotherms of MCM-41 with mercapto (−SH) functionality. Pore size 4.7 nm, pore volume 0.2 cm^3/g, and surface area 135 m^2/g.

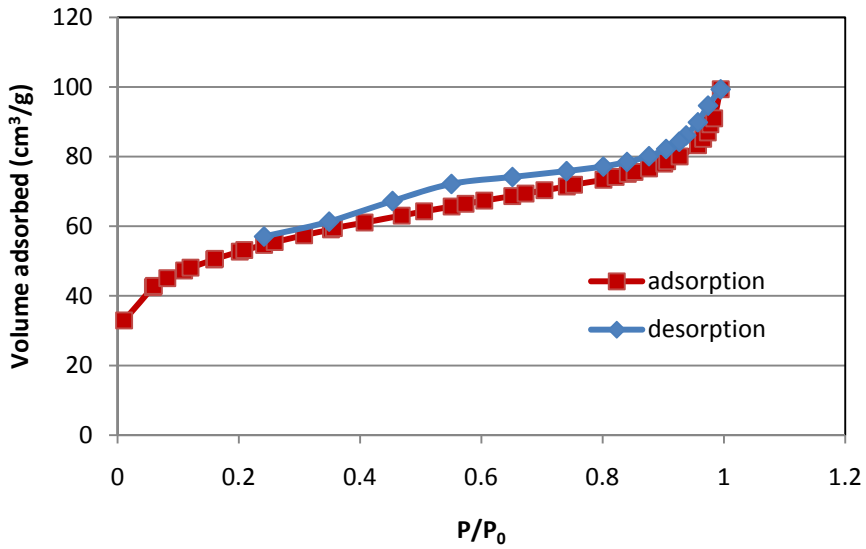

Figure 4.3.11. Nitrogen adsorption/desorption isotherms of MCM-41 with CPTMS functionality. Pore size 3.3 nm, pore volume 0.15 cm^3/g, and surface area 184 m^2/g.

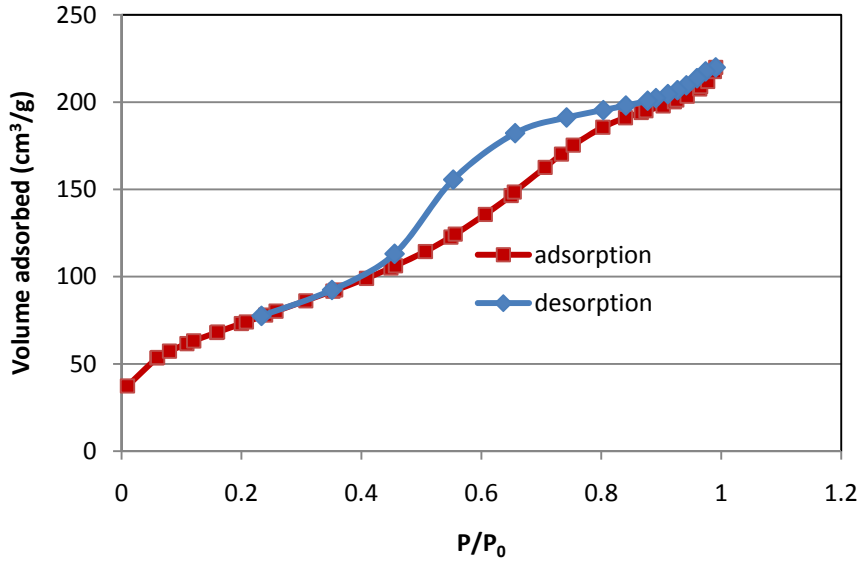

Figure 4.3.12. Nitrogen adsorption/desorption isotherms of MCM-41 with amino functionality. Pore size 5.7 nm, pore volume 0.33 cm^3/g, and surface area 235 m^2/g.

4.4. System Set Up for the Evaluation of Materials for Mercury Oxidation and Adsorption

4.4.1 Mercury Adsorption

The apparatus is shown in Figure 4.4.1. A weighed sample of the catalyst/sorbent to be tested is placed in a 15 cm long x 2 cm i.d. quartz column. The column is mounted in a vertical tube furnace equipped with a temperature controller. Mercury is introduced as saturated vapor in nitrogen flowing through a mercury permeation tube, then through the bed of the catalyst/sorbent in the quartz column. Effluent from the bed passes through a series of four small 30 mL impingers to collect elemental and oxidized mercury, based on a modified version of ASTM D6784-02, 2002. The first impinger contains chilled aqueous 1 M potassium chloride solution, to collect oxidized mercury. The second impinger, to trap elemental mercury, contains an aqueous solution of 5% v/v nitric acid and 10% v/v hydrogen peroxide. The third impinger contains an aqueous solution of 4% w/v potassium permanganate and 10% v/v sulfuric acid, and the last impinger contains silica gel. Each of the first three impingers contains a 30 mL aliquot of the absorbing solution. A one-hour sampling time is planned.

4.4.2. Mercury Analysis by Cold Vapor Atomic Adsorption Spectrophotometry

The amounts of mercuric chloride and elemental mercury captured in the impingers, as described in Section 4.4.1, are determined by Cold Vapor Atomic Adsorption Spectrophotometry, using the analyzer shown in Figure 4.4.2 (top). The analytical method for mercury was established in accordance with EPA Method 245.1. Calibration standards were prepared from certified reference solution, in the range from 0.2 to 10 μg/L, and used to establish a calibration curve, shown in Figure 4.4.2 (bottom).

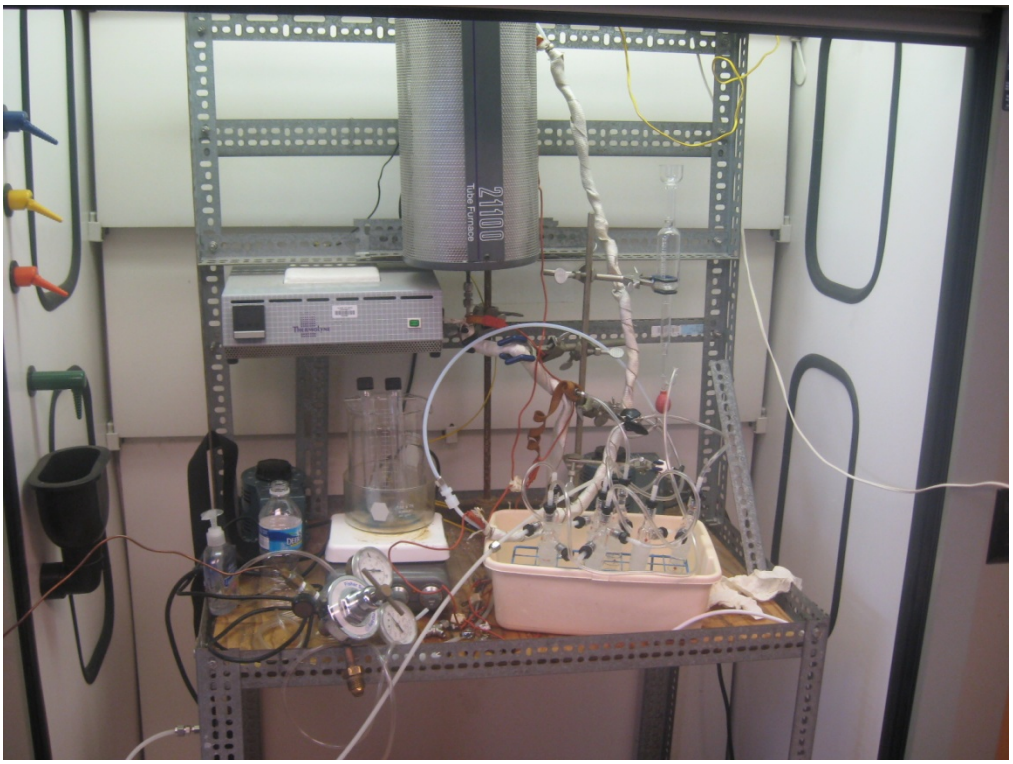

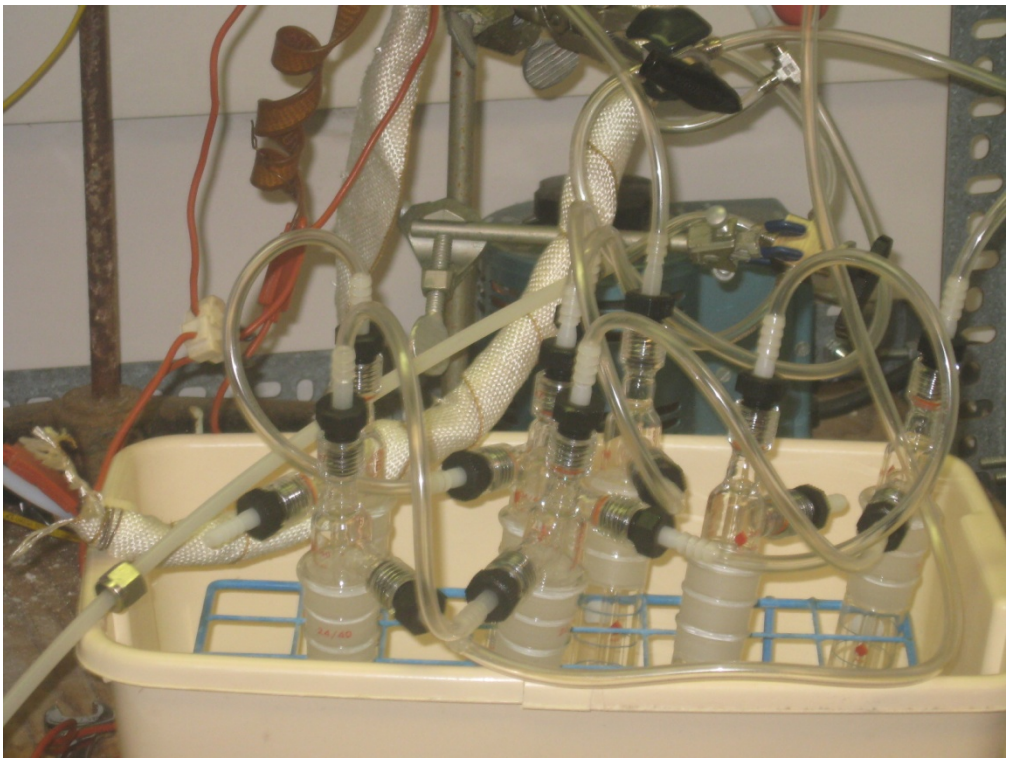

Figure 4.4.1. Photographs of the mercury oxidation/adsorption apparatus: mercury vaporization tube (top), tube heating furnace (top), and impingers and connecting tubes (bottom).

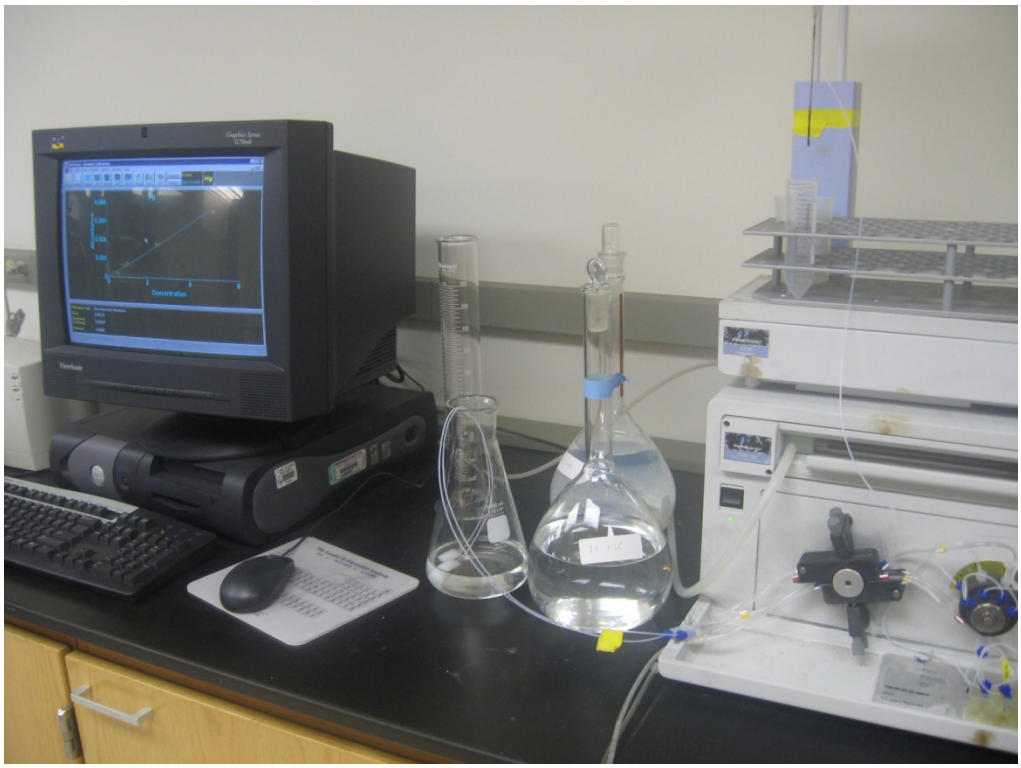

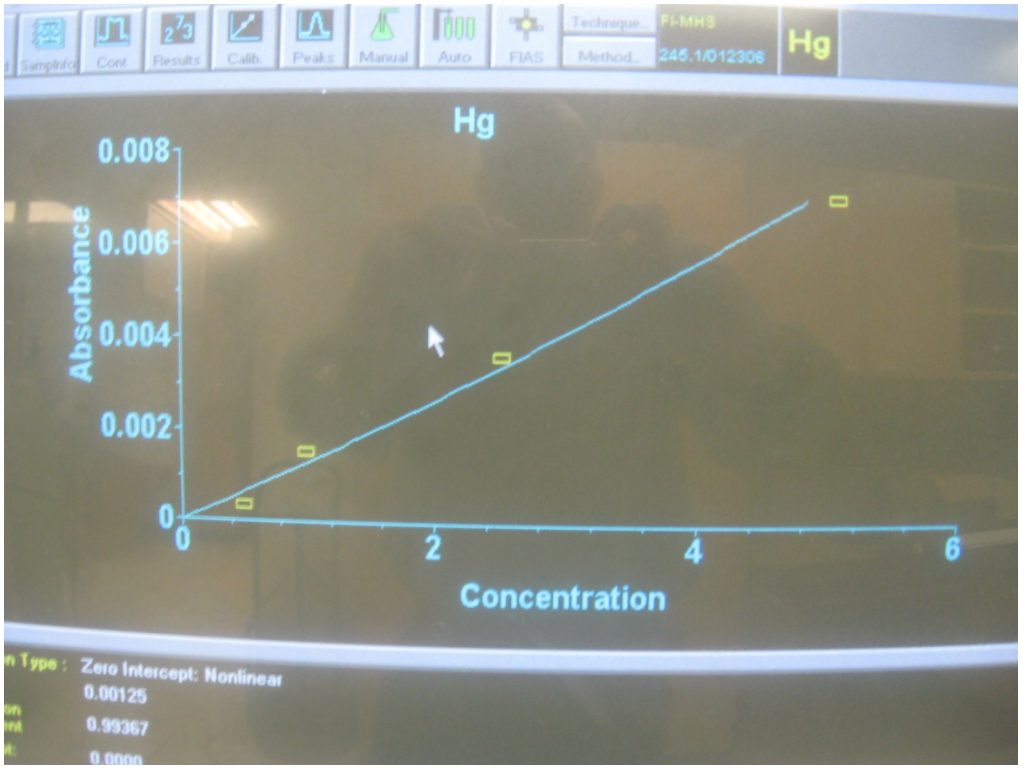

Figure 4.4.2. Photograph of the Perkin Elmer FIMS-100 Cold Vapor Atomic Adsorption Spectrometer, used for mercury analysis (top), and the mercury calibration curve (bottom).

5. Summary and Conclusion

The work performed under the project supports the development and implementation of technology for removal of mercury from flue gas produced by combustion of coal in industrial furnaces and electric utility boilers. The investigation had three components: (1) laboratory measurements of the effects of HCl and CO in coal combustion products on mercury and sulfur dioxide oxidation in the presence of selective catalytic reduction (SCR) catalyst and the effect of NH_3/NO ratio in SCR, (2) simulation of pilot-scale measurements of mercury oxidation and adsorption by unburned carbon and fly ash from combustion of coal, and (3) synthesis of combined catalysts and sorbents for low temperature oxidation and capture of mercury from flue gas.

5.1. Mercury and Sulfur Dioxide Oxidation during Selective Catalytic Reduction of Nitric Oxide

The extent of mercury oxidation over the monolithic V_2O_5-WO_3/TiO_2 SCR catalyst chosen for investigation was examined in the presence of 0 to 100 ppmv of HCl, covering the range from low-chlorine Powder River Basin subbituminous coals to moderate-chlorine bituminous coals. Measurements were made in the absence of NO and NH_3, in the presence of NO and absence of NH_3, and in the presence of both NO and NH_3. The extent of mercury oxidation was highly sensitive to the concentration of HCl at low levels of HCl, as reported by Eswaran and Stenger (2005), and was suppressed in the presence of NH_3, as observed by Machalek et al. (2003), Niksa and Fujiwara (2005b), Senior (2006), and Gale et al. (2006b), because ammonia competes with at least one of the reactants (Hg, HCl) for surface sites toward the entrance to the monolith, before the NH_3 is consumed by reaction with NO and where it is still present at significant concentration (Niksa and Fujiwara, 2005b). The extent of mercury oxidation was most variable in the presence of both NO and NH_3 at NH_3/NO ratios near stoichiometric, when small changes in conditions, such as the inlet levels of NO and NH_3, can cause large changes in the concentration of unreacted NH_3 toward the catalyst exit.

The extent of mercury oxidation was higher in the presence of 300 ppmv NO, without NH_3, than in the absence of both NO and NH_3, for all volume fractions of HCl, consistent with the findings by Hall et al. (1991) and Ghorishi (1998). It appears that NO is able to serve as an oxidizing agent for mercury or, possibly that, when NH_3 is absent, NO removes residual strongly-bound NH_3 left on the catalyst from previous tests, freeing active sites on the catalyst for mercury oxidation. The presence of NO in the absence of NH_3 is a condition that would exist if flue gas were passed through an SCR catalyst when NH_3 addition is not required for NO_X reduction to meet air quality regulations. However, sulfate formation is also enhanced by NO in the absence of NH_3 (Svachula et al., 1993).

The fraction of mercury oxidized was measured as a function of the ratio of NH_3 to NO at the catalyst inlet, at two levels of HCl (1 and 10-11 ppmv), in the presence of

300 to 345 ppmv NO at the catalyst inlet, and in the absence of CO. At the higher concentration of HCl, the effect of increasing the NH_3/NO ratio was small, until the ratio approached and exceeded stoichiometric, when excess ammonia would have been present throughout the length of the catalyst and competing for surface sites with mercury, HCl, or both, over the entire length of the catalyst channels (Niksa and Fujiwara, 2005b). Ammonia may also reduce $HgCl_2$ to Hg(0) by the following homogeneous reaction (Pritchard, 2008):

$$HgCl_2 + NH_3 + \tfrac{1}{4}O_2 \rightarrow Hg(0) + 2HCl + \tfrac{1}{2}N_2 + \tfrac{1}{2}H_2O \qquad \text{(Reaction 2.6)}$$

In the presence of the lower concentration of HCl, the decrease in extent of mercury oxidation with increasing NH_3/NO ratio was more significant, consistent with the predictions of Niksa and Fujiwara (2005b) and Senior (2006) and observations by Gale et al. (2006b). In the presence of 1 ppmv HCl and an NH_3/NO ratio at the catalyst inlet of 0.95, the fraction of mercury oxidized was less than 20%.

The possibility that CO in flue gas might interact with Cl adsorbed on SCR catalysts, and the need for examination of the effect of CO on mercury oxidation, were discussed by Presto et al. (2006) and Presto and Granite (2006). Dependence of the extent of mercury oxidation on CO volume fraction, in the presence of 1.9-2.2, 11-12, and 49-50 ppmv HCl, 313 and 329 ppmv NO, and NH_3/NO = 0.91 to 0.94, was measured over the range from 0 to ~2000 ppmv CO.

In the presence of 2 ppmv HCl, a level expected in combustion products from some Power River Basin subbituminous coals, an increase in CO from 0 to 50 ppmv reduced the extent of mercury oxidation from 24 ± 3 to 1 ± 4%. A level of 100 ppmv of CO was sufficient to completely suppress mercury oxidation when only 2 ppmv of HCl were present. In the presence of 11-12 ppmv HCl, increasing CO from 0 to ~120 ppmv reduced mercury oxidation from ~70% to 50%. Variation in the CO content of flue gas when burning low-chlorine coals, such as those from the Power River Basin, is thus another possible source of variability and uncertainty in the extent of mercury oxidation in SCR, in addition to the high sensitivity of mercury oxidation to HCl itself, at low HCl.

CO had little effect on mercury oxidation in the presence of 50 ppmv HCl. At that HCl level, an increase in CO from 5 to 250 ppmv resulted in no significant decrease in the extent of mercury oxidation, and an increase in CO from 5 to 2053 ppmv was required to reduce the extent of mercury oxidation from 82 ± 4% to 71 ± 3%.

Determination of the dependence of SO_2 oxidation on the three variables, HCl, NH_3/NO at the catalyst inlet, and CO, was undermined by the high degree of scatter in the measurements and the observation that conversion of SO_2 to sulfate in the presence of the SCR catalyst was similar, under many of the conditions investigated, to its conversion in the presence of sea sand used as the filler to maintain the same gas residence time in an "inert" reactor as in the SCR catalyst. It could not be established whether the SCR catalyst and sea sand were equally active as heterogeneous catalysts, whether SO_2 was oxidized by homogeneous reactions in both cases, or whether SO_2 was oxidized by a combination of homogeneous and heterogeneous reactions.

Measurements of sulfate formation as a function of HCl suggested that there is little dependence of SO_2 oxidation to sulfate in the SCR catalyst on HCl, or that the dependence, if it existed, could not be determined from the data. Measurements of sulfate formation versus NH_3/NO ratio, at 1 to 2.2 ppmv HCl and 10 to 12 ppmv HCl suggested that conversion of SO_2 to sulfate was highest in the absence of NH_3 and decreased with increasing NH_3/NO ratio and with increasing HCl, in contrast to the observation regarding dependence on HCl just above. Promotion of SO_2 oxidation in the complete absence of NH_3, and the gradual decline in SO_2 oxidation with increasing NH_3/NO ratio, are both consistent with observations reported by Svachula et al. (1993) and Gale et al. (2006b).

The tentative conclusions that may be drawn from the sulfate measurements are that sulfate formation decreased with increasing NH_3/NO ratio, may have been promoted by CO, and occurred to similar extents in the SCR catalyst and in the reactor containing sea sand. A dependence, or lack of dependence, of sulfate formation on HCl could not be established with any certainty.

A model describing catalytic oxidation of mercury by HCl during NO reduction by ammonia in the absence of CO was based upon the mechanisms and analyses of Niksa and Fujiwara (2005b) and Senior (2006). Niksa and Fujiwara assumed that HCl is adsorbed on the catalyst and reacts with gas-phase mercury, while Senior assumed that adsorbed mercury reacts with gas-phase HCl. Both assumed that gas-phase NO_X reacts with adsorbed NH_3. In the present model, mercury, HCl, and NH_3 are all assumed to be adsorbed on the catalyst surface, with mercury oxidation occurring by reaction of two adsorbed species. Although both NH_3 and HCl are adsorbed, they do not compete with each other for the same surface sites, but each competes for sites with elemental mercury. The flow through a catalyst channel was described as laminar and fully developed, with a one-dimensional treatment of radial diffusion and reaction at the catalyst wall. Pore diffusion in the catalyst wall, considered by Senior (2006), was neglected. The pseudo-steady-state rate equation was integrated step-by-step from the entrance to exit of a catalyst channel.

There are five adjustable parameters in the model for mercury oxidation: the reaction rate coefficients for NO + NH_3 and Hg(0) + HCl, and the adsorption equilibrium constants for NH_3, Hg(0), and HCl at the temperature of the catalyst. The best fit to the mercury measurements was obtained with a small value of the HCl adsorption equilibrium constant, suggesting that HCl is only weakly adsorbed. The proposed mechanism successfully reproduced qualitative features of both the HCl and NH_3/NO ratio dependence of mercury oxidation. However, at NH_3/NO ratios in the range from ~0.8 to ~1, the calculation overestimated the fraction of mercury oxidized at all levels of HCl investigated, a consequence of trying to obtain the best overall fit to the measurements, including those at higher and lower NH_3/NO ratios. Trials using other values of the adjustable parameters showed that, while it was relatively easy to fit the mercury measurements more accurately at HCl levels below about 10 ppmv (though at the expense of the fit to the NH_3/NO ratio trends), it was not possible, using the current

model, to reproduce the low values of the extent of mercury oxidation (80 to 85%) observed at high HCl levels.

Several mechanisms for the inhibition of mercury oxidation by CO were considered: (1) CO competes with mercury for active catalyst surface sites, (2) CO reduces adsorbed HgCl or $HgCl_2$ while one or both of these still reside on the catalyst surface, before desorption, and (3) CO destroys HgCl or $HgCl_2$ in the gas phase, after desorption from the catalyst. None of these mechanisms was able to explain, at least in the form examined, why the effect of CO on extent of mercury oxidation in SCR diminished with increasing HCl concentration. The model was not, therefore, able to capture the dependence of mercury oxidation on both CO and HCl.

Calculations to examine the possible effect of CO on homogeneous oxidation of mercury were performed by Balaji Krishnakumar in Joseph J. Helble's group at Dartmouth College (B. Krishnakumar and J. J. Helble, personal communication, 2008). Based on the simulations of the homogeneous system by Dr. Krishnakumar, CO is not expected to have a significant effect on the gas-phase oxidation of mercury over the entire post-combustion temperature range in coal-fired electric utility boilers, from the furnace exit to the stack (1177 to 77 ^{o}C), consistent with the experimental measurements reported by Kramlich and Castiglone (2004). The effect of CO, in the homogeneous system, is expected to be a slight promotion of mercury oxidation, rather than the inhibition of mercury oxidation observed in the present experiments with SCR catalyst. An explanation for the effect of CO on mercury oxidation in the SCR catalyst remains for future work.

Sulfate formation was treated using the rate expression for SO_3 formation during SCR of NO_X developed by Svachula et al. (1993), which describes the dependence of the rate on all of the species, SO_2, O_2, SO_3, H_2O, NO_X, and NH_3. The empirical factor introduced by these authors to account for the promotion of SO_2 oxidation by NO_X was not included. An effect of HCl was incorporated in the rate expression of Svachula et al. by assuming that it competes with SO_2 for active sites on the catalyst surface. This required a much larger adsorption coefficient for HCl than was needed to describe the competition of HCl with Hg(0) for surface sites.

Calculations of SO_3 formation were compared with the measurements of sulfate versus NH_3/NO ratio and HCl. The calculated dependence of SO_3 formation on NH_3/NO ratio was in satisfactory agreement with the measurements of sulfate at both the intermediate (10 to 12 ppmv) and low (1 to 2.2 ppmv) HCl levels, with the exception of the measurements at high NH_3/NO ratio in the presence of 10 to 12 ppmv HCl, near the detection limit of the controlled condensation procedure, and the measurements at NH_3/NO = 0, where the promotion of SO_3 formation by NO is greatest, a component of the rate expression of Svachula et al. (1993) not included in the calculations. Interpretation of the data using the model is complicated by the uncertainties regarding the effect of HCl on sulfate formation and the contribution of the SCR catalyst to sulfate formation. Effects, if they exist, of CO and HCl on SO_2 oxidation, remain to be established in future work.

5.2. Mercury Oxidation and Removal by Unburned Carbon and Fly Ash

CHEMKIN 4.0.2 (Kee et al., 2005; Reaction Design, 2005, 2006), was used to simulate mercury oxidation and removal measurements obtained while firing bituminous coals (Gale, 2006) and blends of Powder River Basin coal with bituminous coals (Gale, 2005), in experiments at pilot scale in the Combustion Research Facility at Southern Research Institute. The focus, in the experiments, was on moderate-to-low chlorine and moderate-to-low sulfur fuels.

The data set from the pilot-scale experiments consisted of: (1) measurements of the distribution of mercury between elemental and oxidized states and the fraction of mercury adsorbed on fly ash and unburned carbon at the inlet to the baghouse in the CRF while firing blends of Powder River Basin coal with Blacksville and Choctaw America hvAb coals, providing systematic variation of the chlorine and unburned carbon contents of flue gas and the CaO to unburned carbon ratio (Gale, 2005), and (2) measurements of mercury oxidation and removal across the baghouse while firing three high volatile bituminous coals (Galatia, Blacksville, and Choctaw America), with flue gas subjected to two thermal histories (normal and high gas quench rates); and three unburned carbon (UBC) levels in the fly ash (low, < 1% UBC; medium, 1% < UBC < 7%; and high, > 7% UBC) (Gale, 2006).

There was a clear correlation in the experimental data between unburned carbon and mercury removal, but only a weak correlation between unburned carbon and the extent of mercury oxidation. A synergistic effect of coal blending enhanced mercury removal across the baghouse. Change in the HCl volume fraction had relatively weak influence on mercury oxidation or removal, over the range investigated, from 10 to 190 ppmv HCl.

A mechanism consisting of nine homogeneous and heterogeneous reactions for mercury oxidation and removal was developed to interpret the data. The model includes chlorination of carbon sites by reaction with HCl(g) to form the adsorbed species, HCl(C) (the "C" in parentheses is intended to indicate adsorption on solid carbon surface); reaction of elemental vapor phase mercury, Hg(g), with the chlorinated sites to form adsorbed mercurous chloride, HgCl(C); and desorption of HgCl(C) back to the flue gas as HgCl(g). A mechanism proposed by Gale (2005), in which calcium reacts with HgCl(g) vapor after its desorption from carbon surface, but prior to its conversion to $HgCl_2$(g), was adopted to account for the effect of calcium on mercury removal.

The unknown pre-exponential factors, temperature exponents, and activation energies in Arrhenius-type rate coefficients were found by coupling the Simplex Centroid (Nelder and Mead, 1965) FORTRAN code with the CHEMKIN Release 4.0.2 software (Kee et al., 2005; Reaction Design, 2005, 2006) and minimizing the differences between the experimental results and the values calculated using the model.

The removal of mercury by fly ash and unburned carbon in the flue gas from combustion of the bituminous coals, at both high and low temperatures, was reproduced

with good accuracy by the simulation. The mercury removal measurements for the coal blends were approximately reproduced, with removal greatly over-predicted for only two runs. The effect on mercury removal by fly ash and unburned carbon from the blends was due primarily to the increase in mercury capture in the presence of calcium.

The extent of mercury oxidation, on the other hand, in flue gas from combustion of both the bituminous coals and the blends of PRB with bituminous coals, was not so well explained, because of oversensitivity of the oxidation process in the model to the concentration of unburned carbon. Cases whose extents of mercury oxidation were greatly under-predicted by the model were those having the lowest unburned carbon and lowest HCl volume fractions.

A subsequent series of experiments at pilot scale, again in the CRF at Southern Research Institute but under a separate project, was conducted with blends of PRB with Eastern and Western bituminous coals, covering the range of blend composition from 100% PRB to 100% bituminous coal (Gale, Lani, and Offen, 2008). The mercury removal measurements at the inlet and exit from the ESP were fit using an empirical expression containing six terms: linear and quadratic terms in the UBC concentration in flue gas, linear and quadratic terms in the CaO concentration in flue gas, a term containing the product of UBC and CaO concentrations, and a constant. The two variables, UBC and CaO concentration, five coefficients, and the constant were sufficient to reproduce the measurements at the inlet and exit from the ESP while firing the PRB-Western bituminous coal blends and at the exit from the ESP while firing the PRB-Eastern bituminous coal blends, with R^2 values from 0.74 to 0.89 for the least-squares multiple regression analysis (Gale, Lani, and Offen, 2008). The UBC and CaO concentrations alone were therefore able to explain both the effect of UBC and the synergistic effect between UBC and CaO in ash on mercury removal at the entrance and exit from the ESP, under the low chlorine (2 to 50 ppmv HCl) and low SO_3 conditions investigated.

5.3. Toward the Development of Combined Catalysts and Sorbents for Low Temperature Oxidation and Removal of Mercury from Flue Gas

Methods were investigated for the synthesis of combined catalyst/sorbent systems, based on surfactant-templated nanoporous silicas containing a transition metal and an organic functionality. High thermal stability and high capacity to oxidize and capture mercury are the primary performance objectives. The proposed materials are based on the highly ordered, high surface area (~ 1000 m^2/g), thermally stable, surfactant-templated nanoporous (> 2 nm) silicates and aluminosilicates, MCM-41 (Mobil Composition of Matter; Kresge et al., 1992), MSU (Michigan State University; Bagshaw et al., 1995) and SBA-15 (University of California, Santa Barbara; Zhao et al., 1998), that have shown great potential for applications as sorbents, catalysts, and catalyst supports.

The object of the work is to create crystalline or highly ordered multifunctional nanoporous organosilicates, by incorporating both metal ions and organic functionalities within the pore structure of the materials, able to oxidize elemental mercury and adsorb

the resulting oxidized mercury simultaneously. By optimizing composition and physical properties, combination of several desirable characterisitics is expected to be possible in a single material: high thermal and mechanical stability, imparted by the silicate content, and flexible and tunable surface properties, resulting from the incorporation of the proper metal ions and organic functionalities in the framework.

Surfactant-templated mesoporous organic-inorganic silicates were synthesized according to the methods of Burleigh et al. (2004). The introduction of organic functionalities to form the proposed metal-containing nanoporous materials was accomplished by directly co-condensing the organoalkoxysilane precursors with the siloxane silica source. The organosilicate precursors were:

3-aminopropyltriethoxysilane,
mercaptopropyltrimethoxysilane,
3-chloropropyltrimethoxysilane, and
tetraethylorthosilicate.

The surfactant template was cetyltrimethylammonium bromide, $C_{16}H_{33}N(CH_3)_3Br$. Twelve mesoporous organosilicate catalysts/sorbents were synthesized, with and without metals (manganese, titanium, vanadium) and organic functional groups (aminopropyl, chloropropyl, mercaptopropyl).

The x-ray diffraction pattern of the purely siliceous MCM-41 showed the expected diffraction features, attributed to the hexagonally arranged two-dimensional pore structure of the material. Titanium-containing MCM-41 showed similar features. However, those features were absent in materials containing manganese or combinations of transition metal and organic functionalities. The absence of the characteristic peaks in the diffraction patterns of the latter materials may have resulted from a high degree of disorder in their matrices.

Multiple-point BET surface area and pore size analyses were conducted at 77 K using nitrogen adsorbate. The materials all showed mesoporous (> 2 nm) pore size distributions having median pore sizes from 3.3 to 5.7 nm. Their surface areas ranged from 642 m^2/g for purely siliceous SBA-15 to 135 m^2/g for the mercapto-functionalized MCM-41.

A system was set up for measurement of mercury oxidation and adsorption by the candidate materials, to be investigated in future work.

References

Bagshaw, S. A., Prouzet, E., Pinnavaia, T. J., Templating of Mesoporous Molecular Sieves by Nonionic Polyethylene Oxide Surfactants, *Science 269* (1995) 1242-1244.

Bhopatkar, N. S., Prediction of Mercury Speciation in Coal-Combustion Systems, M.S. Thesis, Department of Mechanical Engineering, University of Alabama at Birmingham, 2006.

Bhopatkar, N. S., Gale, T. K., Walsh, P. M., and Ban, H., Prediction of Mercury Speciation in Coal Combustion Systems, Presented at the Huntsville Simulation Conference 2005, Society for Modeling and Simulation International, Huntsville, AL, October 26-27, 2005.

Burleigh, M. C., Jayasundera, S., Spector, M. S., Thomas, C. W., Markowitz, M. A., and Gaber, B. P., A New Family of Copolymers: Multifunctional Periodic Mesoporous Organosilicas, *Chemistry of Materials, 16* (2004) 3-5.

Chang, R., Controlling Mercury Emissions from Power Plants: Status, Issues, and R&D Needs, Symposium on Mercury and other Trace Elements in Fuel: Emissions and Control, Division of Fuel Chemistry, American Chemical Society, 235th National Meeting, New Orleans, LA, April 6-10, 2008. *Preprints of Papers - American Chemical Society, Division of Fuel Chemistry 53(1)* (2008) 18-19.

Dajnak, D., Clark, K. D., Lockwood, F. C., and Reed, G., The Prediction of Mercury Retention in Ash from Pulverised Combustion of Coal and Sewage Sludge, *Fuel 82* (2003) 1901-1909.

Eswaran, S., and Stenger, H. G., Understanding Mercury Conversion in Selective Catalytic Reduction (SCR) Catalysts, *Energy & Fuels, 19* (2005) 2328-2334.

Fujiwara, N., Fujita, Y., Tomura, K., Moritomi, H., Tuji, T., Takasu, S., and Niksa, S., Mercury Transformations in the Exhausts from Lab-Scale Coal Flames, *Fuel 81* (2002) 2045-2052.

Galbreath, K. C., Zygarlicke, C. J., and Toman, D. L., Mercury-Chlorine-Fly Ash Interactions in a Coal Combustion Flue Gas, Paper No. 98-A1045, Proceedings of the Air and Waste Management Association 91st Annual Meeting, San Diego, CA, June 14-18, 1998.

Gale, T. K., Mercury Control with Calcium-Based Sorbents and Oxidizing Agents, Topical Report prepared for the U.S. Department of Energy under Agreement No. DE-FC26-01NT41183, June 2002.

Gale, T. K., Mercury Control with Calcium-Based Sorbents and Oxidizing Agents, Final Report prepared for the U.S. Department of Energy under Agreement No. DE-PS26-04NT41183, July 2005.

Gale, T. K., Understanding Mercury Chemistry in Coal-Fired Boilers, Report No. 1014418, EPRI, Palo Alto, CA, Southern Company Services, Inc., Birmingham, AL, MidAmerican Energy Holdings, Davenport, IA, Dynegy Midwest Generation, Inc., Decatur, IL, Arkansas Electric Cooperative Corporation, Little Rock, AR, American Electric Power Service Corporation, Columbus, OH, Tennessee Valley Authority, Chattanooga, TN, U.S. Environmental Protection Agency, Research Triangle Park, NC, U.S. DOE National Energy Technology Laboratory, Pittsburgh, PA, October 2006.

Gale, T. K., Bhopatkar, N. S., and Ban, H., Kinetics of Ca-C Synergism during Mercury Adsorption on Fly Ash in Coal-Fired Power Stations, Air Quality V Conference, Arlington, VA, September 18-21, 2005.

Gale, T. K., Bhopatkar, N. S., Ban, H., Lani, B. W., and Offen, G. R., Quantitative Prediction of Hg-Capture Enhancement by Calcium, Paper No. 122, Proceedings of the EPA-DOE-EPRI-A&WMA Power Plant Air Pollutant Control "Mega" Symposium, Baltimore, MD, August 28-31, 2006a.

Gale, T. K., Blankenship, G. A., Hinton, W. S., Cannon, J. W., and Lani, B. W., Hg Oxidation Compared for Three Different Commercial SCR Catalysts, Paper No. 55, Proceedings of the EPA-DOE-EPRI-A&WMA Power Plant Air Pollutant Control "Mega" Symposium, Baltimore, MD, August 28-31, 2006b.

Gale, T. K., Lani, B. W., and Offen, G. R., Mechanisms Governing the Fate of Mercury in Coal-Fired Power Systems, *Fuel Processing Technology 89* (2008) 139-151.

Ghorishi, S. B., Fundamentals of Mercury Speciation and Control in Coal-Fired Boilers, U.S. Environmental Protection Agency, EPA-600/R-98-014 (NTIS PB98-127095), February 1998.

Ghorishi, B., and Gullett, B. K., Sorption of Mercury Species by Activated Carbons and Calcium-Based Sorbents: Effect of Temperature, Mercury Concentration, and Acid Gases, *Waste Management & Research 16* (1998) 582-593.

Ghorishi, S. B., and Sedman, C. B., Low Concentration Mercury Sorption Mechanisms and Control by Calcium-Based Sorbents: Application in Coal-Fired Processes, *Journal of the Air & Waste Management Association 48* (1998) 1191-1198.

Ghorishi, S. B., Singer, C. F., Jozewicz, W. S., Sedman, C. B., and Srivastava, R. K., Simultaneous Control of Hg^0, SO_2, and NO_X by Novel Oxidized Calcium-Based Sorbents, *Journal of the Air & Waste Management Association 52* (2002) 273-278.

Hall, B., Schager, P., and Lindqvist, O., Chemical Reactions of Mercury in Combustion Flue Gases, *Water, Air, & Soil Pollution 56* (1991) 3-14.

Kee, R. J., Rupley, F. M., Miller, J.A., Coltrin, M. E., Grcar, J.F., Meeks, E., Moffat, H. K., Lutz, A.E., Dixon-Lewis, G., Smooke, M.D., Warnatz, J., Evans, G.H., Larson, R.S., Mitchell, R.E., Petzold, L.R., Reynolds, W.C., Caracotsios, M., Stewart, W. E., Glarborg, P., Wang, C., McLellan, C. L., Adigun, O., Houf, W.G., Chou, C.P., Miller, S.F., Ho, P., Young, P.D., and Young, D.J., CHEMKIN Release 4.0.2, Reaction Design, San Diego, CA, 2005.

Kolker, A., Senior, C. L., and Quick, J. C., Mercury in Coal and the Impact of Coal Quality on Mercury Emissions from Combustion Systems, *Applied Geochemistry 21* (2006) 1821-1836.

Kramlich, J. C., and Castiglone, L., The Forcing of Mercury Oxidation as a Means of Promoting Low-Cost Capture, Final Report to the U.S. Department of Energy, Grant No. DE-FG26-01NT41288, University of Washington, Seattle, WA, March 2004.

Kresge, C. T., Leonowicz, M. E., Roth, W. J., Vartuli, J. C., and Beck, J. S., Ordered Mesoporous Molecular Sieves Synthesized by a Liquid-Crystal Template Mechanism, *Nature 359* (1992) 710-712.

Krishnakumar, B., and Helble, J. J., Understanding Mercury Transformations in Coal-Fired Power Plants: Evaluation of Homogeneous Hg Oxidation Mechanisms, *Environmental Science & Technology 41* (2007) 7870-7875.

Lissianski, V., Maly, P., Ho, L., Zamansky, V., England, G, and Seeker, R., Multi-Pollutant Control for Boilers Firing PRB Coals, Paper No. 8, Proceedings of the DOE-EPRI-EPA-A&WMA Combined Power Plant Air Pollutant Control Mega Symposium, Washington, DC, May 19-22, 2003.

Machalek, T., Ramavajjala, M., Richardson, M., Richardson, D. C., Goeckner, B., Anderson, H., and Morris, E., Pilot Evaluation of Flue Gas Mercury Reactions across an SCR Unit, Paper No. 64, Proceedings of the EPA-DOE-EPRI-A&WMA Power Plant Air Pollutant Control "Mega" Symposium, Washington, DC, May 19-22, 2003.

Meischen, S. J., Van Pelt, V. J., Zarate, E. A., and Stephens, E. A., Jr., Gas-Phase Mercury Reduction to Measure Total Mercury in the Flue Gas of a Coal-Fired Boiler, *Journal of the Air & Waste Management Association 54* (2004) 60-67.

Merritt, R. L., McCain, J. D., and Cushing, K. M., Evaluation of TVA's Dry Conversion System for Gas Pretreatment Upstream of a Vapor Phase Mercury Monitor, Revised Draft prepared for the Electric Power Research Institute by the Southern Research Institute, Birmingham, AL, February 1, 2005.

Nelder, J. A., and Mead, R., A Simplex Method for Function Minimization, *Computer Journal, 7* (1965) 308-313.

Niksa, S., and Fujiwara, N., Predicting Extents of Mercury Oxidation in Coal-Derived Flue Gases, *Journal of the Air & Waste Management Association 55* (2005a) 930-939.

Niksa, S., and Fujiwara, N., A Predictive Mechanism for Mercury Oxidation on Selective Catalytic Reduction Catalysts under Coal-Derived Flue Gas, *Journal of the Air & Waste Management Association 55* (2005b) 1866-1875.

Niksa, S., Helble, J. J., and Fujiwara, N., Kinetic Modeling of Homogeneous Mercury Oxidation: The Importance of NO and H_2O in Predicting Oxidation in Coal-Derived Systems, *Environmental Science & Technology 35* (2001) 3701-3706.

Niksa, S., Fujiwara, N., Fujita, Y., Tomura, K., Moritomi, H., Tuji, T., and Takasu, S., A Mechanism for Mercury Oxidation in Coal-Derived Exhausts, *Journal of the Air & Waste Management Association, 52* (2002) 894-901.

Pavlish, J. H., Sondreal, E. A., Mann, M. D., Olson, E. S., Galbreath, K. C., Laudal, D. L., and Benson, S. A., Status Review of Mercury Control Options for Coal-Fired Power Plants, *Fuel Processing Technology 82* (2003) 89-165.

Pinto, N. G., and Smirniotis, P. G., Simultaneous Removal of NO_X and Mercury in Low Temperature Selective Catalytic and Adsorptive Reactor, Final Report to U.S. DOE under Grant No. DE-FG26-04NT42180, University of Cincinnati, Cincinnati, OH, August 2006.

Presto, A. A., and Granite, E. J., Survey of Catalysts for Oxidation of Mercury in Flue Gas, *Environmental Science & Technology 40* (2006) 5601-5609.

Presto, A. A., Granite, E. J., Karash, A., Hargis, R. A., O'Dowd, W. J., and Pennline, H. W., A Kinetic Approach to the Catalytic Oxidation of Mercury in Flue Gas, *Energy & Fuels 20* (2006) 1941-1945.

Pritchard, S., Catalyst Management: The Key to SCR Effectiveness, *Modern Power Systems*, Global Trade Media, Progressive Media Group Ltd., May 1, 2008. http://www.modernpowersystems.com/story.asp?sectionCode=88&storyCode=2050553 (accessed February 2009).

Qiu, J., Sterling, R., and Helble, J. J., Kinetic Modeling of Cl-Containing Species Transformations and their Effects on Mercury Oxidation under Simulated Coal Combustion Conditions, Proceedings of the 12th International Conference on Coal Science, Cairns, Australia, November 2003.

Reaction Design, San Diego, CA. CHEMKIN Release 4.0.2, 2005, and CHEMKIN Release 4.1, 2006. http://www.reactiondesign.com/lobby/open/index.html

Senior, C. L., Behavior of Mercury in Air Pollution Control Devices on Coal-Fired Utility Boilers, Power Production in the 21st Century: Impacts of Fuel Quality and Operations, Engineering Foundation Conference, Snowbird, UT, October 28-November 2, 2001.

Senior, C. L., Oxidation of Mercury across Selective Catalytic Reduction Catalysts in Coal-Fired Power Plants, *Journal of the Air & Waste Management Association 56* (2006) 23-31.

Senior, C. L., and Johnson, S. A., Impact of Carbon-in-Ash on Mercury Removal across Particulate Control Devices in Coal-Fired Power Plants, *Energy & Fuels 19* (2005) 859-863.

Senior, C. L., Sarofim, A. F., Zeng, T., Helble, J. J., and Mamani-Paco, R., Gas-Phase Transformations of Mercury in Coal-Fired Power Plants, *Fuel Processing Technology 63* (2000a) 197-213.

Senior, C. L., Helble, J. J., and Sarofim, A. F., Emissions of Mercury, Trace Elements, and Fine Particles from Stationary Combustion Sources, *Fuel Processing Technology 65-66* (2000b) 263-288.

Senior, C., Fry, A., Montgomery, C., Sarofim, A., and Wendt, J., Modeling Tool for Evaluation of Utility Mercury Control Strategies, Paper No. 23, Proceedings of the EPA-DOE-EPRI-A&WMA Power Plant Air Pollutant Control "Mega" Symposium, Baltimore, MD, August 28-31, 2006.

Singer, C. F., Ghorishi, B., and Sedman, C. B., Lime Based Multi-Pollutant Sorbents, Paper No. 242, EPRI-EPA-DOE-A&WMA Combined Power Plant Air Pollutant Control Mega Symposium and A&WMA Specialty Conference on Mercury Emissions: Fate, Effects, and Control, Chicago, IL, August 20-23, 2001.

Sjostrom, S., Smith, J., Hunt, T., Chang, R., and Brown, T. D., Demonstration of Dry Carbon-Based Sorbent Injection for Mercury Control in Utility ESPs and Baghouses, Paper No. 97-WA72A.07, Proceedings of the Air and Waste Management Association 90th Annual Meeting, Toronto, Ontario, June 8-13, 1997.

Sjostrom, S., Starns, T., Amrhein, J., Bustard, J., Durham, M., Penrod, W., Linville, C., O'Palko, A., and Chang, R., Full-Scale Evaluation of Mercury Control by Injecting Activated Carbon Upstream of a Spray Dryer and Fabric Filter on PRB Coal, Presented at PowerGen, Orlando, FL, November 29-December 2, 2004.

Srivastava, R., Lee, C. W., Ghorishi, B., Jozewicz, W., and Hasting, T. W., Evaluation of SCR Catalysts for Combined Control of NO_X and Mercury, Final Technical Report to the Illinois Clean Coal Institute, Project No. 02-1/2.2A-1, 2003.

Starns, T., Bustard, J., Durham, M., Lindsey, C., Martin, C., Schlager, R., Donnelly, B., Sjostrom, S., Harrington, P., Haythornthwait, S., Johnson, R., Morris, E., Chang, R., and Renninger, S., Full-Scale Test of Mercury Control with Sorbent Injection and an ESP at Wisconsin Electric.s Pleasant Prairie Power Plant, Paper No. 43249, Air & Waste Management Association, 95th Annual Conference, Baltimore, MD, June 23-27, 2002.

Svachula, J., Alemany, L. J., Ferlazzo, N., Forzatti, P., and Tronconi, E., Oxidation of SO_2 to SO_3 over Honeycomb DeNoxing Catalysts, *Industrial and Engineering Chemistry Research 32* (1993) 826-834.

Tong, G., Oxidation of Mercury during Selective Catalytic Reduction of Nitric Oxide, Ph.D. Dissertation, Interdisciplinary Engineering, University of Alabama at Birmingham, Birmingham, AL, 2009.

Tong, G., Blankenship, G. A., O'Neal, J. S., Gale, T. K., Ban, H., and Walsh, P. M., Oxidation of Mercury during Selective Catalytic Reduction of Nitric Oxide, Symposium on Mercury and Trace Metal Transformations: Modeling, Division of Fuel Chemistry, American Chemical Society, 234th National Meeting, Boston, MA, August 19-23, 2007. *Preprints of Papers - American Chemical Society, Division of Fuel Chemistry 52(2)* (2007) 513-514.

Tong, G., Walsh, P. M., Blankenship, G. A., and Gale, T. K., Measurements and Modeling of Mercury and Sulfur Dioxide Oxidation during Selective Catalytic Reduction of Nitric Oxide, Symposium on Mercury and other Trace Elements in Fuel: Emissions and Control, Division of Fuel Chemistry, American Chemical Society, 235th National Meeting, New Orleans, LA, April 6-10, 2008. *Preprints of Papers - American Chemical Society, Division of Fuel Chemistry 53(1)* (2008) 174-175.

Van Pelt, V. J., and Meischen, S. J., Determination of Total Mercury in Exhaust Gases, U.S. Patent 5,879,948, 1999.

Widmer, N. C., West, J., and Cole, J. A., Thermochemical Study of Mercury Oxidation in Utility Boiler Flue Gases, Proceedings of the Air & Waste Management Association 93rd Annual Meeting & Exhibition, Paper No. 390, Salt Lake City, UT, June 18-22, 2000.

Yudovich, Ya. E., and Ketris, M. P., Mercury in Coal: a Review Part 2. Coal Use and Environmental Problems, *International Journal of Coal Geology 62* (2005) 135-165.

Zhao, D., Feng, J., Huo, Q., Melosh, N., Fredrickson, G. H., Chmelka, B. F., Stucky, G. D., Triblock Copolymer Syntheses of Mesoporous Silica with Periodic 50 to 300 Angstrom Pores, *Science 279* (1998) 548-552.

Zhuang, Y., Biswas, P., Quintan, M. E., Lee, T. G., and Arar, E., Kinetic Study of Adsorption and Transformation of Mercury on Fly Ash Particles in an Entrained Flow Reactor, Proceedings of the Air & Waste Management Association 93rd Annual Meeting & Exhibition, Paper No. 331, Salt Lake City, UT, June 18-22, 2000.

List of Acronyms, Abbreviations, and Symbols

ads	species adsorbed on a surface
APTES	3-aminopropyltriethoxysilane
ASTM	American Society for Testing and Materials, West Conshohocken, PA
BET	Brunauer, Emmett, Teller (surface area)
C	species adsorbed on carbon surface
CAU	Clark Atlanta University, Atlanta, GA
CPTMS	3-chloropropyltrimethoxysilane
CRF	Combustion Research Facility, Southern Research Institute, Birmingham, AL
CTMABr	cetyltrimethylammonium bromide
DOE	U.S. Department of Energy
EPA	U.S. Environmental Protection Agency
ESP	electrostatic precipitator
FGD	flue gas desulfurization
FT-IR	Fourier transform-infrared spectrometer
g	gas-phase species
GTI	Gas Technology Institute, Des Plaines, IL
HgT	total mercury, elemental and oxidized, ng/m^3
Hg(0), Hg0	elemental mercury, ng/m^3
IPA	isopropyl alcohol
MCM	Mobil Composition of Matter
MPTMS	mercaptopropyltrimethoxysilane
MSU	Michigan State University
PRB	Powder River Basin, Wyoming, subbituminous coal
s	solid-phase species
S*	active site on a catalytic surface
SBA	University of California, Santa Barbara
SCR	selective catalytic reduction (of NO_X)
−SH	mercaptan functional group

SRI	Southern Research Institute, Birmingham, AL
TEAOH	tetraethylammonium hydroxide
TEOS	tetraethylorthosilicate
TVA	Tennessee Valley Authority
UAB	University of Alabama at Birmingham
UBC	unburned carbon
XRD	X-ray diffraction
σ_{FrHgOx}	standard deviation of the fraction of mercury oxidized, %
σ_{HgT}	standard deviation of measurements of total mercury, %
σ_{Hg0}	standard deviation of measurements of elemental mercury, %

Appendix: One-Dimensional Radial Diffusion and Heterogeneous Reaction Model for NO Reduction by NH_3, Mercury Oxidation by HCl, and SO_2 Oxidation to SO_3 in SCR*

```
// Calculate NO Reduction by NH3, Mercury Oxidation by HCl, and SO2 oxidation to SO3 in SCR

#include <stdio.h>
#include <math.h>
#include <stdlib.h>

#define  R  8314.47  //universal gas constant, J/(kmol K)
#define  Pref  101325.  //atmospheric pressure, Pa

double  kNO, Sh, T, P, DNO, dh, S, DNH3, Cg, KNH3, dx, x, NH3toNO, XNOo, CNOo, CNH3o, CNO, a, b, c, CNOs, dCNO, ug;
double  CNH3, kHgs, KHg, KHCl, XHCl, CHCl, kHgbl, kHgeff, DHg, CHgCl, fHgox, CHg, CHgo, CNH3s, dCHgCl, L, KHClpr;
double  KSO2, KSO3, KH2O, kred, kox, kNOx, CSO2, CO2, CH2O, XSO2, XO2, XH2O, Ctot, CSO3, CSO3o, XSO3o, XSO2o,
CSO2o, dCSO3;

        void main(void)
{
        FILE *outfile;
        outfile = fopen("cout1.dat", "w");

        //Catalyst Geometric and Composition Parameters

        S = 571.;  //surface-to-volume ratio, m2/m3
        L = 0.305;  //length of catalyst, m (ends of channels damaged)
```

*P. M. Walsh and G. Tong, unpublished work, 2008.

```
dh = 0.007;  //hydraulic diameter, m
Sh = 2.98;  //Sherwood No., laminar, fully developed, square channel
Ctot = 42000000.;  //total concentration of active sites, dimensionless
dx = 0.001;  //increment of catalyst length, m

//Catalyst Conditions

T = 700.;  //temperature, deg F
T = (T + 459.67) * 5. / 9.;  //temperature, K
P = 101325.;  //pressure, Pa
ug = 0.58;  //average gas velocity, m/s
Cg = P / (R * T);  //gas concentration, kmol/m3
DNO = 1.13e-9 * pow(T, 1.724) * Pref / P;  //molecular diffusion coefficient, O2-N2 [Marrero and Mason, J. Phys. Chem. Ref. Data 1 (1972) 3-118], m2/s
DNH3 = DNO * pow(30. / 17., 0.5);  //diffusion coefficient for ammonia, scaled by square root of molecular weight, m2/s
DHg = 0.470e-9 * pow(T, 1.789) * (Pref / P) * pow(131.3 / 200.6, 0.5);  //Xe-N2 [Marrero and Mason, J. Phys. Chem. Ref. Data 1 (1972) 3-118] scaled by square root of atomic weight, m2/s

//Rate Coefficients

kNO = 0.05;  //surface reaction rate coefficient for NO reduction by ammonia, m/s
kHgs = 0.014;  //rate coefficient for reaction between adsorbed Hg and adsorbed Cl or HCl, kmol/(m2 s)
kred = 0.01;  //rate coefficient for reduction of active vanadium oxide and oxidation of adsorbed SO2, kmol/(m3 s)
kox = 0.01;  //rate coefficient for reoxidation of active vanadium sites, kmol0.5/(m1.5 s)
kNOx = 0.;  //factor accounting for enhancement of SO3 formation rate by NOx ["b" in the notation of Svachula et al., Ind. Eng. Chem. Res. 32 (1993) 826-834], m3/kmol

//Adsorption Equilibrium Constants

KNH3 = 3000000.;  //NH3 adsorption equilibrium constant, m3/kmol
KHg = 750000;  //Hg adsorption equilibrium constant, m3/kmol
KHCl = 7.5;  //HCl (or Cl) adsorption equilibrium constant, competing with Hg, m3/kmol
kHClpr = 5000000.;  //HCl (or Cl) adsorption equilibrium constant, competing with SO2, m3/kmol
```

```
KSO2 = 0.00000015;  //SO2 adsorption equilibrium constant, m3/kmol
KSO3 = 5700000.;  //SO3 adsorption equilibrium constant, m3/kmol
KH2O = 0.;  //H2O adsorption equilibrium constant, m3/kmol

//Gas Composition

XHCl = 1.e-6;  //mole fraction HCl
XSO2o = 877.4e-6;  //mole fraction SO2
XO2 = 0.05;  //mole fraction O2
XH2O = 0.10;  //mole fraction water vapor
NH3toNO = 0.0;  //ammonia to NO mole ratio
XNOo = 300.e-6;  //mole fraction NO at inlet
XSO3o = 1.e-6;  //mole fraction SO3 at inlet
CNOo = XNOo * Cg;  //inlet NO concentration, kmol/m3
CHgo = (10000.e-12 / 200.6) * (293.15 / T) * (P / Pref);  //inlet elemental mercury concentration (10,000 ng/m3), kmol/m3
CSO3o = Cg * XSO3o;  //inlet SO3 concentration, kmol/m3
CHCl = Cg * XHCl;  //concentration of HCl (constant to good approximation, no axial or radial gradient), kmol/m3
CSO2o = Cg * XSO2o;  //concentration of SO2, kmol/m3
CO2 = Cg * XO2;  //concentration of oxygen, kmol/m3
CH2O = Cg * XH2O;  //concentation of water vapor, kmol/m3

while (NH3toNO <= 1.20)
{

CNH3o = CNOo * NH3toNO;  //inlet NH3 concentration, kmol/m3
CNO = CNOo;  //initialize NO concentration
CHgCl = 0.;  //initialize HgCl concentration
CHg = CHgo;  //initialize Hg concentration
CSO3 = CSO3o;  //initialize SO3 concentration
CSO2 = CSO2o;  //initialize SO2 concentration
x = 0.;  //initialize position
```

```
while (x <= L)
{

        //Calculate CNOs, concentration of NO at catalyst surface

        a = (kNO + (Sh * DNO / dh)) * DNO / DNH3;
        b = kNO * CNH3o - kNO * CNOo + kNO * CNO * (1. - (DNO / DNH3)) - 2. * (Sh * DNO / dh) * CNO * DNO /
        DNH3;
        b = b + (1. / KNH3) * (Sh * DNO / dh) + (Sh * DNO / dh) * CNH3o - (Sh * DNO / dh) * CNOo + (Sh * DNO / dh) *
        CNO;
        c = - (Sh * DNO / dh) * CNO * ((1. / KNH3) + CNH3o - CNOo + CNO * (1. - (DNO / DNH3)));

        CNOs = (- b + pow((pow(b, 2.) - (4. * a * c)), 0.5)) / (2. * a);

        //Calculate Mercury Oxidation

        CNH3 = CNH3o - (CNOo - CNO);
        CNH3s = CNH3 - (DNO / DNH3) * (CNO - CNOs);
        kHgbl = (kHgs * KHCl * CHCl * KHg) / ((1. + KNH3 * CNH3s + KHCl * CHCl) * (1. + KHCl * CHCl));
        kHgeff = 1. / ((1. / (Sh * DHg / dh)) + (1. / kHgbl));
        dCHgCl = (1. / ug) * kHgeff * S * CHg * dx;
        CHgCl = CHgCl + dCHgCl;
        CHg = CHg - dCHgCl;
        fHgox = CHgCl / CHgo;

        //Calculate SO3 formation [after Svachula et al., Ind. Eng. Chem. Res. 32 (1993) 826-834]

        dCSO3 = (dx / ug) * kred * KSO2 * KSO3 * Ctot * CSO2 * CSO3 * (1. + kNOx * CNOs)/(1. + KSO3 * CSO3 * (1. +
        KSO2 * CSO2 * (1. + (kred / (kox * pow(CO2, 0.5)))) + KH2O * CH2O + KNH3 * CNH3 + KHClpr * CHCl));
        CSO3 = CSO3 + dCSO3;
        CSO2 = CSO2 - dCSO3;
```

```
        //Calculate NO and NH3 Decay

        dCNO = (1. / ug) * (Sh * DNO / dh) * S * (CNO - CNOs) * dx;
        CNO = CNO - dCNO;
        CNH3 = CNH3o - (CNOo - CNO);

        x = x + dx;  //increment position

        //printf("\n%6.3lf   %6.4lf   %5.2lf   %4.2lf   %6.3lf", x, CNO / CNOo, CNO * XNOo * 1.e6 / CNOo, CNH3 * 1.e6 /
        Cg, fHgox);
        //fprintf(outfile, "\n%10.6lf    %10.6lf    %10.6lf    %10.6lf    %10.5lf"    , x, CNO / CNOo, CNO * XNOo * 1.e6 /
        CNOo, CNH3 * 1.e6 / Cg, fHgox);
    }
        printf("\n%6.3lf   %6.4lf   %5.2lf   %4.2lf   %6.3lf   %6.4lf", NH3toNO, CNO / CNOo, CNO * XNOo * 1.e6 / CNOo,
        CNH3 * 1.e6 / Cg, fHgox, CSO3 / CSO2o, KNH3 * CNH3, KHClpr * CHCl);
        fprintf(outfile, "\n%10.6lf    %10.6lf    %10.6lf    %10.6lf    %10.5lf    %10.5lf"    , NH3toNO, CNO / CNOo, CNO *
        XNOo * 1.e6 / CNOo, CNH3 * 1.e6 / Cg, fHgox, CSO3 / CSO2o);

        NH3toNO = NH3toNO + 0.05;  //increment NH3 to NO ratio

    }

    return;
}
```